

KAUNAS UNIVERSITY OF TECHNOLOGY

EVELINA JASELSKĖ

FORMATION AND FUNCTIONALIZATION OF
POLYMER DOSE GELS USING PHOTON AND
ELECTRON BEAMS

Doctoral dissertation
Technological Sciences, Materials Engineering (T 008)

Kaunas, 2021

The doctoral dissertation was prepared at Kaunas University of Technology, Faculty of Mathematics and Natural Sciences, Department of Physics, during the period of 2015–2020. The scientific research was done in the Faculty of Electrical and Electronics Engineering, Institute of Metrology, and LUHS Kaunas Clinics, Oncology and Hematology Clinic, Radiotherapy Department, Neurosurgery Clinic, Gamma Knife Department. The studies were supported by the Research Council of Lithuania.

Scientific Supervisor:

Prof. Dr. Diana ADLIENĖ (Kaunas University of Technology, Technological Sciences, Materials Engineering, T 008).

Doctoral dissertation has been published in: <http://ktu.edu>

Edited by Brigita Brasienė (Publishing House “Technologija”).

KAUNO TECHNOLOGIJOS UNIVERSITETAS

EVELINA JASELSKĖ

POLIMERINIŲ DOZIMETRINIŲ GELIŲ
FORMAVIMAS IR FUNKCIONALIZAVIMAS
NAUDOJANT FOTONŲ IR ELEKTRONŲ
SPINDULIUOTE

Daktaro disertacija
Technologijos mokslai, medžiagų inžinerija (T 008)

Kaunas, 2021

Disertacija rengta 2015–2021 metais Kauno technologijos universiteto Matematikos ir gamtos mokslų fakulteto Fizikos katedroje. Dalis mokslinių tyrimų atlikta Elektros ir elektronikos fakulteto Elektronikos inžinerijos katedroje, Metrologijos institute bei LSMUL Kauno klinikų Onkologijos ir hematologijos klinikoje, Spindulinės terapijos skyriuje bei Neurochirurgijos klinikos Gama peilio sektoriuje. Mokslinius tyrimus rėmė Lietuvos mokslo taryba.

Mokslinė vadovė

prof. dr. Diana ADLIENĖ (Kauno technologijos universitetas, technologijos mokslai, medžiagų inžinerija T 008).

Interneto svetainės, kurioje skelbiama disertacija, adresas: <http://ktu.edu>

Redagavo Brigita Brasienė (leidykla „Technologija“).

ACKNOWLEDGEMENTS

The author of the dissertation would like to express gratitude to scientific supervisor Prof. Dr. Diana Adlienė for patience, her professional advices, and support during all doctoral studies as well as help in the process of preparing the dissertation.

The author would like to thank KTU research group of Radiation and Medical Physics and the medical physicists from the Hospital of Lithuanian University of Health Sciences.

TABLE OF CONTENTS

LIST OF FIGURES	8
LIST OF TABLES	12
LIST OF ABBREVIATIONS	13
1. INTRODUCTION	14
2. LITERATURE REVIEW	17
2.1. Ionizing radiation-induced processes in polymer gels.....	17
2.2. Polymer gels	18
2.2.1. Polymer gels composition	18
2.2.2. The influence of gelatin concentration in dose gels	22
2.2.3. The role of the oxygen scavenger in gels	24
2.3. Polymerization in nPAG and VIPAR gels	25
2.4. The impact of irradiation parameters on dose gel properties	26
2.4.1. The impact of the radiation beam type on dose gel properties	27
2.4.2. Dose rate effect.....	28
2.4.3. The impact of temperature on dose gel properties.....	29
2.5. Reading-out techniques for the irradiated dose gels	30
2.5.1. MRI read-out method	30
2.5.2. Optical read-out method	35
2.5.3. Raman spectroscopy	36
2.5.4. Microscopy methods for the read-out of dose gels.....	38
2.6. Uncertainties during the read-out of irradiated dose gels.....	38
2.7. Dose gels applications in the medical field	40
2.7.1. Dose gels in radiotherapy and radiosurgery dosimetry	40
2.7.2. The application of polymer gels for 3D and 4D printing	42
3. INSTRUMENTS AND METHODS	44
3.1. Dose gels fabrication	44
3.1.1. Fabrication of nPAGF dose gels.....	46
3.1.2. Fabrication of VIPARnd dose gels.....	47
3.2. Irradiation techniques	48
3.2.1. Gamma photon irradiation facilities	49
3.2.2. High dose rate brachytherapy units	50
3.2.3. Medical linear accelerator	51
3.3. Experimental methods	52
3.3.1. Characterization methods of materials	53
3.3.2. Dose read-out/dosimetry methods	57
4. RESULTS AND DISCUSSION.....	62
4.1. Modified dose gels evaluation.....	62
4.2. Characterization of the dose gel properties	62
4.2.1. Evaluation of radiation sensitivity of experimental gels using UV-VIS spectrophotometry	62
4.2.2. Investigation of the optical density changes in the irradiated gels	67
4.2.3. Analysis of polymerization processes in irradiated dose gels using Raman spectroscopy	68

4.2.4. X-ray attenuation properties of dose gels	76
4.2.5. Evaluation of polymerized gel properties using magnetic resonance imaging.....	78
4.2.5.1. Evaluation of dose sensitivity using MRI scanning method.....	78
4.2.5.2. Dose mapping using polymerizable nPAGF gels.....	81
4.2.5.3. Comparison of dosimetric features of nPAGF and VIPARnd gels .	83
4.3. Evaluation of dose resolution in irradiated gels	85
4.4. Ionizing radiation-induced 3D printing of free standing gels.....	89
4.5. Formation of free standing gels.....	90
4.6. Clinical exploration of polymerizable gel properties	95
4.6.1. Clinical application of free standing gel shapes	95
4.6.2. Application of dose gels for individualized dosimetry.....	97
4.6.3. Clinical microdosimetry concept.....	100
CONCLUSIONS	107
LIST OF REFERENCES.....	109
LIST OF PUBLICATIONS.....	120
ANNEXES	124

LIST OF FIGURES

Fig. 1. Radiolysis of water [9].....	17
Fig. 2. Relative maximum absorbance vs. the dose of VIPAR nd [27].....	21
Fig. 3. Different polymer structures after irradiation: (a) initial gel solely composed of monomer (AAM); (b) gel composed of low initial Bis fraction; (c) gel composed of high initial Bis fraction; (d) initial gel composed solely of crosslinker (Bis) [17]...	22
Fig. 4. Principal scheme of heating and cooling effect in the gel [29].....	23
Fig. 5. Dose sensitivity dependence on the gelatin concentration [32].....	23
Fig. 6. The effect of THPC concentration on the nPAG polymer gel dose response [35]	24
Fig. 7. Principal polymerization scheme of vinyl group polymers [36].....	26
Fig. 8. Dose rate dependence on the dose principal scheme [48, 49].....	28
Fig. 9. Dose and polymerization rate dependency scheme	29
Fig. 10. a) Random alignment of hydrogen nuclei in the material (tissue) and b) hydrogen nuclei behavior in a strong magnetic field, according to the magnetic field direction (B ₀) [59].....	31
Fig. 11. a) External RF pulse, b) displaced magnetic moment (vector M) [60].....	31
Fig. 12. Illustration for TE and TR parameters in T1 and T2 weighted images [60]	32
Fig. 13. The parameter measurement function of MRI, where x, c – any parameters for measure [63]	34
Fig. 14. An example of polymer gel dose mapping, with a) irradiated dose gel and b) dose map in TPS [65]	34
Fig. 15. Energy level diagram of Raman spectroscopy [76]	37
Fig. 16. The mathematical definition of accuracy and precision.....	39
Fig. 17. 2D projection of VMAT plan: a) calculated by TPS and b) verified with portal dosimetry	41
Fig. 18. Polymerization scheme for acrylamide (L) and N-vinylpyrrolidone based crosslinked polymers (R).....	44
Fig. 19. a) Fabrication of nPAG ^F dose gels, b) freshly prepared gels, c) an example of the irradiated dose gel sample	47
Fig. 20. a) VIPAR nd dose gel preparation, b), freshly prepared dose gel, c) an example of irradiated VIPAR nd dose gel.....	48
Fig. 21. a) The experimental setup for the irradiation of gel samples in Teletherapy unit Rokus M, b) location of samples and ionization chamber during the experiment, c) nPAG ^F dose gels irradiated to the doses up to 4 Gy for catheter-based dosimetry calibration purposes.....	49
Fig. 22. a) The experimental setup for the gel irradiation in the Gama knife facility, b) dose gel samples positioning during the treatment, c) irradiated VIPAR nd and d) nPAG ^F dose gels.....	50
Fig. 23. The experimental setup for the irradiation of obtaining free standing dose gels in a) HDR brachytherapy unit Flexitron Icon TM , b) and c) PAG ^F dose gel samples after the irradiation with ¹⁹² Ir source inserted into the catheter, d) the removal of polymerized gel shape from the gel volume, e) measuring the size of the polymerized shape.....	51

Fig. 24. a) Principal scheme of the samples irradiation with a linear accelerator, b) e-beam irradiated nPAG ^F samples.....	52
Fig. 25. Dose gel evaluation and characterization methods	53
Fig. 26. Experimental setup for controlled heating method: a) Ametek JOFRA RTC-158 thermostat with gel sample inserted instead of the calibration sleeve; b) dynamometric measuring stand Sauter TVM 5000N230N with calibrated dynamometer Sauter F1k.....	55
Fig. 27. Radiation attenuation values (Hounsfield Units) [104]	57
Fig. 28. a) Spectrophotometer Ocean optics with USB 400, b) dose mapping system with UV-VIS spectrophotometer Ocean Optics with USB650 and sample positioning stage.....	58
Fig. 29. NMR imaging: a) experimental sample mounted in the head coil; b) irradiated gel filled sample and MRI scan of the same sample	59
Fig. 30. Dosimetric sensitivity of electron beam irradiated nPAG dose gels at the selected wavelengths	60
Fig. 31. Transmittance spectra of gamma irradiated VIPAR nd gel	63
Fig. 32. Transmittance spectra of gamma irradiated nPAG ^F gel.....	64
Fig. 33. Transmittance spectra of electron irradiated nPAG ^F gel.....	64
Fig. 34. OD changes of VIPAR nd dose gel irradiated with gamma photons at 750 nm wavelength.....	65
Fig. 35. OD changes of nPAG ^F dose gel irradiated with gamma photons at 750 nm wavelength.....	66
Fig. 36. OD changes of nPAG ^F dose gel irradiated with electron beam at 750 nm wavelength.....	66
Fig. 37. Absorbed dose related refractive index of polymerized gels irradiated with gamma photons.....	68
Fig. 38. Raman spectra of pure materials.....	69
Fig. 39. Full Raman spectrum of nPAG ^F dose gels irradiated with 6 MeV X-ray photons	70
Fig. 40. Full Raman spectrum of nPAG ^F dose gels irradiated with 6 MeV electrons	70
Fig. 41. Polymerization of nPAG ^F dose gels: A) irradiated with 6 MeV X-ray photons, B) irradiated with 6 MeV electron beam	73
Fig. 42. Raman spectrum segments of nPAG gels: A) electron beam irradiated, B) X-ray irradiated.....	73
Fig. 43. Full Raman spectrum of VIPAR nd dose gels irradiated with 60Co gamma photons	74
Fig. 44. Raman spectrum segments for gamma irradiated VIPAR nd gels	76
Fig. 45. Raman spectrum segments for gamma irradiated VIPAR nd gels	76
Fig. 46. a) nPAG cuvettes irradiated in linear accelerator with 6 MeV X-ray photons, b) dose dependency of X-ray attenuation in the irradiated gels	77
Fig. 47. Dose dependency of X-ray attenuation in nPAG ^F gels irradiated with gamma photons	77
Fig. 48. Variations of pixel intensities with a dose of nPAG ^F samples at the selected points in MRI scans obtained by applying different echo times.....	79

Fig. 49. Comparison of dose assessment sensitivity using MRI and Gafchromic films	79
Fig. 50. Gafchromic Kodak X Omat V films (top row) and RTQA2 films (bottom row) irradiated in Gamma knife facility using 4 mm collimator to doses 1 Gy, 4 Gy, and 6 Gy, respectively	80
Fig. 51. Spin-spin relaxation rate R2 versus absorbed dose curve constructed for Gamma knife irradiated nPAG ^F dose gels	81
Fig. 52. Gammaplan TPS simulated dose distributions with Dmax in the isocenter: 1–10 Gy, 2–13 Gy, 3–18.6 Gy, 4–26 Gy, 5–43.3 Gy.....	83
Fig. 53. MRI scanned nPAG ^F dose gel image: 1–10 Gy, 2–13 Gy, 3–18.6 Gy, 4–26 Gy, 5–43.3 Gy	82
Fig. 54. Dose distribution maps of irradiated nPAG ^F dose gels created using Matlab programming software: 1–10 Gy, 2–13 Gy, 3–18.6 Gy, 4–26 Gy, 5–43.3 Gy	82
Fig. 55. Relative pixel intensity variations in MRI scanned irradiated dose images after the first shot at the first target.....	83
Fig. 56. Relative pixel intensity variations in MRI scanned irradiated dose images after the second shot at the second target	84
Fig. 57. Comparison of T2 time values that are needed for obtaining the irradiated dose gel images of the first target for both types of irradiated dose gels	84
Fig. 58. Comparison of T2 time values needed for obtaining the irradiated dose images of the second target for both types of irradiated dose gels	85
Fig. 59. R2 calculations for nPAG ^F and VIPAR nd dose gels with differently absorbed doses	86
Fig. 60. Dose sensitivity of nPAG ^F and VIPAR nd dose gels evaluated at different echo times	87
Fig. 61. Dose resolution (p=95%) calculations for nPAG ^F dose gels.....	88
Fig. 62. Dose resolution (p=95%) calculations for VIPAR nd dose gels	88
Fig. 63. Gelatin concentration related dose response in terms of relaxation rate R2 of gamma photons irradiated nPAG ^F gels.....	89
Fig. 64. A – nPAG ^F dose gel samples irradiated in Elekta Flexitron IconTM in brachytherapy unit with 192Ir source with different doses, B – example with free standing dose gel shape inside the bottle, C – free standing polymerized gel removed from the whole gel volume.....	91
Fig. 65. Measurement of the polymerized shape with digital caliper.....	91
Fig. 66. Comparison of TPS proposed treatment volume (2D dose distribution map, transverse view from TPC) (a) with radiation produced polymerized free standing dose gel volume: (b) image of just irradiated gel filled beaker with a polymerized part in gelatin matrix, (c) separation of polymerized gel part from the gelatin, (d) image of radiation produced 3D free standing polymerized gel shape; notice that the scales are different	92
Fig. 67. Adhesion force versus time for nPAG ^F gels, applying the dry air method .	94
Fig. 68. Adhesion force versus temperature gradient time for nPAG ^F gels, applying controlled heating method	95
Fig. 69. Views of TPS plan prepared for head and neck cancer patient with squamous cell lip carcinoma	96

Fig. 70. The high energy photon based 3D printing of free standing gel shape: (a) image of just irradiated gel filled beaker with a polymerized part in gelatin matrix, (b) separation of polymerized gel part from the gelatin, (c) image of radiation produced 3D free standing polymerized gel shape; notice that the scales are different [A2] .. 96

Fig. 71. Catheter implantation process in brachytherapy 98

Fig. 72. Comparison of measured dose errors during two independent treatment sessions 98

Fig. 73. Relative errors, % between two independent fractions 99

Fig. 74. Comparison of the in vivo dosimetry results using of nPAG^F gel filled catheter as a dosimeter in catheter based dosimetry..... 100

Fig. 75. A – distribution of isodoses in the target simulated by the Gammaplan treatment planning system for single shot geometry, where the yellow line indicates 8 mm collimator area, corresponding to the delivery area of 16 Gy, B – the horizontal dose profile within the area, irradiated with open field of 8 mm collimator 102

Fig. 76. Images of irradiated S1.2 gel samples: A – a photograph, B – MR-scanned image 102

Fig. 77. Variations of pixel intensities of nPAG^F samples at the selected points in MR scans obtained at different TE 103

Fig. 78. Variations of pixel intensity values in MRI images of the irradiated nPAG^F gels for each of three single dose delivery shots at different echo times (TE) 103

Fig. 79. A – Distribution of isodoses in three treatment isocenters simulated by the Gammaplan treatment planning system for multiple shot geometry, B – dose profile along the distance, covering all three dose isocenters 104

Fig. 80. Images of S2.3 sample: A– photograph of nPAG^F gel-filled vial after 3-shot irradiation with clearly seen three polymerized 3D shapes at the selected isocenters, indicated as I, II, and III, B – corresponding MRI DICOM view of the same sample 105

Fig. 81. Dose profiles obtained for the nPAG^F samples: a) irradiated with 4 Gy dose in Gamma knife facility by applying different collimators and from TPS Gammaplan irradiated using b) 16 mm, c) 8 mm, and d) 4 mm open sector collimators 106

LIST OF TABLES

Table 1. Possible manufacturing components of a gel [16].....	19
Table 2. Possible compositions of nPAG dose gels.....	21
Table 3. Reactions of polymer radicals in PAG and NIPAM dosimeters.....	25
Table 4. Advantages and disadvantages of the optical read-out systems	36
Table 5. Raman shifts of different photon beam irradiated gels: methacrylic acid based (nMAG), polyacrylamide based (nPAG), N-Isopropylacrylamide based (NIPAM), polyacrylic acid based (PAA), polyhydroxyethylmethacrylate (PHEMAG) based dose gels	37
Table 6. The main advantages and disadvantages of 4D printing method.....	43
Table 7. Chemical composition of the advanced nPAG ^F and VIPAR nd dose gels...	45
Table 8. Irradiation facilities and irradiation parameters.....	48
Table 9. Reference and experimental values of nPAG ^F dose gel refractive index...	54
Table 10. nPAG ^F and VIPAR nd dose gel sample quantities used in the experiments	61
Table 11. The main vibrational band assignments for nPAG gels.....	71
Table 12. The main Raman vibrational band assignments for VIPAR nd gels.....	75
Table 13. Radiation based 3D printing of free standing dose gel shapes	93
Table 14. Irradiation parameters of nPAG ^F gel samples in Gamma knife facility	101
Table 15. Comparison of the output factors.....	105

LIST OF ABBREVIATIONS

Aam – acrylamide
Bis – *N,N'*-methylene bisacrylamide
FWHM – full width half maximum
Gy – ionizing radiation dose unit Gray
HU – Hounsfield units
MAG – methacrylic acid dose gels
MRI – magnetic resonance imaging
NIPAM – *N*-isopropylacrylamide
NMR – nuclear magnetic resonance
nPAG – normoxic polyacrylamide based dose gels
OCT – optical computed tomography method
OSL – optically stimulated luminescence
PAG – polyacrylamide gel
R2 – transverse relaxation rate
RPR – radiolytic polymerization reaction
RRR – radiolytic reduction reaction
SEM – scanning electron microscopy
SNR – signal-noise ratio
SSD – source to skin surface
TE – echo time
THPC – tetrakis hydroxymethyl phosphonium chloride
TLD – thermoluminescent dosimeter
TPS – treatment planning system
TR – repetition time
UV-VIS – ultraviolet and visible light spectra
VIPARnd – *N*-vinylpyrrolidone based normoxic double dose gels
VMAT – volumetric modulation arc therapy
XCT – X-ray computer tomography

1. INTRODUCTION

Ionizing radiation is a tool to detect and visualize cancer injured tissues and tumors and treat cancer. Different types of equipment can be used for radiotherapy treatment; however, in all cases, adequate dosimetry procedures are required. Dosimeters are made from ionizing radiation sensitive materials, which chemical and physical properties are sensitive to the energy (dose) that is absorbed in the irradiated target. Ionizing chambers, optically stimulated luminescence (OSL) or thermoluminescence (TLD) dosimeters, chemical, semi-conductor dosimeters are well established for 2D absorbed dose measurements; however, polymer gel dosimetry only provides 3D information on dose distribution and shape of the irradiated volume, which is present when the irradiated gel polymerizes upon irradiation. The polymer gels as dosimeters are widely used in radiotherapy, brachytherapy, proton therapy, neutron capture therapy, etc. [1], however, not for clinical routine dosimetry, but mainly in research applications [2].

The main obstacle for the clinical use of polymer dose gels is their low dose sensitivity and relative high uncertainties related to the applied dose evaluation methods. A few different studies [3–7] have been performed on investigating various ionizing radiation sensitive materials, and it has been found that the polymer gels are most promising materials, because the properties of fabricated dose gels may be altered by changing their chemical components and concentrations and a broad variety of different dose read-out methods might be selected, following the main objectives of the performed research. Since the amount of absorbed dose is tightly related to the radiation-induced polymerization processes in the gel, magnetic resonance imaging (MRI), optical computed tomography (OCT), X-ray computed tomography (CT), Raman spectroscopy, Infrared spectroscopy (FTIR), and other optical evaluation methods as well as echoscopy can be applied for the dose evaluation in polymerized gels.

Despite of relatively intensive research in the dose gel field, the specific dose gel applications, like small-scale dosimetry in radiosurgery or individualized patient care dosimetry for individualized radiotherapy treatment, which will be one of the main challenges in the health sector for the next decade, have not been addressed and fully covered until now.

In this work, the modified formulations of polyacrylamide and *N*-vinylpyrrolidone based polymer gels were fabricated, and their applicability for dosimetry purposes in e-beam therapy, brachytherapy, and Gamma knife radiosurgery was investigated. The dose evaluation was based on radiation-induced polymerization of dose gels irradiated with high energy photons and electrons.

Aim and objectives of the dissertation

The aim of the doctoral dissertation is to form, analyze, and functionalize dose gels for high dose small scale radiation treatment and propose radiation based 3D printed dosimetry concept for the individual treatment plan verification in radiotherapy and radiosurgery.

In order to achieve this aim, the following objectives were set:

1. To select, fabricate, and analyze a set of polymeric gels viable for small scale high dose dosimetry applications;
2. To investigate and evaluate dose gel read-out methods and their suitability in terms of practical application;
3. To develop and realize ionizing radiation based 3D printing concept of free standing gels;
4. To perform pilot study on the dose gel use for individualized patient dosimetry in high dose small scale radiosurgery and functionalize it.

Originality of the research

1. It was shown that some types (modified nPAG^F and VIPARnd) of polyacrylamide and *N*-vinylpyrrolidone based polymer gels are sensitive enough to record small-scale high-dose radiation-induced optical property changes in polymerized gel structures. The highest sensitivity to the dose was 0.081 Gy⁻¹s⁻¹ and 0.121 Gy⁻¹s⁻¹ for nPAG^F and VIPARnd, respectively. VIPARnd gels were as well sensitive enough in a high dose region (10 Gy to 40 Gy), indicating 0.035 Gy⁻¹s⁻¹ sensitivity.

2. Radiation-induced 3D printing method was firstly proposed, and free standing dose gel structures were created.

3. The applicability of dose gels for individualized patient dosimetry purposes in brachytherapy and gamma knife surgery has been assessed and implemented during the pilot projects.

Author's contribution

The experimental work was carried out at:

1. Kaunas University of Technology, Faculty of Mathematics and Natural Sciences, Department of Physics;
2. Hospital of Lithuanian University of Health Sciences, Kaunas Clinics, Oncology and Hematology Clinic, Radiotherapy Department;
3. Hospital of Lithuanian University of Health Sciences, Kaunas Clinics, Neurosurgery Clinic, Gamma Knife Department;
4. Faculty of Electrical and Electronics Engineering, Institute of Metrology with the support of Dr. Benas Gabrielis Urbonavičius;
5. Institute of Materials Science (Raman spectroscopy).

The selection, formation, and characterization of dose gels and dose read-out methods as well as the interpretation of the obtained results were performed by the author. The author of the dissertation contributed to the development of ionizing radiation based 3D printing concept of free standing dose gels with the experimental investigation of adhesion forces between polymerized and not polymerized part of the gel and development of part separation method. The author performed all clinical experiments related to the dose gel applicability in radiotherapy and radiosurgery.

Two papers related to the topic of dissertation were prepared in collaboration with other doctoral students. Neringa Šeperienė presented the investigations of dose

sensitivity of polymer composites that are irradiated to low doses up to 10 Gy in her dissertation, and Benas Gabrielis Urbonavičius developed the plasmonic sensors with polymer gels for radiation dose measurements for a small dose (< 10 Gy) registration.

PhD thesis approbation

The main doctoral dissertation results were published in 10 scientific publications: 3 papers related to the dissertation topic are published in journals included in Clarivate Analytics Web of Science database, 5 papers are published in conference proceedings that are included in CAWoS database without impact factor; 2 articles and 2 conference proceedings papers included in the CAWoS database are out of the scope of this dissertation.

The main results of the performed research were presented in 15 international and national conferences.

The author participates/was participating in two related research projects supported by the Lithuanian Research Council:

1. P-MIP-17-223 “Development of 3D phantom for individualized dosimetry in radiotherapy”, 2017–2019;
2. Joint LUHS/KTU project under programme Healthy ageing P-SEN-20-10 “Development of neurosurgical treatment options for Parkinson`s disease applying molecular markers, gamma knife technology and individualized dosimetry”, 2020–2022.

Structure of the dissertation

This doctoral dissertation consists of five chapters. The first chapter includes introduction, aim, objectives, author’s contribution, work originality and PhD thesis approbation. The second chapter includes a literature overview related to the newest information about the polymer dose gel application. The instruments and methodology are described in the third chapter. The fourth chapter is dedicated to the results and their interpretation. The dissertation concludes with the final fifth chapter. At the end of the dissertation, there are presented a list of references (143), two annexes, a list of scientific publications related to the topic of the dissertation and participated conferences. The total dissertation size is 130 pages, including 81 figures and 15 tables, 143 references.

2. LITERATURE REVIEW

2.1. Ionizing radiation-induced processes in polymer gels

Dose gels (and polymer gels or hydrogels) contain monomers that are tending to polymerize upon the exposure to ionizing radiation. The main processes that are resulting from the interaction of ionizing radiation with dose gels are cross-linking, long-chain branching, oxidation and chain scission, polymerization and grafting.

One of the main parts of polymerization processes are water radiolysis. Radiolytic reduction reaction (RRR), radiolytic oxidation reaction (ROR), and radiolytic polymerization reaction (RPR) are chemical radiation reactions produced from the radiolysis of water [8].

It is as a source of radicals responsible for the polymerization reactions. The ionization of water molecules is indicated by irradiation ($h\nu$). This process is illustrated below (Fig. 1):

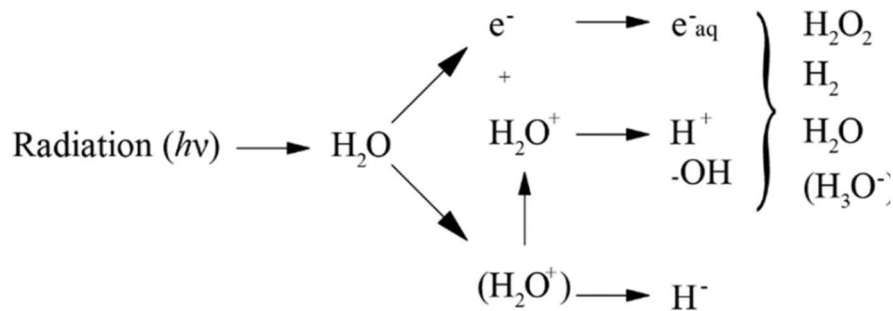


Fig. 1. Radiolysis of water [9]

Hydrogen is a product of molecule, which escapes with chemical insertion. Hydrogen peroxide (H_2O_2) is a molecular product as well, which reacts with reducing species (e^-_{aq} , $\text{H}\cdot$) after retaining in water and produce $\cdot\text{OH}$ and other related species. After some time in the radiation field, H_2O_2 concentration becomes steady if the water is pure. From H_2O^+ reaction formed positive ions can form hydroxyl radical ($\text{OH}\cdot$) as well, when dissociating into the $\text{H}\cdot$ and $\cdot\text{OH}$ form. The radicals of hydroxyl and hydrogen can be formed through the water molecule excitation and produce pairs of H^+ and OH^- ions, a pair of free radicals $\text{H}\cdot$ and $\cdot\text{OH}$ as a radiolysis reaction result [9].

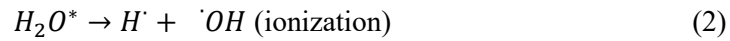
The cross-linking is related to the polymer chemistry process that is called stabilization, when a bond links polymer chains together and restricts the movement ability, thus changing the liquid polymer into “solid” or “gel” consistent [10].

The intensity of polymerization process and cross-linking of monomers depends on the amount of absorbed energy. Free radicals, which are important reactive species in polymer processing by ionizing radiation, are created either through scission of the main polymer chain or through the dissociation chain [8].

Cross-linking and chain scission are related to different polymer response to ionizing radiation and causes the formation of three-dimensional polymer network

(polymerized gel) and an increase in the molecular weight of the polymer. The result of two molecules junction combination (head–head, head–tail, or tail–tail) is called radiation cross-linking. The opposite process is polymer degradation or chain scission [8]. Different quantities of selected components during the polymer gel manufacturing process affect the polymerization processes and gel sensitivity to radiation.

The primary interaction with ionizing radiation with water molecules is excitation or ionization (Eq. 1–2):



The process when monomers are bonded and polymerized as a side chain onto the main polymer chain is called grafting [11]. Polymerization is a process when monomer molecules of radiosensitive materials form polymer chains, i.e., volumetric networks during the chemical reactions. The selection of individual components, physical and chemical conditions during the fabrication has a significant influence on the manufactured dose gel as a final product. A parameter called “gel fraction” is the ratio of the insoluble part divided by the initial weight of the polymer [12].

For the evaluation of different polymers response to irradiation strength, G-value evaluation is used quite frequently. It represents the chemical yield of chain scission, double bonds, crosslinks etc. G-value is the radiation by the number of molecules reacted per 100 eV ($1.6023 \times 10^{21} \text{ J}$) that are dissipated in the material. For cross-linking, it is denoted as G(X). For example, the value of G(X) 4.5 means that 4.5 cross-links are formed in the polymer per 100 eV under certain radiation conditions [13].

Long chain branching effect on the polymer physical properties makes the polymers less dense and may increase strength, toughness, etc. as a result. Polymer crystallographic geometry depends on “g” parameter, which is related to nuclear magnetic resonance conditions after samples read-out, and they are provided in equation 3:

$$hf = gm_B B; \quad (3)$$

where h is the Planck’s constant = $6.62 \times 10^{-34} \text{ J}\cdot\text{s}$; f – frequency (Hz); g – Lande factor; m_B – Bohr magneton equivalent to $9.2740154 \times 10^{-24} \text{ J/T}$; B – magnetic field induction (T).

2.2. Polymer gels

Polymer gels are the oldest known gelation system with three dimensional interconnected molecular framework, composed of cross-linked long macromolecular chains and specific physical and chemical properties [14].

2.2.1. Polymer gels composition

The sensitivity to the absorbed energy (dose) of polymer gel depends on the chemical structure. Usually, the dose gels contain monomer, cross-linker (not in all cases), gelatin, as a matrix for polymerized structure, water, and oxygen scavenger. Due to the high amount of water (> 80%), polymer gels are nearly water equivalent

hydrogels. The physical mass density of the gel can be 2–6% higher as compared with water, depending on the monomer and the amount of gelatin in the fabricated gel; however, it stays close to the density of the human tissue, keeping the dose gels tissue equivalent [15]. The alteration of gel's components and their concentrations allows for achieving different sensitivity (high and low) of dose gels to the irradiation. Several components of dose gels are given in Table 1.

Table 1. Possible manufacturing components of a gel [16]

Components	Weight/weight fractions	
	High sensitivity (HS)	Low sensitivity (LS)
C	0.1419	0.1418
H	0.1008	0.1008
N	0.0209	0.2089
O	0.7364	0.7361
Cu	3.2×10^{-7}	-
S	1.6×10^{-7}	1.6×10^{-4}
Fe	-	2.8×10^{-4}

The radiation sensitivity of dose gels (dosimeters) as well depends on the type of particles that are interacting with gels and dose rate, provided by the treatment unit.

The composition of the selected polymer gel dosimeters is strongly dependent on the preset dosimetry goals. The chemical compositions of polymer gels that are widely used in dosimetry applications are provided in Annex 1.

Despite of the impressive number of polymer gels that are already in use, new compositions of gels are constantly investigated, seeking to improve their dose sensitivity, stability, and other characteristics, such as toxicity.

Polyacrylamide based PAG dosimeters are widely used for dosimetry purposes (even if dose sensitivity of these gels is rather low 0.08–1.10), because of their low dose rate dependency, low sensitivity to the temperature changes, and fabrication simplicity at room temperature [17]. The replacement of high toxic acrylamide with other derivatives of acrylamide or other components reduced the toxicity of the entire gel, as it was shown in [18, 19] by using 2-acrylamido-2-methyl-1-propane sulfonic acid (AMPS) sodium salt monomer instead of acrylamide (PASSAG and PAMPSGAT gels). In some studies [20–22], acrylamide was changed to *N*-isopropyl acrylamide with the purpose to manufacture less toxic (NIPAM) dosimeters; however, the polymerized gel was cloudy, thus excluding the application of some optical methods for their read-outs. One more polymer gel (HPC) consists of less toxic monomers, and hydroxypropyl cellulose was proposed in [8]. Unlike PAG, PAGAT dose gels HPC did not become cloudy after the irradiation up to 10 Gy; but it was less dose sensitive as PAG gels.

Genipin gel based dosimeters [23] are changing from colorless to deep blue after the irradiation, and this change can be optically quantified. Different derivatives of genipin gel composition are suitable for the dose evaluation within the range of 0–100 Gy or 100–1000 Gy.

The polymer gel that contains dithiothreitol and methacrylic acid (MAGADIT) demonstrates linear dose response after the irradiation up to 24 Gy and was suitable for small field measurements [24]. Dithiothreitol was added as oxygen scavenger to replace more toxic THPC.

Radiochromic micelle hydrogel dosimeters are indicating high accuracy in 3D dose measurements [25].

Leuco crystal violet (LCV) based micelle gelatin hydrogels can be used in dosimetry applications due to the induced radiation, increasing the intensity of violet color [92]. A wide selection of dose gels could be applied for dosimetry purposes, and most of them could be modified with the purpose to achieve better dosimetry results.

However, the research performed in the frame of this dissertation focuses on the modification and functionalization of acrylamide based (nPAG) and *N*-vinylpyrrolidone based (VIPAR) gels that can be used in some new medical dosimetry applications.

VIPAR type gels. This type of gels is used for dosimetry purposes because of their wide dose sensitivity range and good agreement with the data calculated by the TPS of radiotherapy unit [26, 27, 9].

VIPAR dose gel consists of 90.5 wt% pure deionized water, 3.5 wt% gelatin from porcine skin (type A/300 Bloom), 2 wt% of *N,N'* methylene bisacrylamide (BIS), 397 mM ASC (ascorbic acid), 32 mM of copper sulfate pentahydrate ($\text{CuSO}_4 \cdot 5\text{H}_2\text{O}$), and 4 wt% of *N*-vinylpyrrolidone (NVP) [9]. The optimal concentrations of copper sulfate pentahydrate and *N*-vinylpyrrolidone are 0.0008 wt% and 0.007 wt% [27].

This gel composition demonstrates the ability to absorb a dose in a wide energy range; however, the dose response in the low energy region is low. With the purpose to extend VIPAR gel sensitivity, i.e., dose response to low dose region, the original recipe was modified, and NVP concentration was doubled to 8 wt%. Moreover, the proportion of gelatin was increased. A new formulation of VIPAR was called VIPARnd (VIPAR-normoxic-doubled) and had significantly lower dose registration threshold with expanded dose registration region from 30 Gy to 35 Gy [28]. According to the performed optical spectrophotometry measurements, VIPARnd provides linear dose response in the region between 3 Gy and 20 Gy (Fig. 2).

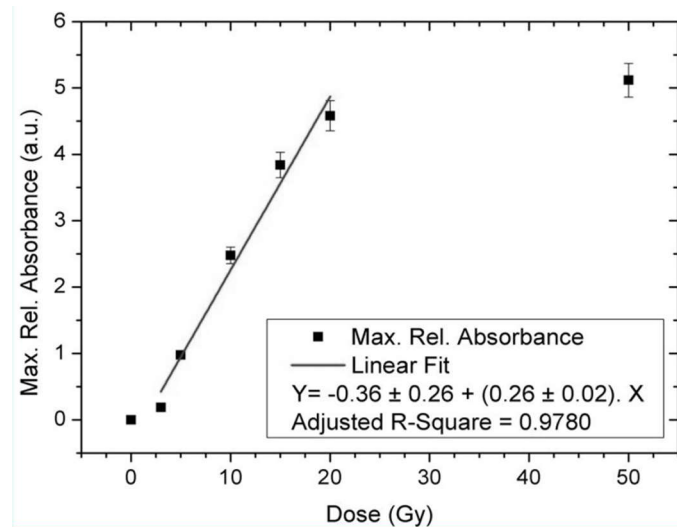


Fig. 2. Relative maximum absorbance vs. the dose of VIPARnd [27]

VIPARnd preparation differs from nPAG, but it is still available at room conditions. It remains suitable for the application for around 4 weeks, but demonstrates better energy absorption ability few days after the preparation [27]. Moreover, the time span between the irradiation and evaluation of these gels does not play any role, since the dosimetric data in irradiated gels remain unchanged for at least two weeks after the irradiation. The repeatability and reproducibility of gel response were 0.5% and 5%, respectively [26].

PAG type gels. Normoxic nPAG gels consist of acrylamide (Aam), *N,N'* methylene bisacrylamide (Bis), gelatin (gelatin (300 Bloom, type A) hydroxymethyl phosphonium chloride (THPC) as oxygen scavenger, and pure water.

The concentrations of gel components may slightly vary when applied for different dosimetry purposes, as it is indicated in Table 2. Moreover, some other additives may be included in the basic recipe.

Table 2. Possible compositions of nPAG dose gels

Acrylamide, %	Bis acrylamide, %	Gelatin, %	Deionized water, %	THPC, mM	Reference source
3	3	5	89	4.65	[64]
3	3	5	89	10	[65]
3	3	5	89	10	[95]
3	3	8	83	3	[96]
3	3	5	89	2–100	[97]
6		3, 6, 9		5	[98]

nPAG dose gels are characterized by lower dose sensitivity, are almost independent from the dose rate and temperature. These properties indicate potential for the nPAG gel application for dosimetry purposes. However, it should be noted that nPAG gels are sensitive to the oxygen exposure.

Different polymer structures can be created in the gels upon irradiation (Fig. 3). Due to relative high amount of crosslinker in the composition of PAG gel, the created fragments of the polyacrylamide network can be seen as microgel particles encapsulated in the gelatin matrix. The size of the polymer structures varies with the dose. As a result, the polymer chain density in the irradiated PAG gels can be expected to be far from the uniform, indicating large heterogeneities in highly crosslinked nPAG gels.

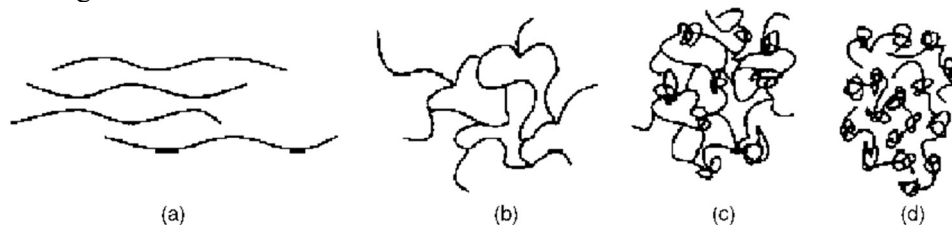


Fig. 3. Different polymer structures after irradiation: (a) initial gel solely composed of monomer (AAm); (b) gel composed of low initial Bis fraction; (c) gel composed of high initial Bis fraction; (d) initial gel composed solely of crosslinker (Bis) [17]

If the initial gel consists of Aam monomer only, long, linear chains are formed with no crosslinks. If the gel contains low initial crosslinker Bis fraction, the predominant gel formation is an ordered, crosslinked network. If the gel contains a high initial crosslinker fraction, it begins to form a larger number of knots due to the irradiation. If the initial gel is composed solely of crosslinker, the predominant structures are knots, loops, and doublets, which together form beads.

2.2.2. The influence of gelatin concentration in dose gels

Gelatin is a widely used gelling agent. Gelatin chains are water-soluble; they dissolve readily in the water heated to $\sim > 35$ °C. Upon cooling, the chains form coils and undergo a helix. Gelatin provides a physical matrix to support the polymerized network structure [29–31] and create a stable gel upon cooling due to the formation of triple helices, stabilized by the intermolecular hydrogen bonds. The heating of the gel results in the reverse process of gel liquefaction (Fig. 4).

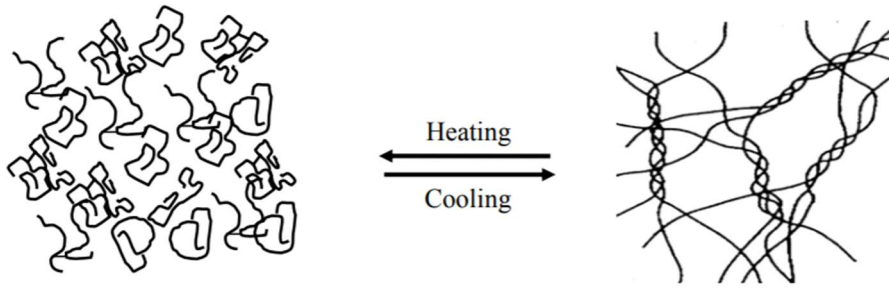


Fig. 4. Principal scheme of heating and cooling effect in the gel [29]

Gelatin concentration in the gel solution could affect the size and number of the polymerized gel segments, thus influencing the dose sensitivity. Gelatin concentration could vary for different types of polymer gels, but should ensure the mechanical stability of the gel and stiffness, which are based on three dimensional polymer network formation in gelatin water solution after the irradiation. The role of gelatin in MRI visualization relates to the determination of the transverse relaxation rate R_2 . The gels with a lower gelatin concentration will receive less intense, but larger range of R_2 values (Fig. 5).

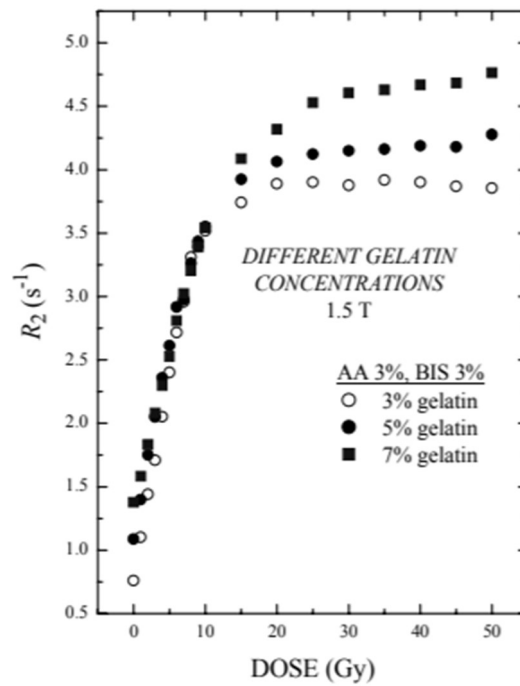


Fig. 5. Dose sensitivity dependence on the gelatin concentration [32]

The polymer formation rate is directly dependent on the amount of gelatin in the examined dose gel. The polymerization rate decreases with the increased amount of gelatin in the gel. The polymerization rate is influenced by the gelatin network morphology as well, the formation of which is temperature dependent. It is known that gelatin network becomes weaker when the temperature of the gel solution is increasing. This feature was used when removing the polymerized gel part from the gel.

2.2.3. The role of the oxygen scavenger in gels

Tetrakis hydroxymethyl phosphonium chloride (THPC) is an oxygen scavenger, which is designated to remove reactive oxygen from the gel solution. THPC contributes to the kinetic changes of the subsequent reactions at the end of gel irradiation. THPC concentration in gel influences the dose response, especially in the regions of high dose gradients. These findings are summarized in a simple model that is disclosing the action of the oxygen scavenger in the irradiated gel, which allows the estimation of the dose and dose gradient dependent polymerization kinetic changes and dose response in the irradiated gels [33].

It should be noted that the application of a certain amount of oxygen scavenger does not secure the recombination of all oxygen, and the problem of minor oxygen leakage from the already prepared gel samples leading to the post polymerization of dose gels still remains [34].

THPC concentration in the gel influences the rate of oxygen scavenging and the dose response of the polymerized nPAG gel (Fig. 6).

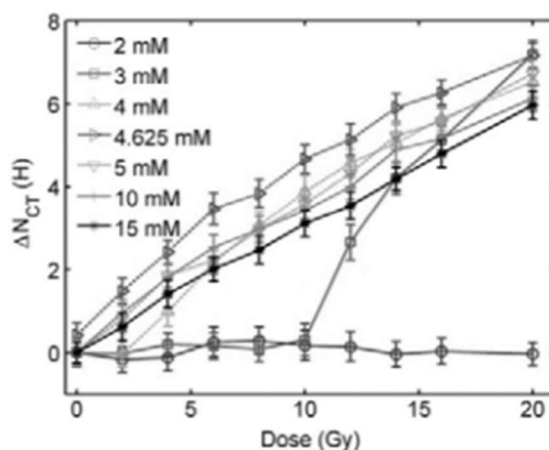


Fig. 6. The effect of THPC concentration on the nPAG polymer gel dose response [35]



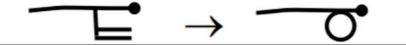

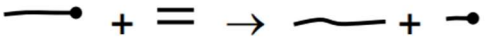
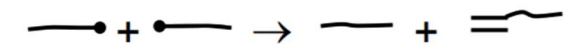
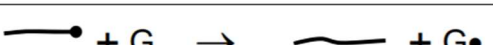
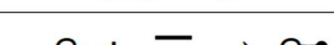
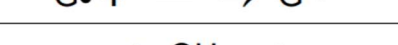
As it can be seen from Fig. 6, THPC concentration should vary within a small range. However, the too low concentration indicates that not all oxygen is scavenged from the gel, which turns into the weak (flat) dose response. Higher THPC quantities will not provide any additive effect on the polymerization, since with the increased crosslinking of the gel, the dose response appears to weaken. In one of the studies

[35], the maximum dose response was achieved with the exact THPC concentration (4.65 mM).

2.3. Polymerization in nPAG and VIPAR gels

During the water radiolysis, several types of free radicals are generated, which can react with vinyl group monomer molecules. One of the most commonly used dose gels component *N,N*'methylene bisacrylamide (Bis) has two vinyl groups. Bis molecule is propagating reaction with one of the vinyl groups; thus, the second is left for the next reaction (cyclization or cross-linking). Polymeric radicals as well can react with gelatin and leave fewer radicals to initiate the polymerization. The reaction rate of gelatin radicals with monomers depends on the type of the dose gel. The reactions in polyacrylamide gel (PAG) and *N*-isopropylacrylamide (NIPAM) dosimeters are demonstrated in Table 3.

Table 3. Reactions of polymer radicals in PAG and NIPAM dosimeters [35]

a) Generation of primary radicals by radiolysis	$H_2O + Radiation \rightarrow H_2, H_2O_2, e_{aq}^-, H^\bullet, OH^\bullet$
b) Propagation with monomer	
c) Propagation with crosslinker	
d) Primary cyclization	
e) Crosslinking	
f) Chain transfer to monomer	
g) Termination	
h) Chain transfer to gelatin	
i) Propagation of gelatin-centred radicals	
j) Termination with primary radicals	

For *N*-vinylpyrrolidone based (VIPARnd) dose gels, the polymerization of free radicals is a mandatory synthesis to obtain vinyl polymers.

The polymerization scheme of vinyl group polymers is shown in Fig. 7.

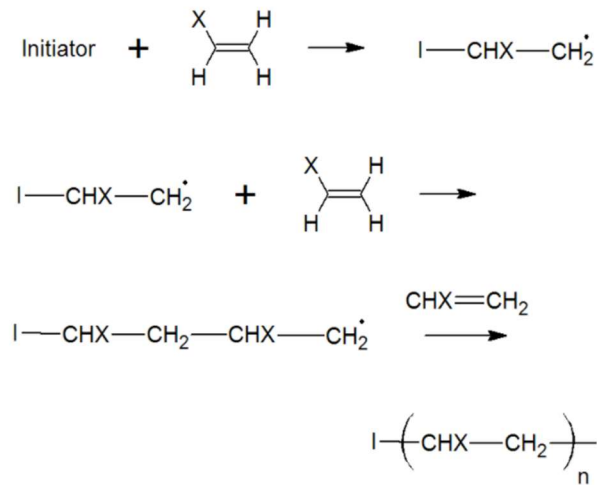


Fig. 7. Principal polymerization scheme of vinyl group polymers [36]

The molecular fragments with unpaired electrons, called free radical initiators, are created due to the irradiation.

Through the reaction with monomers, they create new radicals, thus starting the chain growth polymerization [36].

2.4. The impact of irradiation parameters on dose gel properties

The dose response and dose sensitivity of irradiated polymer gels depend on several factors, such as energy, dose rate and temperature independence, spatial integrity, and temporal stability. Ideal 3D dosimeters should demonstrate high spatial resolution and be independent from dose rate. However, the spatial resolution is limited by the voxel size of the imaging modality and typically is around 1 mm^3 [24]. In several types of polymer gels, such as PAG group, metacrylic acid based group, or proprietary PAG dosimeters made of a mixture of acrylic monomers (BANG-3), the dose registration sensitivity is decreasing with the increasing dose rate [37].

Monomer polymerization rate and cross-relaxation efficiency affect the dose sensitivity. It has been found that the hydroxyl group is more efficient in the magnetization exchange, compared to the amino-group. However, Aam monomer's reaction rate in PAG is much higher than in acrylic acid based dose gel. This compensates the processes in both gels, making the dose sensitivity of both monomers very similar. However, the same dose sensitivity expands over the larger dose range for the AAm based gels as compared to the acrylic acid based gels [38].

It has been found that the dose sensitivity linked to the transverse relaxation rate (R2) of MRI is decreasing with the increased Bis concentration, presumably because crosslinking is not required to induce precipitation. Bis is less reactive than methacrylic acid; thus, fewer polymer chains are formed per Gy of the absorbed radiation [35].

Jirasek and Duzneli [39] investigated the different ratios of monomer AAm or crosslinker Bis in dose gel compositions and found that in order to achieve reasonable dose sensitivity, the amount of Bis in gel's composition should not exceed 3 wt%.

According to Maryanski et al. [40], the optimal sensitivity of PAG dosimeter can be achieved by having equal amounts of AAm and Bis. Nevertheless, PAG dosimeter with higher concentration of Bis in gel's composition is more sensitive. Since cross-linker *N,N'*methylene bisacrylamide is used in almost all dose gel formulations, this finding is of great importance, when developing new gels.

In addition, Jirasek and Duzneli [39], using FTIR analysis, have found almost two times larger Bis consumption rate, comparing with AAm in nPAG gels, which explained the differences in polymerized gel viscosity and polymerized part shape that is related to the absorbed dose.

The calculated polymerization yield (G) of the gel was 5×10^5 [29] with a contributing factors of 2.54×10^5 and 2.54×10^5 for AAm and Bis, respectively. The polymer chain size and density in the irradiated PAG dose gels are responsible for the transparency of polymer. Since the size and density of formed polymer chains are directly linked to the absorbed dose, the whole polymerization process can be expressed as a function of absorbed dose.

It should be noted that the dose response must be stable during the entire scanning time and not vary too much with a dose rate, at which the irradiation was performed [41].

The average dose response of irradiated polymer gels is ~ 1.0 Gy for the doses > 20 Gy and ~ 0.1 Gy for doses < 5 Gy and is highly affected by the capabilities of the read-out system [42]. The capability to differentiate between two absorbed doses with confidence limit p is dose resolution (Eq. 4) [23]:

$$D_{\Delta}^p = k_p \sqrt{2\sigma_D}; \quad (4)$$

where D_{Δ}^p is dose resolution, σ_D is the sample standard deviation, k_p is the factor of coverage.

The dose resolution depends on the beam type, absorbed dose, dose rate, and gel type. It has been shown [41] that for *N*-vinylpyrrolidone based gels, 0.45 Gy dose resolution was achieved when the gel was irradiated up to 20 Gy and 0.97 Gy dose resolution for up to 56 Gy irradiated dose gel.

It is higher within the dose: for example, 0.45 Gy/ irradiated 20 Gy and 0.97 Gy/56 Gy for *N*-vinylpyrrolidone-based polymer gels, respectively [41]. It should be noted that the dose resolution does not include stochastic variations in the chemical concentrations in dose delivery or the calibration procedure [17].

2.4.1. The impact of the radiation beam type on dose gel properties

The irradiation of polymers with electron beam at high dose rates is responsible for the generation of higher number of radicals per unit time as compared to the irradiation at low dose rates. If the time for the diffusion of electrons is insufficient, they recombine without any effect. Gamma irradiation is usually characterized as low dose rate irradiation. It is responsible for a weak generation of radicals that experience

difficulties with the recombination but are tending to diffuse and participate in polymer cross-linking and scission processes [43].

2.4.2. Dose rate effect

According to other studies [44–46], the dose response of polymer gels depends on the dose rate and may reduce its accuracy.

The dose rate in external radiotherapy varies in the range of 100–600 monitor units (MU/min), and typically, 1 MU corresponds to 1 cGy or 0.01 Gy of the delivered dose. The treatment time depends on the calculated MU in TPS and selected dose rate. If the dose rate is increased, the equipment could fail to terminate the beam and a larger overdose could be delivered before the automatic beam off. If the dose rate is decreased, the radiotherapy unit could end the treatment time before the total set dose is delivered to the target [47]. Both situations may cause health problems for the treated patient, since the dose rate is one of the most important factors, which determines the biological effect of realized dose, using the photon beams (X-rays, gamma rays) (Fig. 8).

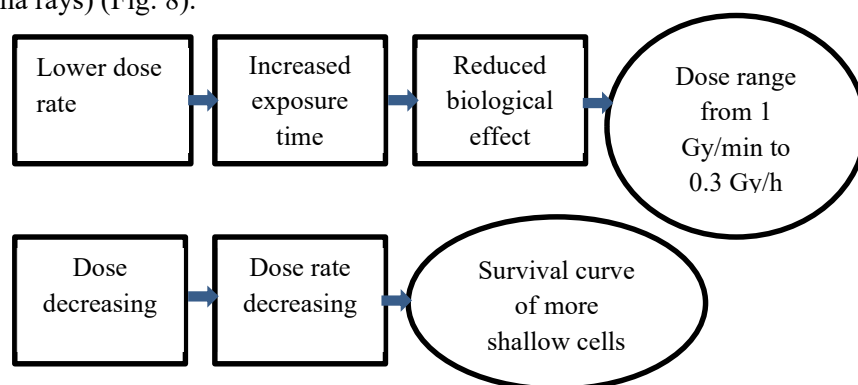


Fig. 8. Dose rate dependence on the dose principal scheme [48, 49]

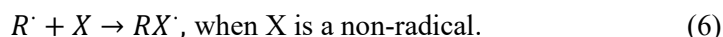
In some cases, the dose rate lowering leads to the enhancing of cell killing effect and indicates inverse dose rate effect [49].

The dose sensitivity of acrylamide and THPC based gel dosimeters demonstrate a small dependency on the dose rate. For example, the dose-rate dependence on the dose sensitivity for nPAG dose gels at the dose rate of 600 cGymin^{-1} amounts to 5% only, as compared to the dose sensitivity at a dose rate of 400 cGy min^{-1} [50].

The dose response of *N*-vinylpyrrolidone based polymer gels are less influenced by the dose rate; however, the dose gels of this type need some dose sensitivity increasing additives.

There is a linear dependence between the high dose rates and low polymer concentration combination, especially when electron beams or intensity modulated photon irradiation is used. In this case, hundreds of radicals are generated on each chain at once, thus reducing the intermolecular recombination. On the contrary, the low dose rate with high polymer concentration indicates gel formation.

The effect of dose rate was described by S. Alex et al. [51]. It has been noted that the importance of radical plus non-radical reactions decreases when the dose rate increases (Eq. 5, 6):



C. Dispenza et al. [80] analyzed the radiation-induced polymerization in hydrogels and found that within the higher dose rate, the initiating radicals concentration is higher as well. This indicates a shorter incubation period and faster particle nucleation, which increases the rate of polymerization (Fig. 9).

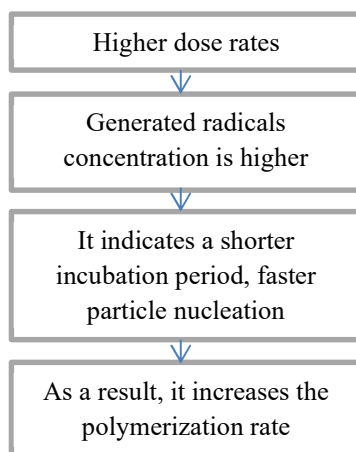


Fig. 9. Dose and polymerization rate dependency scheme

However, the dose rate has an effect on the generated numbers of polymer particles and particle size. Higher dose rate generates higher radical concentration and higher particle number, but the size of polymer particles is lower.

For intermolecular crosslinking and obtaining nanogels with tailored molecular weight, mainly continuous irradiation at low dose rate is used. Nanogels shrink and intramolecular crosslinking occurs when irradiating polymer gels with low dose, but keeping the high dose rate [52].

2.4.3. The impact of temperature on dose gel properties

The temperature differences during the gel fabrication and small variations of separate chemical components may influence the irradiation response. However, the polymerized gels must be temperature independent during the irradiation and visualization procedures. It is recommended that during the irradiation, the range of gel temperatures would not exceed 2 °C and 1–2 °C during the dose visualization procedure.

The temperature differences during the fabrication and post-manufacturing of dose gels may affect the dosimetric accuracy of the gels. It has been found [35] that the temperature changes by 1 °C in the irradiated gels during the MRI scanning have contributed by less than 1% to the uncertainty of dose response evaluation. It was

shown [17] that acrylamide based (nPAG) dose gels are less temperature dependent than many other dose gels.

nPAG gels are less susceptible (7% variation at 10 Gy) to the gel cooling rates during the solidification process as compared with nMAG gels (67% at 10 Gy). The polymer gel cooling rates are influenced by their surrounding atmosphere and the amount of the gel.

Various physical and chemical properties of the irradiated gels may be indicators of induced radiation and absorbed dose that is related to the polymerization of gels. Since the absorbed dose in the irradiated gels may be assessed by using different read-out/visualization methods, the estimated dosimetric sensitivity of gels is dependent on the dose evaluation methods as well. It should be noted that the random errors, such as phantom calibration, positioning errors, temperature, energy or dose rate-dependent response, polymer homogeneity, and equivalency with human tissue, may have an impact on the dosimetric sensitivity of dose gels and evaluated dose values [39].

2.5. Reading-out techniques for the irradiated dose gels

Polymerized gel based dosimeters can be scanned by different techniques, but a special resolution of distributed doses depends on the selected read-out method [2].

S. Sheib and W. Vogelsanger noted that the optimized MRI protocols allow achieving 1 mm spatial and up to 5% dose resolutions by using MAGIC gel as a dosimetry tool [53]. Y. Roed et al. [54] have shown that the polymer gels as well could be used with new generation MR, guided linac for volumetric dosimetry and demonstrate promising results with more than 85% conformity. P. Mann, N. Saito et al. [55] performed 4D dose calculations by combining 3D polymer gel dosimetry (PAGAT) and Calypso tracking system. They have found that 4D dose calculation with polymer gel is very accurate for dynamic targets and is a promising technique in adaptive radiation therapy [55]. Several types of electron microscopies, Raman spectroscopy, different optical methods, computer tomography, etc., could be used for ionizing radiation-sensitive dose gel scanning.

2.5.1. MRI read-out method

MRI tool is the most suitable read-out method for the irradiated polymer dose gels [56–58] and provides several possibilities for dose assessment.

The principle of nuclear magnetic resonance imaging is based on strong magnetic field interactions with charged particles (especially with hydrogen nuclei/protons). The hydrogen nuclei affected by strong magnetic field align themselves within the magnetic field direction. This process is called Larmor precession, and the related Larmor frequency is directly proportional to the magnetic field strength. The principal scheme of Larmor precession is given below (Fig. 10).

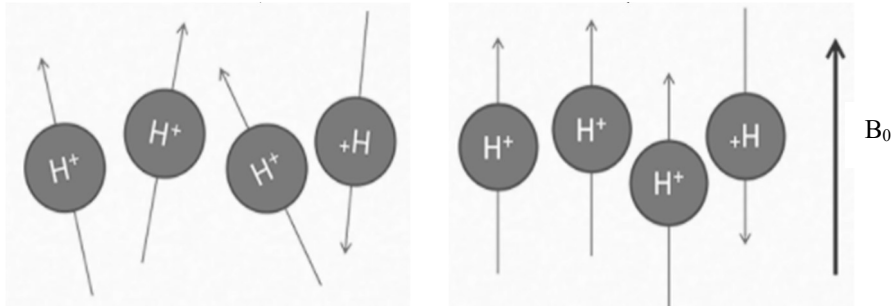


Fig. 10. a) Random alignment of hydrogen nuclei in the material (tissue) and b) hydrogen nuclei behavior in a strong magnetic field, according to the magnetic field direction (B_0) [59]

Larmor frequency could be calculated by (Eq. 7), where γ is gyromagnetic ratio and B_0 is magnetic field strength [60]:

$$\omega_0 = \gamma B_0 \quad (7)$$

For protons (hydrogen nuclei), the gyromagnetic ratio is 42.6 MHz/T or 42.6 MHz/T \times 1.5T = 63.9 MHz, if the MR unit is 1.5 T strength. The corresponding Larmor frequency depends on the magnetic field strength.

In order to register and visualize images, the external radio frequency pulse (RF) is applied. RF is equal to Larmor frequency and introduces a magnetic moment of hydrogen nuclei (M) (Fig. 11). The generated NMR signal, which has been produced by the RF pulse induced magnetic moment, can be detected by special coils.

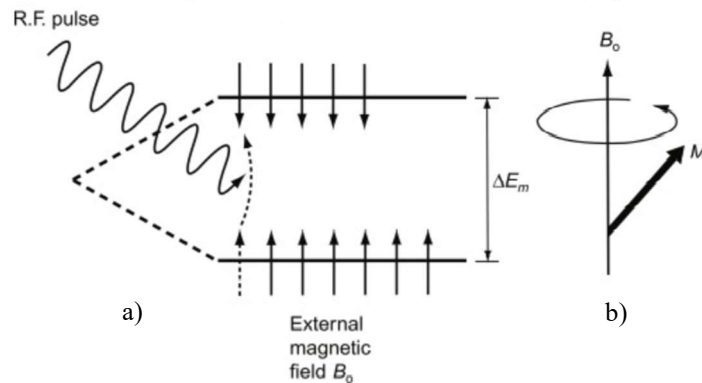


Fig. 11. a) External RF pulse, b) displaced magnetic moment (vector M) [60]

When the RF pulse is switched off or decreased exponentially in time, the nuclei return to their normal state via two different mechanisms described as:

- T1 – spin-lattice relaxation time (recovery);
- T2 – spin-spin relaxation time (decay).

T1 signal is described as a time, which requires recovering for M_z 63% of its maximum value. T2 is a time for transverse magnetization to decay to 37% of its value or lose 63% of maximum signal.

T1 depends on the surrounding tissue and structure density. T2 is related to the magnetic field strength.

Within the external RF pulse application, all nuclei vectors are turning to 180 degrees, and it takes time. The same time interval is needed to return to the primary position. The time between phases termed echo and the time at which echo is produced (how often RF pulse turning on/off) is called echo time (TE). The repetition time (TR) is the time between 90° external RF pulses (Fig. 12).

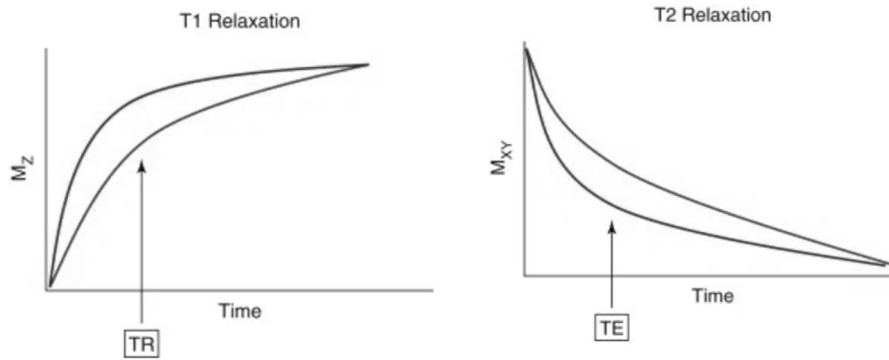


Fig. 12. Illustration for TE and TR parameters in T1 and T2 weighted images [60]

The nuclear magnetic resonance related images are displayed in the field of view (FOV), which consists of fixed number voxels.

Moreover, other parameters are being used when performing the analysis of images. One of them is an inverse to the relaxation time parameter, i.e., relaxation rate R (Eq. 8), which is used for graphical visualization [59]:

$$R1 = 1/T1; R2 = 1/T2 \quad (8)$$

Water protons in the polymer gel system exist in four environments: pour water, in water hydrating monomer, in gelatin of porcine skin, and in polymer itself. The spin relaxation is almost equal in hydrating monomer and pour water, but molecular motions in hydrating monomer are faster because of smaller molecular size. Moreover, the water protons are joining larger molecules. Otherwise, gelatin and polymer motion are slow, and it forms the conditions to increase the relaxation rate, which can be converted to the absorbed dose by using R2 sequence and calibration curve [38].

The formed polymers are highly restricted in their mobility within the gel matrix. The mobility is affected by the size of the polymer molecules and the total amount of polymer and is related to the MRI relaxation time T2. Actually, both R1 and R2 relaxation rates can be used, but spin-spin relaxation rate R2 is more effective because of reducing of bound water molecules mobility after the irradiation [39].

The spin-spin relaxation rate expressed by formula $R_2 = 1/T_2$ can be measured by using the optimized MRI echo sequences (TE) and converted to T2 maps for the evaluation of dose distribution. This can be done after the dose gel calibration with different absorbed doses [55].

R2 sequence dose sensitivity can be measured by the following equation 9:

$$R_2 \text{ dose sensitivity} = \frac{\Delta R_2}{\Delta D}; \quad (9)$$

where ΔR_2 are R2 changes and ΔD are dose changes.

R2 of polymerized gels may decrease with the increased temperature. R2 values depend on the echo time: more accurate R2 values will be received with increased echo time; however, a longer echo time can affect the signal intensity, and higher noise could be registered, which may lead to significant R2 evaluation errors [61].

In order to visualize MRI read-out results, several quantitative mapping methods, such as gradient measurement, fat/water separation, B0, B1, T1, T2, T* mappings are used.

The most important parameters to evaluate the MRI image quality are signal to noise ratio, spatial resolution, and tissue contrast. These parameters are directly interdependent and can be hardly improved. The reduction of voxel size or precise tissue contrast indicates the SNR decrease and limits resolution of $> \approx 1 \text{ mm}^3$ (1 μl) [61].

Gradient measurement calculation can be approached within the excitation of a thin slice in position x by following equations (10–11):

$$d\varphi/dt = \gamma G(t)x, \quad (10)$$

$$\varphi = \gamma \int_0^t G(t)x dt = 2\pi k_x t x; \quad (11)$$

where G is gradient, k – space trajectory (scaled, unwrapped etc.), x – thickness of the thin slice; γ – gyromagnetic ratio [63].

When performing gradient measurements, it is possible to separate effects, such as Eddy currents, off-resonance, concomitant gradient terms, and get better resolution $< \approx 1 \text{ mm}^3$. The advantage of this recalculation method is that no additional scanning is required, just few more TE pulse sequences [62].

Fat/water separation could be applied by analyzing MRI views voxel by voxel in the selected computer system. This method requires high precision during the scanning process to get acceptable results after the calculations. Fat/water separation model is phase-based. The fat signal is in 6 peaks different from the water: at -244.3 , -221.7 , at -244.3 , -221.7 , calculations. Fat/water separation model is $\text{phae}^{-i\pi 0.181}$, 64.66 , $9.67e^{i\pi 0.046}$, $2.26e^{-i\pi 0.567}$, $2.22e^{-i\pi 0.244}$, $8.83e^{-i\pi 0.089}$. Water and fat have different R2 values: $W=42\text{s}^{-1}$ for water and $F=54\text{s}^{-1}$ for fat, respectively. The single-peak or multi-peak fat modeling is applicable for the further analysis [64].

Any parameter (x, c) of MR imaging can be recalled by using function $s=f(x,c)$ (Fig. 13).

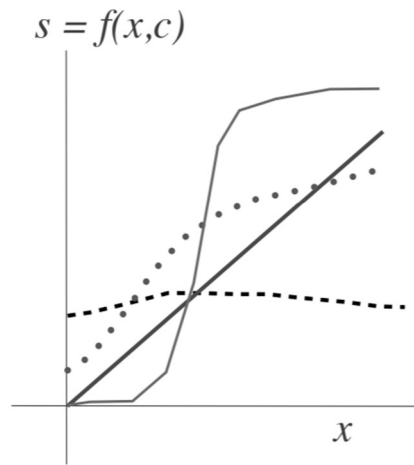


Fig. 13. The parameter measurement function of MRI, where x, c – any parameters for measure [63]

Different techniques can be suggested for the evaluation of scanned MRI views, applying different echo sequences. Several techniques (B0, B1, T1, T2, T* mappings) might be used to visualize the dose distribution in the irradiated gel. An example of dose mapping is provided in Fig. 14.

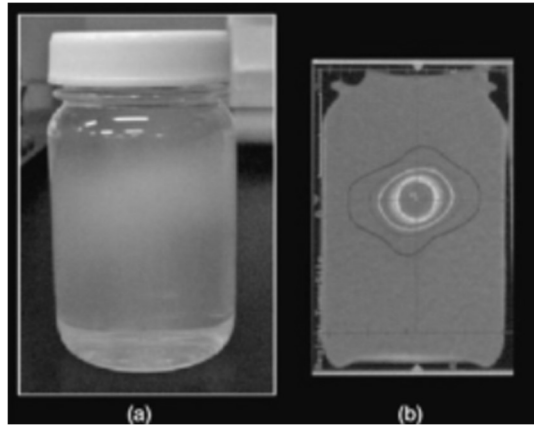


Fig. 14. An example of polymer gel dose mapping, with a) irradiated dose gel and b) dose map in TPS [65]

R2 maps of T2 weighted images can be calculated from signal pixel intensities (point by point) and with the application of two-point method. This method is suitable when two different echo times (TE) for the same sample are applied (Eq. 12).

$$R2 = \frac{\ln S1 - \ln S2}{TE2 - TE1}; \quad (12)$$

where TE is transverse relaxation rate, R2 – calculated transfer relaxation rate and S1, S2 – measured signal (pixel) intensities.

Conversion of R2 maps to dose maps is realized using Equation 13:

$$R2 = \alpha D + R_0; \quad (13)$$

where α is the slope of R2-dose curve, R_0 is the background of R2; R2 is the relaxation rate of the irradiated gel [66, 67].

For more precise dosimetry, T2 calculation for each pixel of the image is required. R2 can be obtained by using the maximum-likelihood estimation from pixel intensities of the reference images. This method is based on the standard deviation calculations. If this parameter is unknown, the maximum likelihood must be estimated by minimizing X^2 , which is performed by applying special algorithms. Direct calculation of R2 value is possible when standard deviations of the reference image are known (Eq. 14):

$$R2 = \frac{S_x S_y - S_{xy}}{S_{xx} - S_x^2}; \quad (14)$$

where S_x, S_{xy}, S_y, S_{xx} are calculated standard deviations [68].

It shall be noted that some methods allowing for compensation of MRI artifacts are used during the read-out procedure [1].

It is as well important that such factors as speed, costs, spatial resolution, precision, and accuracy are affecting the final quality of read-out result [69]. Thus, it is recommended that the precision errors in polymer gel dosimetry should not exceed 5% limit [2].

2.5.2. Optical read-out method

The optical dose gel evaluation method is highly spatially resolved and could measure small physical sizes; however, very often, the inhomogeneities (artifacts) in irradiated gels are found, which require additional refractive index matching.

Depending on the aim of the investigation, UV-VIS spectroscopy or optical CT methods can be used. The main difference between the two methods are that in UV-VIS spectroscopy, 2D dose maps can be easily extracted from the irradiated dose gels, and when using the Optical CT method, 3D images can be reconstructed. Both types of measurements, i.e., optical absorbance and transmittance measurements, are suitable for the read-out of irradiated gels, and the obtained data (optical density maps) can be converted to dose maps in irradiated gels. The measurement uncertainties by using this method are < 1%. Optical density maps can be created by analyzing the pixel values of the obtained optical image, using Eq. 15:

$$OD = \alpha \log\left(\frac{I_0(i,j)}{I(i,j)}\right); \quad (15)$$

where OD – optical density; α – calibration factor; I_0 and I are intensities of each i, j pixel of the image (pixel values) before and after the irradiation.

It is as well possible to obtain dose maps and dose response from the absorbance values measured using UV-VIS spectrophotometry; however, proper wavelength must be selected. For commonly used dose gels, this wavelength interval is between

500–680 nm [70]. The wavelength selection depends on the highest sensitivity with saturation value and is different for each dose gel type.

The calculations are performed using optical spectral data (Eq. 16):

$$\Delta A = A_i - A_0 = mD + n ; \quad (16)$$

where ΔA is absorbance difference; A_i and A_0 – optical absorbance at the selected wavelength in irradiated and unirradiated sample, respectively; D – dose; m – slope of the A-D curve; n – dose threshold in the material [71].

Often, more complicated optical systems are used to get information from point and reconstruct images, for example, optical computed tomography (OCT) scanners [72–3]. The main principle of the optical CT system is the same as in X-ray CT and is based on the photon attenuation phenomena in the investigated objects. However, it should be noticed that with the increasing dose, the polymerization degree in irradiated gels increases as well, thus leading to the increased optical attenuation and making data acquisition impossible.

Optical imaging systems are widely used for the read-out of the irradiated gels because of several significant advantages (Table 4).

Table 4. Advantages and disadvantages of the optical read-out systems [73, 74]

Optical imaging system	
Advantages	Disadvantages
Portable scanning system	Limited dose range of gels (0–10 Gy)
Cheap	Signal losses at the vial edges
Low image distortion	Lower doses may lead to lower contrast
Lower noise level	Limited size of the experimental samples

2.5.3. Raman spectroscopy

Raman spectroscopy is a technique based on the light scattering and different molecular vibrations induced by the light photons. The examined samples are irradiated with a monochromatic laser beam, which interacts with sample molecules. Since different molecules are scattering light (energy) at different frequencies, the Raman spectrum of the investigated material is created. Raman spectrum represents the intensity of scattered radiation as a function of the energy difference between the incident and scattered photons. The units of energy are conveniently plotted as wave numbers or wavelength⁻¹ (sometimes it is called a Raman shift) [75]. An example of the energy level diagram of Raman spectrum is illustrated in Fig. 15.

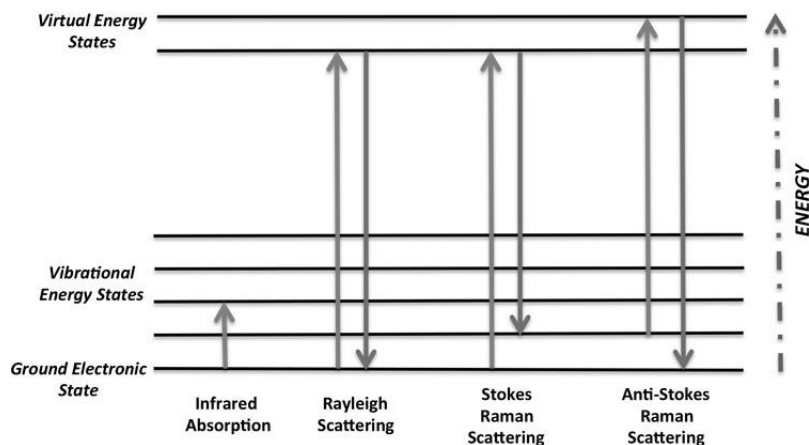


Fig. 15. Energy level diagram of Raman spectroscopy [76]

The light absorption in infrared region and following transition from one energy state to another is an internal feature of a particular molecule [76]. Raman scattering strongly depends on a wavelength of incident radiation [77]. Depending on the energy, there are several possibilities for light scattering from molecular structure. The frequency of Rayleigh scattering is equal to the frequency of incident radiation and constitutes. Stokes Raman scattering is the frequency of incident radiation, which is higher than the scattered radiation frequency. Anti-Stokes Raman scattering appears when scattered radiation frequency is lower than the incident radiation frequency.

Raman spectroscopy is often used to detect radiation-induced changes in polymer gel structure. In the gel polymerization process, the most important role is dedicated to highly polarizable C–C and C=C bonds in monomer and crosslinking agent of the dose gel. The Raman shifts that correspond to the vibrational modes of C=C bonds in polymerized and C=O bonds in non-polymerized materials are of high importance as well [71]. Several most important Raman shifts (intensity peaks) for commonly used dose gels are provided in the Table 5.

Table 5. Raman shifts of different photon beam irradiated gels: methacrylic acid based (nMAG), polyacrylamide based (nPAG), N-Isopropylacrylamide based (NIPAM), polyacrylic acid based (PAA), polyhydroxyethylmethacrylate (PHEMAG) based dose gels

	Raman shift 1, cm^{-1}	Raman shift 2, cm^{-1}	Raman shift 3, cm^{-1}	Source
nMAG	809	1687	2937	[64]
nPAG	1253	1280	-	[65]
nPAG	1256	1285	-	[63]
NIPAM	815	1025	2353	[66]
NIPAM	815	1025	2353	[67]

PAA	629	1406	1714	[68]
PHEMAG	1635	1640	-	[69]

Moreover, the full width at half maximum (FWHM) method could be applied for getting additional information about the accuracy of the performed Raman spectroscopy measurements of the irradiated polymer gels. The FWHM for the indicated Raman peak positions can be expressed as in Eq. 17 [75]:

$$FWMH = 2\sqrt{2\ln 2} \sigma \approx 2.355\sigma; \quad (17)$$

where σ is the standard deviation. Depending on the focus of the laser in Raman spectroscopy system, the dose gels demonstrate potentially higher spatial resolution (0.75 mm), compared to the MRI techniques, which is especially important for specific brachytherapy procedures [78].

2.5.4. Microscopy methods for the read-out of dose gels

Various types of microscopes could be applied for dose gel read-out, for example, visible light microscopes, short-wavelength fluorescence, phase contrast (optical methods), electron microscopes. In most studies related to the investigation of polymer gels, the scanning electron microscopy (SEM) or transmission electron microscopy (TEM) are used [79]. The scanning principle is based on the materials surface topography in cooperation with image analysis. For the measurements of texture analysis, the parameters, such as sample homogeneity, entropy, energy, and contrast, are important. Cheng-Ting Shih et al. [80] applied SEM for microscale dose response evaluation in the irradiated polymer gels. The modified NIPAM gels were prepared, irradiated with 5–20 Gy doses with 5 Gy step, and frozen. The dried samples were sliced and prepared for scanning. The average deviation of the SEM evaluated dose from the TPS planned dose was 20.05%.

2.6. Uncertainties during the read-out of irradiated dose gels

The structures of irradiated polymer gels can be read-out/evaluated by using MRI, optical-CT and UV_VIS spectroscopy, Raman spectroscopy, x-ray CT, ultrasound, or other imaging techniques.

Systematic (type B) and random (type A) errors that are related to the scanning parameters, such as voxel size, dose-related imaging artifacts, scanning temperature, spatial inaccuracy, may affect the imaging results and must be kept under control [37, 39, 40], since they are influencing the accuracy and precision of the dose evaluation (Fig. 16).

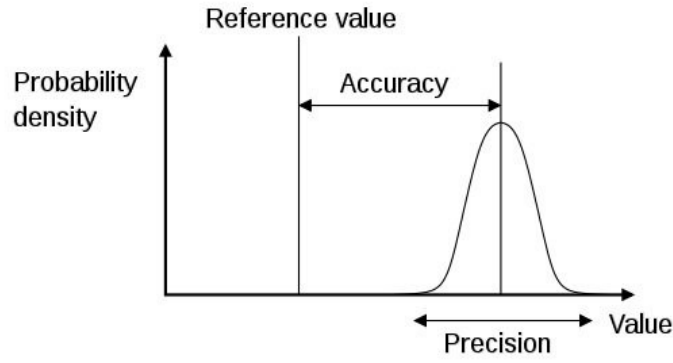


Fig. 16. The mathematical definition of accuracy and precision

For example, the maximal overall uncertainty in absolute dose measurements should not exceed 5% within the minimum voxel size of 5 mm³ during the MRI read-out [73]. This accuracy may be achieved by very careful performing the read-out of independently calibrated polymer gel based dosimetry system [74].

The accuracy of the dose that has been measured by a detector depends on the accuracy of the original signal that has been recorded in the 3D dosimeter medium and the precision of the dose-response data or the calibration data, which are used to convert the raw signal data to the absorbed dose. Considering this information, 3D polymer gel dosimeter can be used for absolute dose measurements [2].

If the absolute dose D can be expressed as (Eq. 18):

$$D = aX^2 + bX + c \quad (18)$$

Then, the uncertainty of D can be given as the function of uncertainties of raw data X and three calibration related coefficients: a , b , and c (Eq. 19):

$$\delta D = \{(X^2\delta a)^2 + (X\delta b)^2 + (\delta c)^2 + [(2aX + b)\delta X]^2\}^{1/2} \quad (19)$$

If the calibration equation is constructed correctly, i.e., $\delta a = \delta b = \delta c = 0$, the equation 14 can be modified as follows (Eq. 20):

$$\delta D/D = (X/D) \times (dD/dX) (\delta X/X) = \{(2aX + b)X/D\} \times (\delta X/X) \quad (20)$$

It could be seen that the relative uncertainty of dose is proportional to the relative uncertainty of X , which means that X is directly linked to the dose uncertainty: smaller X value corresponds to the smaller possible dose uncertainties.

According to A. Venning [37], the polymer gel dosimeters have two types of instability: spatial instability, which is related to the diffusion of monomers from high to low dose regions, and temporal instability. Temporal instability may affect R2 background or R2 dose response curve and indicate it as increasing. In order to reduce this type of instability, it is recommended to perform calibration and experimental measurements with the gels from the same batch.

Baldock et al. [38] performed a very detailed comparison between the uncertainties in A and B groups for polymer gel dosimeters and found that within the

group A uncertainties, the chemical composition of gels may have less than 2% influence on the gel dosimeter accuracy after the irradiation. Moreover, 1 mm gel phantom positioning failure or increasing the imaging noise during the MRI scanning may lead to the enhancement of the uncertainties. It was shown, that the most significant uncertainties that are occurring during CT scanning are from the range of 2 to 8% and are related to the standard deviation of CT numbers.

In the second group of B uncertainties, it has been found that non-uniformity correction during MRI may affect the accuracy up to 3% and image processing during CT, up to 5%.

Kesthar et al. [61] has investigated whether MRI evaluation based polymer gels can be used for dosimetry purposes in radiotherapy if the dose mapping uncertainties are properly estimated. The investigation of MAGIC gels that are irradiated with high energy photons has shown significant (18.96%) mismatching of the experimental and theoretical results for low doses (1 Gy), which was reduced to 4.17% for higher doses (10 Gy). The performed assessment of the results using the homemade MATLAB programme indicated two main uncertainty sources related to the polymerized gels: results mismatching due to the calibration issues and uncertainties from R2 dose map.

According to A. Venning [37], the polymer gel dosimeters have two types of instability: spatial, which is related to monomers diffusion from high to low dose region, and temporal instability. The temporal instability may affect R2 background or R2 dose response curve and indicate it increasingly. In order to reduce this type of instability, it is recommended to perform calibration and experiments with the gels from the same batch.

2.7. Dose gels applications in the medical field

Polymer dose gels could be a useful tool for dose distribution in the selected geometry registration.

2.7.1. Dose gels in radiotherapy and radiosurgery dosimetry

Dose gels have unique features, which could be explored for dosimetry applications in radiotherapy. The 3D polymer gel dosimeters are perfect tools to provide 2D dose maps of the irradiated areas and register 3D dose distribution in a simple geometry and “record” the heterogeneity effects, where two-dimensional or point detectors are not suitable. The recorded dosimetry results are quite accurate due to the relatively high spatial resolution (0.1–0.2 mm) of the gels.

Novotny et al. [81] irradiated the polymerized gels with gamma rays and compared two measurable parameters of the irradiated gel with those calculated by TPS.

The geometrical differences between the measured and calculated points characterized by a certain dose were defined as position misalignment between the center positions (ΔX , ΔY , ΔZ). The second parameter is dose differences between the measured and calculated values, according to the isodose curves. There was found a good agreement between the compared dose profiles 0.1–0.7 mm and 3–7% dose discrepancies between the experimentally measured and TPS indicated values, depending on the selected dose plans. Using linear accelerator for prescribed dose

delivery, the TPS calculated and performed dose could be verified with portal dosimetry [82], thus creating maps of dose profiles (see Fig. 17).

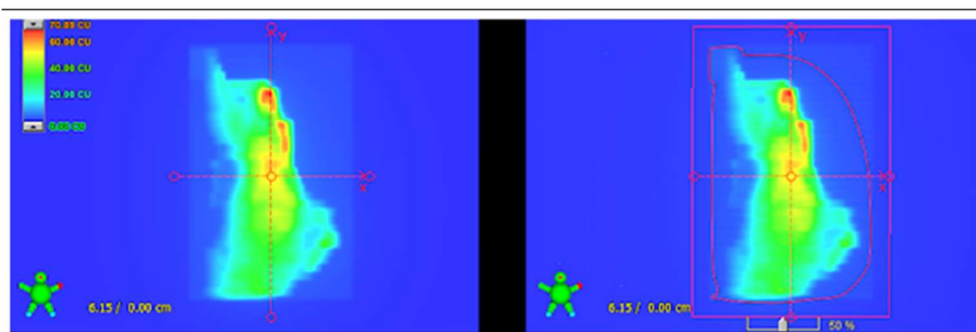


Fig. 17. 2D projection of VMAT plan: a) calculated by TPS and b) verified with portal dosimetry

The same dose mapping has been performed by using irradiated nPAG gels [83]. The MRI evaluated doses were very similar to those obtained from TPS calculations (gamma index > 1), and relative dose deviation of 1.2% at 10 cm depth in the gel was registered. Despite of the highly accurate dosimetric results of nPAG gels and their suitability to be used in radiotherapy for dosimetry purposes, these gels have a limited dose range if applied for hypofractionated techniques.

Polymer gel dosimetry might be successfully applied in catheter based interstitial brachytherapy. Brachytherapy is high dose radiation treatment method when a small (point) radioactive source is attached for a certain amount of time as close as possible to the cancerous tissue. There is no other method than gel dosimetry, which can experimentally visualize 3D dose distribution within the patient's body. This is realized by filling up a special catheter up with the gel, which is surgically preimplanted into the tumor. Read-out dosimetry catheter provides dose delivery to the target information and can be compared with the results that are simulated by using TPS of brachytherapy unit. Three dimensional dose distribution measurements can be performed with all radioactive sources that are used in brachytherapy systems: cesium-137 [84], iodine-125 [85], iridium-192 [2, 26, 86], Rhenium-188, Yttrium-90 [82], or Ruthenium [87]; three dimensional polymer dose gels based measurements can be applied [83, 87, 88].

The application of VIPAR dose gels for dose measurements in prostate brachytherapy with Ir-192 source used by P. Kipouros et al. [26] have shown 5% difference between the calculated and experimentally measured dose values.

Fragoso et al. [86] performed 3D dose distribution measurements in Ir-192 source brachytherapy, and 1–3 mm beam positioning differences between the calculation and dose gel measurement results were obtained. Another experiment was performed by using low dose rate Cs-137 source in intracavitary brachytherapy [84]. In this experiment, homogeneous (filled with dose gel) and heterogeneous phantoms (with polymer dose gel partly filled phantom with the left air cavity) were employed.

The estimated dose difference between the experimental and TPS calculated results was around 5%.

The polymer dose gels can be as well applied for three dimensional dose verification in Gamma knife. A. Moutsatsos et al. [89] used VIPAR dose gels for the output factor evaluation of the smallest possible Gamma knife field that was formed with 4 mm collimator. There was observed a 3% lower output factor than it is recommended in the guidelines.

Watanabe et al. [2] noted that the 3D visualization of the small irradiated volume, which is less than 1 mm³ (small field dosimetry), may be very problematic, since there is a lack of suitable dosimetry tools. Only radiochromic films (2D dosimeters) or dose gels (3D dosimeters) could be applied. When using polymer dose gels, it is possible to visualize small, irradiated points in the volume (pixels or voxels) that were obtained after scanning the irradiated dosimeter in the MRI unit [90]. The performed measurements of irradiated nPAG gels have shown that the differences between prescribed 5, 10, 15, 20 Gy and measured doses were 27.60%, 5.80%, 2.53%, 0.95%, respectively. This indicates that higher absorbed doses installed microscale structural changes in the irradiated gels, which were sufficient to keep a high accuracy of results. It should be noted that this accuracy decreases when the prescribed doses are lower.

2.7.2. The application of polymer gels for 3D and 4D printing

The 3D printing is a perspective and one of the most growing technology with possible application in science, engineering and especially for clinical purposes. Following the demand from the health sector to have individualized health care for each patient, the 3D printing technology becomes a powerful tool for the creation of patient specific artificial organs and tissues or mimicking patient's specific organs as phantoms, which are used in the pretreatment stage to adjust the treatment procedure (relevant for radiotherapy treatment). There are few 3D printing techniques to perform the same tasks: electron beam melting, stereolithography, selective laser melting, fused deposition modelling, direct ink writing, etc. [91]; however, the 3D printing where thermoplastics, ceramics, or metal materials are used is the most progressing technique. Nevertheless, A. Elter et al. [91] used PAGAT dose gels and PolyJet/MultiJet volumetric printing technique to create suitable radiation sensitive printing materials, containing polymer gel with some additives. It was found that in a small square (1.0 x 1.0 cm²) of the produced material that is irradiated with 5 Gy dose, the dose response between pure gel and 3D printed gel was deflected by < 3%, and the geometrical deviation was < 1% [92].

A significant evolution of smart materials enables additional inclusion of the time factor for the 3D printing technology. The most popular materials that are suitable for 4D printing are shape memory polymers and stimuli-responsive hydrogels. Customized smart materials are able to transform the size and shape in response to any external stimulation and within the 3D printing base, create a concept of the 4D printing.

The main characteristics of 4D printing are the following: expansion, folding after printing, shrinkage, and bending. These shape transformations could be stimulated by light, pH, temperature, humidity, etc.

The 4D printing is as well possible with gel-based materials by printing the required structure/shape, following the shape morphing due to the selected stimulant.

Otherwise, the suitable materials for 4D printing are very limited, because of the early stage of the research that is related to this new printing method [91]. The main advantages and disadvantages of 4D printing are provided in Table 6.

Table 6. The main advantages and disadvantages of 4D printing method

4D printing	
Advantages	Disadvantages
Created structure is independent from the fabrication devices	Limited number of suitable materials and devices
Defects, time, and cost reduction	Almost all materials are limited by one type of stimulus
Wide application	More studies are needed to analyze the physical and chemical properties
High potential for further application	Limited size of the structure
	Precision is needed only for macroscale structures

In this dissertation, a new method of ionizing radiation based 3D printing was proposed. This method requires deep knowledge and more investigations; however, it could be considered as a concept for new individualized dosimetry/visualization method for the assessment of irradiated structures.

The performed literature analysis has shown that the development, characterization, and exploration of unique properties of 3D polymer dose gels as well as functionalization of these gels for the new applications in medical radiation field has invaluable potential for the implementation of the individualized patient health care (patient specific radiotherapy treatment, optimized by using gel dosimetry). According to this statement, two types of polymer dose gels were selected, modified, and applied for high dose small-scale radiotherapy and radiosurgery treatment dosimetry purposes. Moreover, the most promising (UV-VIS, MRI, etc.) read-out techniques were selected for the estimation of polymer dose gels sensitivity to the absorbed energy. After the review of analyzed literature, there was observed a limited development of polymer dosimeters in 3D dose distribution registration field. Because of this, the ionizing radiation based 3D printing and individual treatment plans verification concepts were developed and functionalized.

3. INSTRUMENTS AND METHODS

Considering the level of investigation and the experience gathered from the scientists of KTU research group of “Radiation and Medical Physics”, nPAG and VIPAR dose gels were selected for further modification. The decision was based on the fact that these gels might be produced under normal ambient conditions, the polymerization in both types of gels proceeds via cross-linker BIS acrylamide (Fig. 18), and both types of gels are sensitive enough to the radiation, thus being suitable for dosimetry applications [93–95].

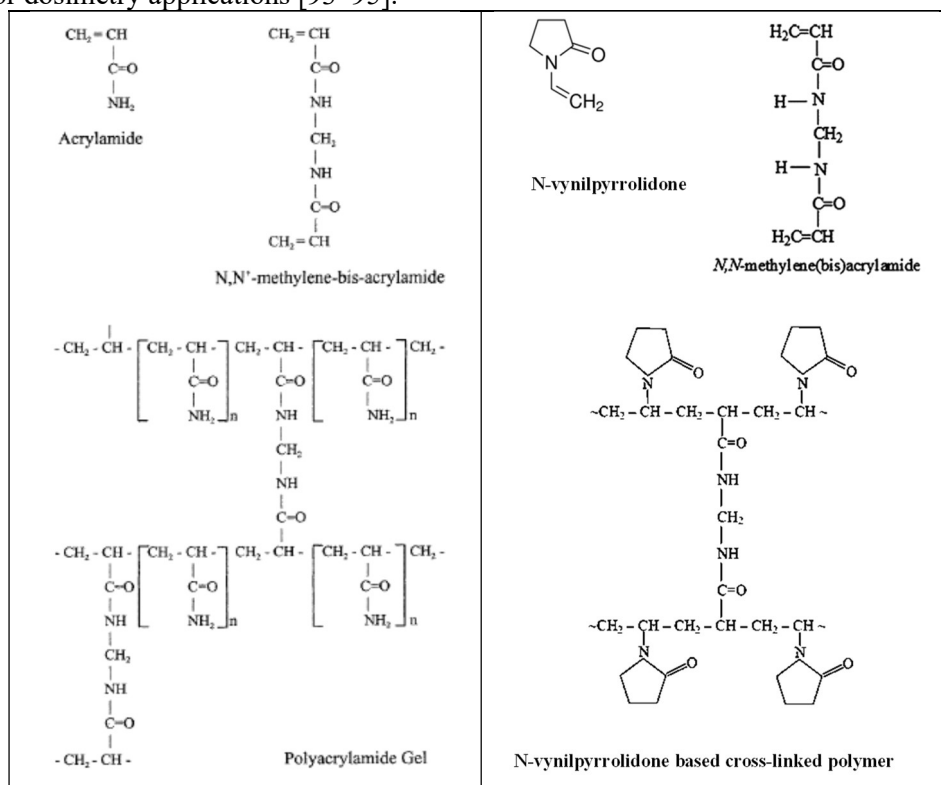


Fig. 18. Polymerization scheme for acrylamide (L) and *N*-vinylpyrrolidone based crosslinked polymers (R)

3.1. Dose gels fabrication

Another technique that is called free standing polymerization is the separation of irradiated and non-irradiated volumes with the purpose to compare theoretically modulated and experimentally irradiated volumetric shapes [69, 96].

Seeking to improve the sensitivity of polymer gels to ionizing radiation and create free standing dose gel structures, which may record polymerized target volume, the initial gels of both types were modified by adjusting their chemical content as compared to the standard gel recipe.

The modification of a standard nPAG gel recipe was undertaken, and the properties of new gels were evaluated with the aim to discover the most appropriate gel formulation for achieving the free standing dose gels structures after the irradiation that correspond to the irradiated volume. The evaluation of gels was based on the fact [39] that the chemical changes and polymerization processes in dose gels depend on the concentration of separate components in the total volume. In fact, monomer and cross-linker concentration affects the dose gel sensitivity due to the formed polymer network size and polymerized part density [99, 98].

The acrylamide concentration in percent (%T) can be expressed as follows (Eq. 21):

$$\%T = ((\text{grams acrylamide} + \text{grams crosslinker}) / \text{total volume (ml)}) \times 100, \quad (21)$$

and bis-acrylamide concentration in percent (%C) is expressed as follows (Eq. 22):

$$\%C = ((\text{grams crosslinker}) / (\text{grams acrylamide} + \text{grams crosslinker})) \times 100. \quad (22)$$

It should be noted that the increasing crosslinker concentration leads to the transverse relaxation rate R2 (MRI evaluation) increase until 50%C when %T is constant 6%. The further crosslinker concentration increase indicates the polymerization rate decrease, which could be related to the reduced monomer diffusivity [92]. Another investigation based on Raman analysis of polymerized structures [91] has shown that R2 is affected more by the number of crosslinks that have been formed than the polymerized monomer amount. The higher reactivity of cross-linker as compared to the acrylamide was considered when choosing concentrations of monomers for the gel fabrication, and higher gelatin concentration, which ensures mechanical dose stability (free standing polymerized structure), was taken into account.

The chemical composition of the advanced nPAG^F and VIPARnd dose gels are provided in Table 7.

Table 7. Chemical composition of the advanced nPAG^F and VIPARnd dose gels

Chemicals	Role	Amount*	
		nPAG ^F	VIPAR nd
Gelatin (from Porcine skin A/300 strength, bloom, Sigma Aldrich)	Dose gel matrix	2–5 wt%	7–7.5–8 wt%
<i>N,N'</i> methylene bisacrylamide (purity grade ≥ 98%, Sigma Aldrich)	Cross-linker	3–3.5 wt%	4–5 wt%
Acrylamide (purity grade ≥ 99%, Sigma Aldrich)	Comonomer	3–3.5 wt%	
(Hydroxymethyl) phosphonium chloride, THPC +hydroquinone (80% in H ₂ O, Sigma Aldrich)	Oxygen scavenger	10–11 mM	
<i>N</i> -Vinylpyrrolidone (purity grade ≥ 99%, Sigma Aldrich)	Comonomer		8–9 wt%
CuSO ₄ ·5H ₂ O (purity grade ≥ 99%, Sigma Aldrich)			32 mM

Ascorbic acid (99%, Sigma Aldrich)	Oxygen scavenger		0.007 wt%
Water (pure deionized)		~ 87–89 wt%	~ 80 wt%

*The final amount of the chemicals that are used in this work is indicated in **Bold**. The gelatin concentration was changed by 1%, monomer/comonomer 0.5% step.

It is known that separate chemical components affect polymer gel's sensitivity to the absorbed dose. Gelatin concentration is directly responsible for the polymerized gel segment size and number. The equal quantities of monomer AAm and crosslinker Bis (for nPAG dose gels) are responsible for successful monomer consumption and polymer formation processes. Aam and Bis quantities out of 2.5–3.5% range may indicate long chain formation and no crosslinking or large number of knots due to the irradiation and lower dose gel sensitivity.

3.1.1. Fabrication of nPAG^F dose gels

Varying initial concentrations of gel components, all nPAG type gels were fabricated under normal conditions, following the same procedure described below. Gelatin was mixed with water at room temperature and left to swell for 20–30 minutes. The whole mixture was heated up to 40–45 °C, mixed using magnetic stirrer Heidolph MR 3001K (300–500 rpm) until the gelatin was completely dissolved, and the solution became clear. The corresponding amounts of acrylamide monomer and cross-linker *N,N'*methylene bisacrylamide were admixed one by one into the prepared gelatin solution maintaining 35 °C temperature and continuously stirring for the next 10 min. Then, the whole mixture was cooled down to 30 °C, and a certain amount of the oxygen scavenger hydroxymethyl phosphonium chloride with hydroquinone was admixed under continuous stirring for the next 5 min. The prepared gels were poured into borosilicate beakers (DIN 12 331. ISO 3819; D=4.8 cm, H=8.0 cm) or special vials/cuvettes, tightly closed, and stored for at least 24 hours in the dark. The experimental setup and examples of prepared and irradiated (with clearly seen polymerized structure) nPAG^F dose gels are shown in Fig. 19. It should be noted that the fresh gels were almost transparent.

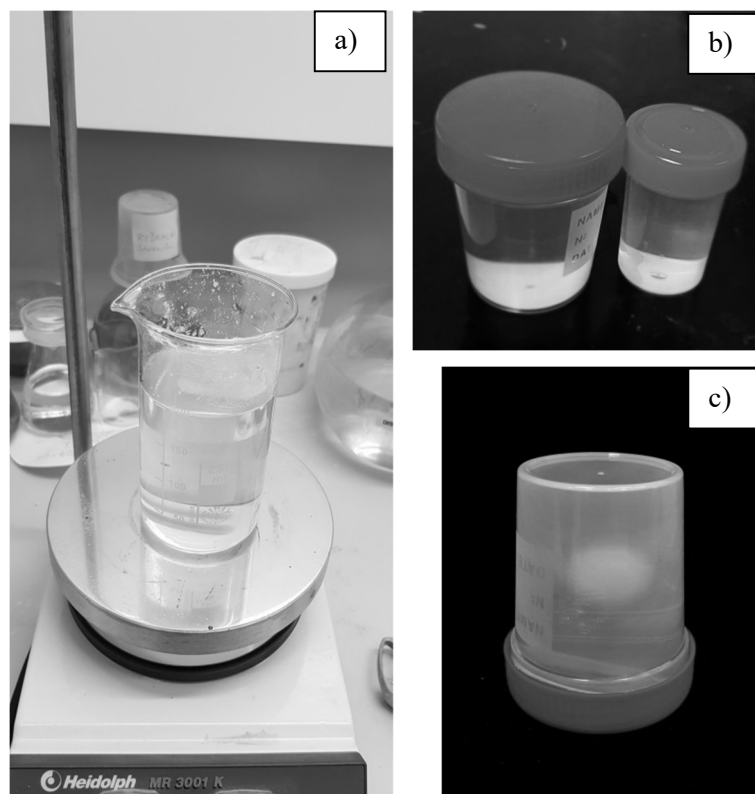


Fig. 19. a) Fabrication of nPAG^F dose gels, b) freshly prepared gels, c) an example of the irradiated dose gel sample

3.1.2. Fabrication of VIPARnd dose gels

The fabrication procedure of the modified VIPARnd (normoxic-double) dose gel, having a relative high amount of gelatin, was slightly different from the previous one, which was used to produce nPAG^F dose gels.

Preparing VIPARnd dose gel [41], a part of water was used to swell the gelatin and another part to dissolve *N,N'*methylene bisacrylamide (BIS). After 30 min of swelling, the gelatin was dissolved under continuous stirring in magnetic stirrer, keeping temperature at 40–45 °C. The rest of the water was heated up to 40 °C, and *N,N'*methylene bisacrylamide was dissolved. The temperature of both suspensions was reduced to 30–33 °C, and then, both of them were mixed together. After additional 5 min of stirring, all other gel components were added to the solution.

The prepared gels were poured into borosilicate beakers (DIN 12 331. ISO 3819; D=4.8 cm, H=8.0 cm) or standard disposable PMMA cuvettes, tightly closed, and stored in the dark for 24 hours. Fig. 20 provides insights on VIPARnd gel preparation and irradiation and shows an example of irradiated gel.

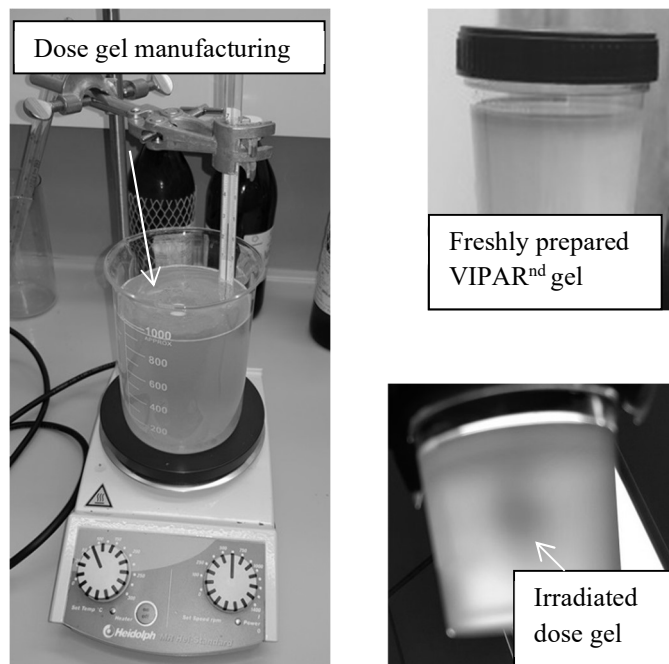


Fig. 20. a) VIPARnd dose gel preparation, b), freshly prepared dose gel, c) an example of irradiated VIPARnd dose gel

Prepared VIPARnd dose gels indicated characteristic yellow/blue/green color tone and were slightly less transparent compared to nPAG^F dose gels.

3.2. Irradiation techniques

In order to cover all multitasks, which were set for the development of dose gels, the experimental samples were irradiated with photons and electrons in different radiotherapy facilities; the related information is summarized in Table 8.

Table 8. Irradiation facilities and irradiation parameters

Parameters	Irradiation facility			
	Teletherapy unit Rokus M	Leksell Gamma knife Icon TM	Microselectron V2 (Nucletron) and Flexitron Icon TM (Elekta)	Linac Truebeam 2.7
Radiation source	⁶⁰ Co	⁶⁰ Co	¹⁹² Ir	Electrons
Activity, Bq	4.28 * 10 ¹³	189–244 * 10 ¹² (< 1.3 * 10 ¹² for 1 source)	0.35 * 10 ¹² and 0.39 * 10 ¹²	-
Dose rate, Gy/min	0.25	3.45	0.73 and 0.82	1–6 Gy/min

Characteristic energies, MeV	$\gamma_1 = 1.17$ MeV, $\gamma_2 = 1.34$ MeV	$\gamma_1 = 1.17$ MeV, $\gamma_2 = 1.34$ MeV	$\gamma = 0.37$ MeV, $\beta = 1.454$ MeV	6–20
Dose per fraction, Gy	Up to 40	Up to 40	Up to 13	Up to 40
Geometry	Broad field (10 x 10 cm ²)	Point source	Point source	Broad field 10 x 10 cm ²

3.2.1. Gamma photon irradiation facilities

Gamma photon irradiation impact on the gel properties and the applicability of dose gels for gamma dosimetry research in clinical environment was assessed and evaluated by examining the dose gels irradiated in teletherapy unit Rokus M (Fig.21) and Lexell Gamma knife Icon™ (Fig. 22). Considering the high workload of the Gamma knife facility, it was decided to simplify the procedure and assess the sensitivity of nPAG^F and VIPARnd gels to gamma irradiation in dose region up to 40 Gy, including the dose calibration, using teletherapy unit Rokus M. The experimental setup with Rokus M unit is shown in Fig. 18. It should be noted that gelfilled samples were irradiated from the bottom side, and 0.5 cm thick bolus was applied during the samples treatment order to deliver the maximum dose at 0.5 cm depth. One of the experimental gamma irradiated nPAG^F dose gel batches (dose range: 0–4 Gy) is shown in the same figure as well. The delivered doses were checked independently by using ionization chamber PTW Semiflex C31010. The actual ⁶⁰Co source activity and corresponding dose rates were calculated on the exact day of the treatment.

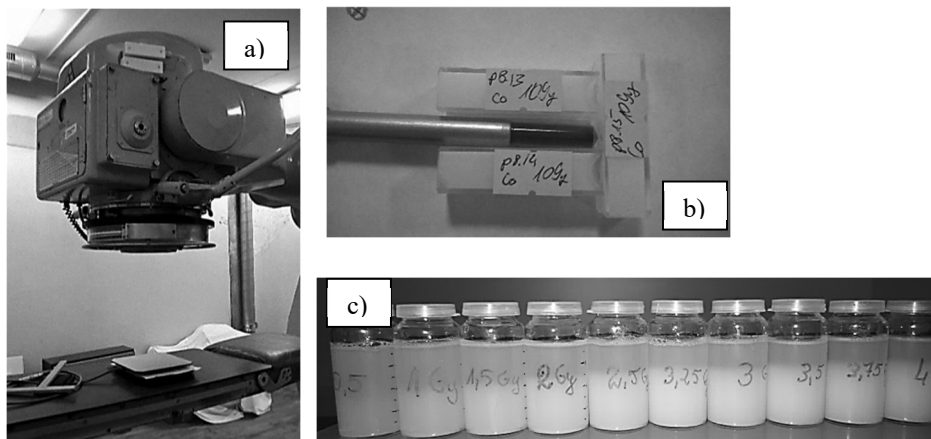


Fig. 21. a) The experimental setup for the irradiation of gel samples in Teletherapy unit Rokus M, b) location of samples and ionization chamber during the experiment, c) nPAG^F dose gels irradiated to the doses up to 4 Gy for catheter-based dosimetry calibration purposes

The gamma knife facility was involved mainly in microdosimetry experiments. It consists of 192 ⁶⁰Co sources, divided into eight sectors, which provide internal

collimation system and point sources geometry. In all cases, the dose gel samples were placed on the film holder tool, which ensures the appropriate position (Fig. 22 b) during the treatment procedure.

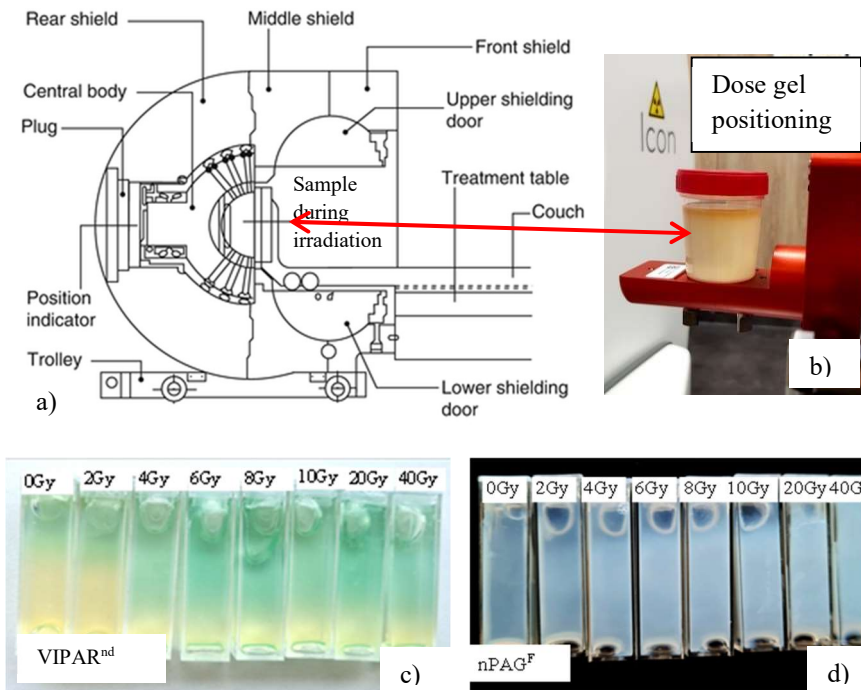


Fig. 22. a) The experimental setup for the gel irradiation in the Gama knife facility, b) dose gel samples positioning during the treatment, c) irradiated VIPARnd and d) nPAG^F dose gels

3.2.2. High dose rate brachytherapy units

Two types of High Dose Rate (HDR) brachytherapy units with ^{192}Ir source and $\gamma=0.37$ MeV and $\gamma=1.454$ MeV characteristic energies were used in dose gel irradiation experiments.

MicroSelectron v2 was used for the implementation of catheter based dosimetry concept in HDR brachytherapy. The concept is based on the dose measurement in specifically arranged and dose gel filled Fr6 ($D=2$ mm) catheters.

Flexitron HDR was mainly used for the development of free standing dose gel structures, which record the radiation treated volume, corresponding to the size and shape of the tumor (ionizing radiation based 3D printing). This was possible, according to the prepared patient's dose treatment plan, inserting catheters at certain positions into the gel-filled volume (Fig. 23) [99].

In both cases, the activity of radiation source was assessed on the day when the experiments were performed.

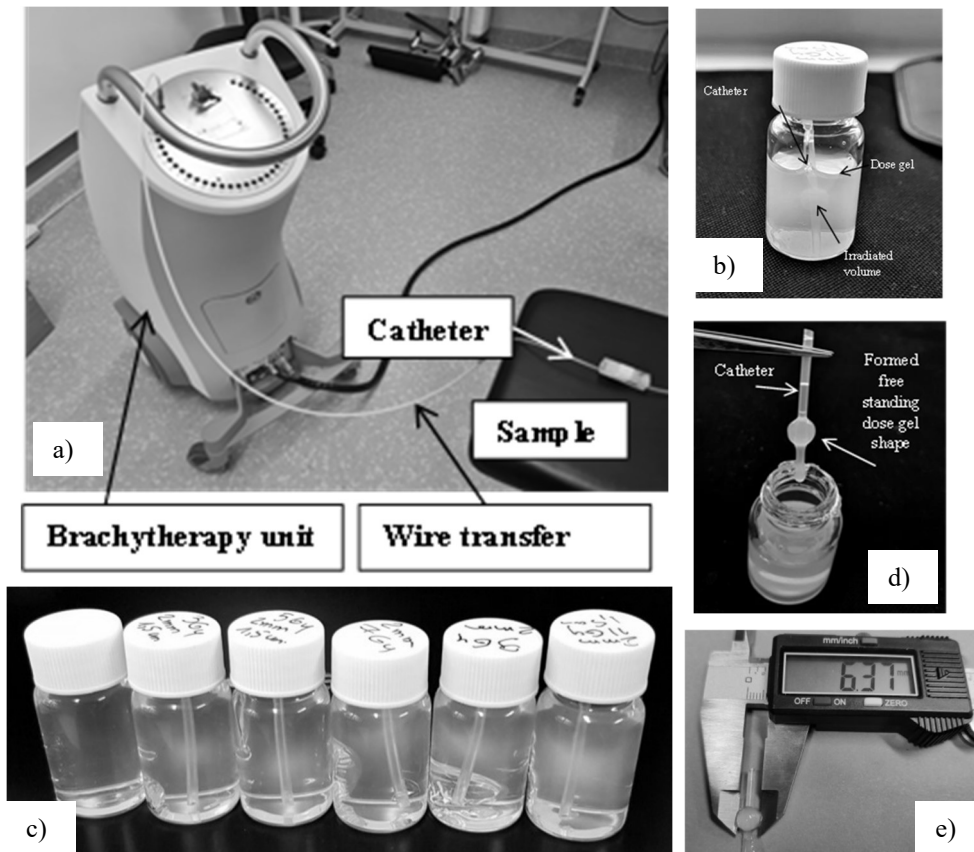


Fig. 23. The experimental setup for the irradiation of obtaining free standing dose gels in a) HDR brachytherapy unit Flexitron Icon™, b) and c) PAG^F dose gel samples after the irradiation with ¹⁹²Ir source inserted into the catheter, d) the removal of polymerized gel shape from the gel volume, e) measuring the size of the polymerized shape

3.2.3. Medical linear accelerator

Linear accelerator Varian Truebeam 2.7 with integrated treatment planning system (TPS) Eclipse 15.5 was used for dose gels irradiation with 6 MeV electron beam in order to assess the dosimetric sensitivity of gels. The irradiation of samples was performed by using broad field (10 cm x 10 cm) geometry, applying 3 Gy/min dose rate.

The electrons in linear accelerator are accelerated by following straight trajectories in special evacuated structures that are called accelerating waveguides. The energy transfer from the high power radio-frequency (RF) fields is set up in the accelerating waveguide and is produced by the RF power generators, i.e., magnetrons and klystrons. The electrons originating in the klystron are accelerated in the accelerating waveguide to the desired kinetic energy and “travel” through a special accelerating tube into the linac treatment head. The electron beam is formed to a narrow 3 mm pencil beam before they left the accelerating tube. The electron beam

scattering over a relatively large area (up to 25 cm × 25 cm) could be achieved by placing thin foils of high Z material into the flattening filter or, as an alternative using electron beam scanning technique when two computer controlled magnets deflect the pencil beam in two orthogonal planes.

The gantry of the accelerator was rotated to 180 degrees, and 100 cm source-sample distance (SSD) was kept. The centrally placed nPAG^F gel filled bottles were irradiated to different doses (0 Gy, 2 Gy, 4 Gy, 6 Gy, 8 Gy, 10 Gy) from the bottom side. One extra sample was irradiated with 12 MeV electrons, delivering 8 Gy dose in order to see the influence of electron beam energy [100] on the polymerization process in the gel.

The experimental setup and electron irradiated nPAG^F gel samples are shown in Fig. 24.

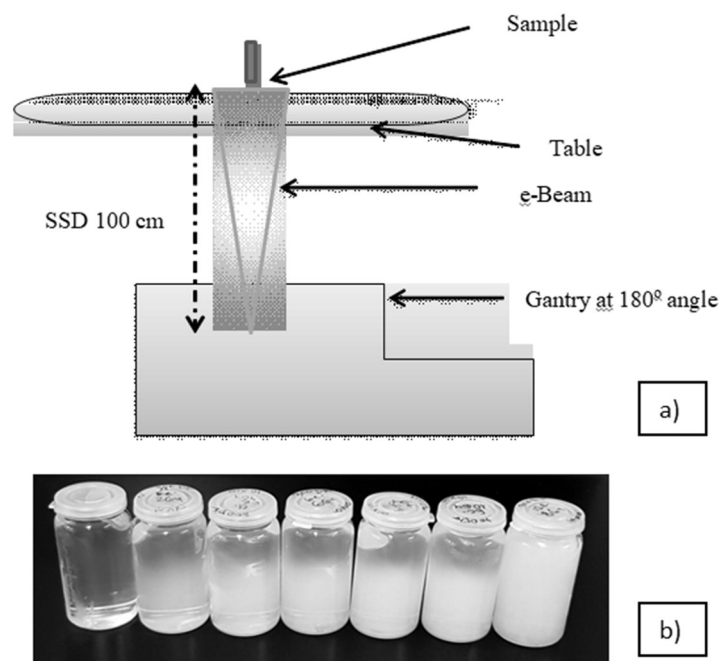


Fig. 24. a) Principal scheme of the samples irradiation with a linear accelerator, b) e-beam irradiated nPAG^F samples

3.3. Experimental methods

nPAG^F and VIPARnd dosimetric gels were analyzed by using several evaluation and characterization techniques demonstrated in Fig. 25.

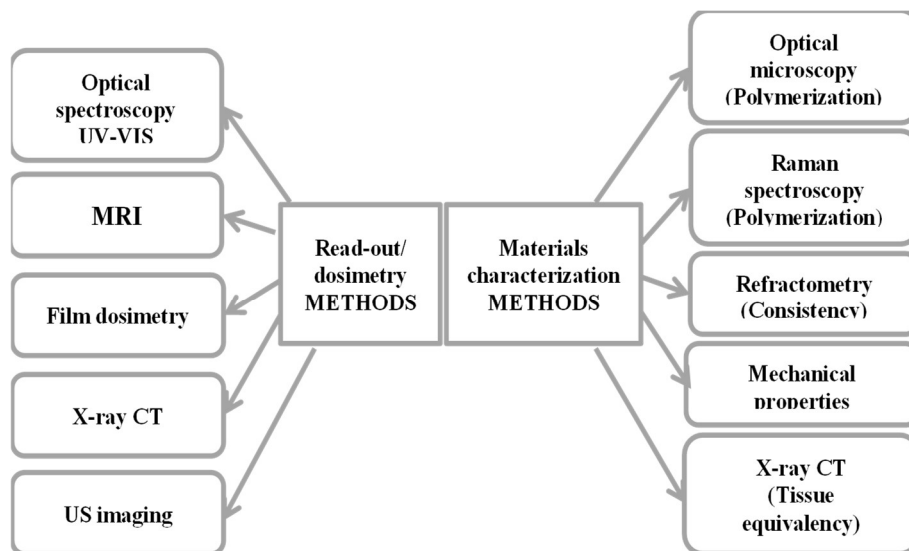


Fig. 25. Dose gel evaluation and characterization methods

3.3.1. Characterization methods of materials

Raman spectroscopy. Raman spectroscopy is an analytical technique where scattered light is used to measure the vibrational energy modes of a sample. When the exciting monochromatic laser beam interacts with a sample, different molecules are scattering light differently, thus forming a Raman spectrum. Raman scattering is an inelastic scattering process with a transfer of energy between the molecule and scattered photon. Raman spectrum represents the intensity of scattered radiation as a function of the energy difference between the incident and the scattered photons.

Raman spectroscopy can provide both chemical and structural information as well as the identification of substances through their characteristic Raman ‘fingerprint’. Raman spectroscopy is often used to detect radiation-induced changes in polymer gel structure. In the gel polymerization process, highly polarizable C-C and C=C bonds groups in monomer and crosslinking agent play the most important role. The Raman shift can be observed in irradiated gels, which can be attributed to the vibration differences between C=C bonds in polymerized and C=O bonds in non-polymerized materials [71].

In this work, the polymerization of irradiated gel samples was assessed analyzing the data obtained from performing measurements with Raman microscope Reinshaw inVia.

The excitation beam from a diode laser of 532 nm wavelengths was focused on the sample using a 20× objective. Laser power at the sample surface was 2 mW. For all measurements, the integration time was 10 s; a signal was accumulated at once. The Raman Stokes signal was dispersed with a diffraction grating (2400 grooves/mm), and the data were recorded using a Peltier cooled charge-coupled device (CCD) detector (1024 × 256 pixels). This system yields a spectral resolution

of about 1 cm^{-1} . The silicon material was used to calibrate the Raman setup in both Raman wavenumber and spectral intensity.

Raman spectroscopy method was applied in the range of $600\text{--}3200 \text{ cm}^{-1}$ wavenumbers. Molecule structural changes cause spectral shifts due to the chemical composition of the dose gels.

A normal distribution method was applied for the data interpretations when searching and defining Raman peaks. The data analysis of Raman peaks and full width at half maximum (FWHM) calculations was performed by using the OriginPro2021 program package. RStudio plugin Chemospec was used for data baseline corrections and normalization.

Refractometry. It is known [101] that radiation-induced polymerization is responsible for physical and optical density changes in the irradiated dose gels. Since the refractive index directly depends on the optical density of the investigated materials, the refractometry measurements may provide supplementary information regarding the radiation-induced polymerization of samples.

Possible random errors that may occur in the evaluation of physical parameters of dose gels during the samples fabrication and solidification processes were estimated by analyzing the refraction indexes of nPAG^F dose gel samples. For this reason, two batches of nPAG^F gels of the same composition, 5 samples of each, were produced.

The refraction indexes of the initial (solid) samples and liquefied dose gel samples (heated up to $40 \text{ }^\circ\text{C}$ for 30 min until the gelatin is liquified) were measured using KRÜSS AR3 refractometer. The measured values are provided in Table 9.

Table 9. Reference and experimental values of nPAG^F dose gel refractive index

Dose gels	Refractive index of nPAG ^F gels	
	Initial sample (solid)	Liquefied sample (heated up to $40 \text{ }^\circ\text{C}$ for 30 min.)
nPAG ^F 1 series	1.3550	1.3552
nPAG ^F 2 series	1.3551	1.3553

There was found no significant difference between the refraction indexes of initial sample and liquified sample.

Obtaining free standing polymerized gel shapes. One task of this research was to create stable free standing polymerized gel shapes, mimicking the tumor volume, which should be treated according to the prepared patient's treatment plan. It is known [102] that gels are able to maintain polymerized 3D structure after the termination of ionizing radiation; however, the polymerized volume of the gel remains surrounded by the remaining part of not polymerized gel.

In order to fully implement the developed concept [103] of ionizing radiation-induced 3D printing of free standing anatomic shapes (tumors) in medical practice and open new possibilities for the direct analysis of polymerized structure, it should be separated from the gel.

Experimental bottles (D=2.5 cm, H=4.5 cm) with nPAGF dose gel were supplied with one centrally arranged 4 Fr (D=2 mm) catheter: a number of which are used for the insertion of ^{192}Ir source during the catheter-based HDR brachytherapy procedures. The samples were irradiated with Elekta Flexitron IconTM brachytherapy unit with ^{192}Ir source at the same day. The delivered doses were 0, 3, 5, 7, 9, 11 Gy, respectively, and a single target was set 15 mm from the bottom of the bottle for all experiments. The activity of ^{192}Ir source on the day of performed irradiation was 0.36×10^{12} Bq; the dose rate was 0.77 Gy/min.

It is known that long-lasting exposure to different temperatures and visible light shrinks the gelatin matrix, and the polymerized volume remains “free” after the liquifying. However, this process is relatively long and does not correspond to the clinical needs where the immediate investigation of polymerized structure is requested in order to improve the treatment of a patient.

Several possible polymerized gel shape separation methods were tested to speed up this process. Two of them, i.e., **Controlled heating method** and **Dry air method**, are described below.

Controlled heating method. The irradiated gel was heated for 30 min in Ametek JOFRA RTC-158 thermostat (Fig. 26 a b)) keeping 40 °C temperature. After half an hour, the non-irradiated part of whole gel sample volume liquifies and becomes mechanically volatile. The irradiated (polymerized) sample part keeps its shape/form, since it is denser due to the radiation-induced polymerization and may be removed from the gel’s solution. The removal of the polymerized shape was performed by using a dynamometric measuring stand Sauter TVM 5000N230N with calibrated dynamometer Sauter F1k (resolution 1 mN) (Fig. 26 c). The measured separation force (adhesion force) was depended on the temperature and was in 45–308 N range.

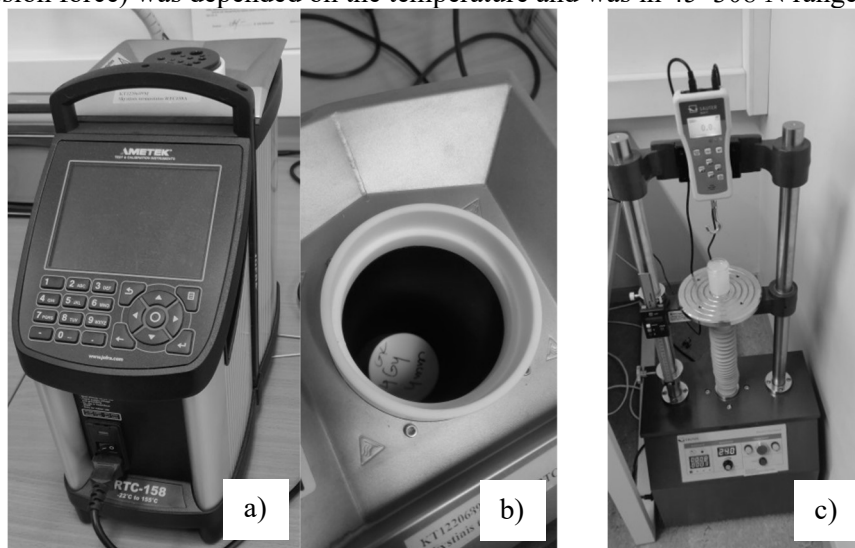


Fig. 26. Experimental setup for controlled heating method: a) Ametek JOFRA RTC-158 thermostat with gel sample inserted instead of the calibration sleeve; b)

dynamometric measuring stand Sauter TVM 5000N230N with calibrated dynamometer Sauter F1k

It should be noticed that the controlled heating method applies at least 40 °C temperature for gelatin liquefaction; thus, the mechanical properties of gelatin matrix are changed. In order to avoid this, a series of experiments were performed using a dry air generator (commercial fruit/vegetable dryer).

Dry air method. Applying this method, the samples were dried at 30% relative humidity conditions in order to obtain the polymerized gel shape separately from the whole volume. Keeping these conditions for 72 hours, most of the non-irradiated gel solution, which consist of a large amount of water (> 80%), evaporates. It is very important to provide a mechanical holder for the polymerized gel shape, since it remains “hanging” after the evaporation of non-irradiated solution and can be removed from the vial. However, the separated shape differs from the originally created one due to the fact that some water is extracted from it during the drying procedure as well. A detailed information, regarding the separation of polymerized dose gel shapes, is provided in the Results section.

X-ray computed tomography (CT). This method was applied for two reasons: 1) the evaluation of fabricated dose gels in terms of tissue equivalency, which is absolutely necessary when performing clinical dose measurements, and 2) the assessment of correlation between the irradiation dose and X-ray attenuation properties in the irradiated dose gels.

The properties of irradiated dose gels can be assessed by performing CT scans of samples and quantitatively evaluated by using a Hounsfield units scale. The calculation of Hounsfield units is based on linear attenuation coefficient transformation in relationship with constant air/water values [104]. The tissues or materials with higher density better absorb the X-rays and are displayed brighter on the Hounsfield scale versus lower density tissues (lower density, darker view). Hounsfield units scale, indicating X-ray attenuation (radiodensity) of materials, is provided in Fig. 27.

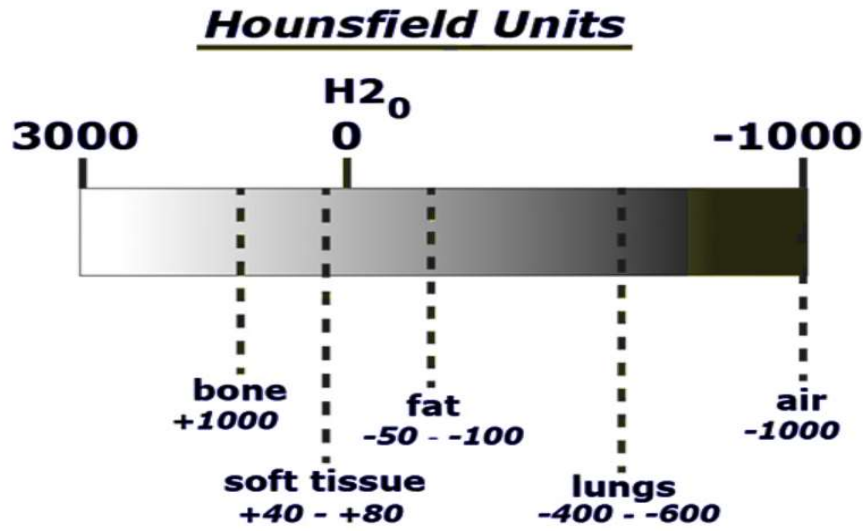


Fig. 27. Radiation attenuation values (Hounsfield Units) [104]

It should be noted that CT image contrast is related to the material density. If pixel intensities in CT are expressed in Hounsfield units (CT units), it is possible to evaluate the dose gel density in relationship with water density (Eq. 23):

$$HU = 1000 \times \frac{\mu - \mu_w}{\mu_w}; \quad (23)$$

where μ is the measured linear attenuation coefficient in sample of dose gel and water, respectively [105].

Theoretically, the density of the irradiated dose gel (ρ_g) should increase with higher doses; thus, it became equivalent to Hounsfield units (Eq. 24).

$$\Delta \rho_g = \Delta HU \quad (24)$$

The irradiated gel samples (cuvettes) were scanned in Computed Tomography unit Siemens Magnetom Avanto 1.5T, following the typical CT protocol: 120–140 kV, 100 mA, 200 s, slice thickness 2.5 mm. The cuvettes were placed on the table along the central CT axis. The dose profile measurements were performed by using special quality assurance phantom.

3.3.2. Dose read-out/dosimetry methods

Since the dose gels are considered for 3D dosimetry applications in clinical radiation procedures, the physical principles and methods applied for the dose evaluation from irradiated gels play a crucial role.

Optical spectrophotometry. Optical spectrophotometry method [106] is one of the simplest methods to investigate radiation-induced changes of the optical properties of irradiated gels. In this work, UV-VIS spectrometer Ocean Optics with USB4000 and 2D dose mapping photospectrometric system Ocean Optics with USB650 supported by homemade sample positioning system (Fig. 28) allow to measure the

optical characteristics of differently shaped samples (bottles, cuvettes, vials) and read-out irradiated samples in vertical and horizontal directions with 0.15 mm and 0.125 mm step, respectively.

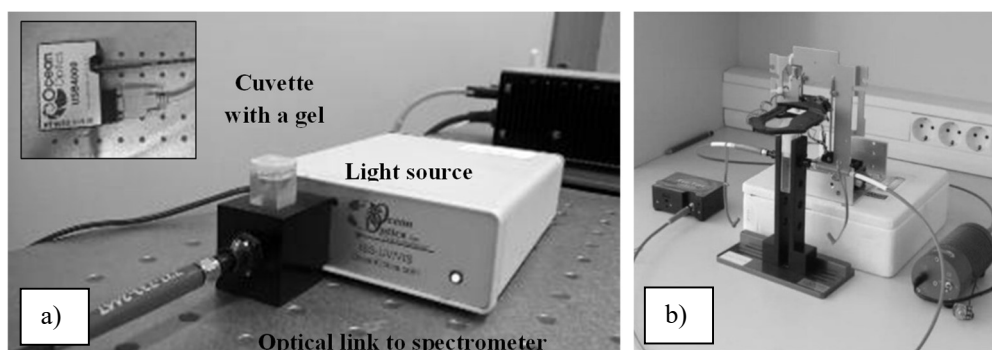


Fig. 28. a) Spectrophotometer Ocean optics with USB 400, b) dose mapping system with UV-VIS spectrophotometer Ocean Optics with USB650 and sample positioning stage

The technical calibration of spectrometers has been performed prior to each measurement: an empty cuvette was measured, and the reference absorbance intensity and transmittance data of cuvette were automatically removed from further measurements. The UV-VIS transmittance and absorbance spectra in the wave range of 250–850 nm were measured and analyzed.

It should be noticed that all irradiated samples were analyzed not earlier than 24 hours after the exposure.

Optical microscopy method was applied as well for possible structural changes due to the detection of polymerization in the samples; however, more detailed data were obtained by using other methods, and the optical microscopy method results have not been considered.

Magnetic resonance imaging (MRI). MRI tool is the most suitable read-out method for polymer dose gels, and it provides several possibilities for dose assessment.

The evaluation of dosimetry characteristics of experimental samples was performed by analyzing the images obtained by scanning irradiated dose gels in Siemens MAGNETOM Avanto 1.5T MRI system. MRI scanning was performed by using a 64 multiple spin-echo pulse sequence (T2 weighted basic sequence) and head scan coil (HE 3, 4). The gel filled vials were centrally positioned to ensure proper signal detection, as it can be seen in Fig. 29 a). The example of the irradiated VIPARnd and the obtained MRI image are provided in Fig. 29 b) as well.

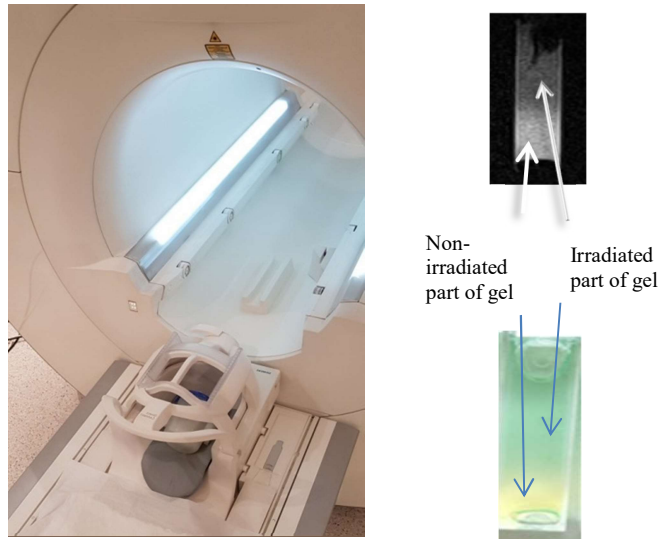


Fig. 29. NMR imaging: a) experimental sample mounted in the head coil; b) irradiated gel filled sample and MRI scan of the same sample

The parameters for each scanning were chosen according to the set tasks. MR images of irradiated samples that were acquired after the calculation of T2 values were subsequently analyzed using open source software Weasis v2.5.0 and program package ImageJ2.

Film dosimetry. There is a recommendation of ICRP [60] that the indirect dose measurements (as it is in the case of MRI) and construction of dose calibration curves shall be verified by another independent dosimetry method.

The film dosimetry using Gafchromic films RTQA2 and Kodak X-OmatV films was applied to verify the absorbed doses that were obtained in Gamma knife facility. The films were cut into 27 x 27 mm pieces and placed in the central position of calibrated film holder with stereotactic space coordinates of (100, 100, 100) mm for the irradiation. The same position was used for the irradiation of gel-filled samples.

After the irradiation to different doses, the films were scanned using free software NAPS2 6.1.2.25834 (24-bit color and 1200 dpi) and analyzed with free image analysis software ImageJ 1.52p version. The obtained data were used for the verification of the dose evaluation results that were obtained using MRI scanner.

The output factor was calculated as the ratio between the dose value measured at prescribed (planned) D_{max} location (when the collimator is positioned at the selected point, local isocenter) and the D_{max} ' dose value measured when the collimator is at the standard calibration position (Eq. 25).

$$OF = \frac{\text{measured } D_{max} \text{ at local isocenter}}{D_{max} \text{ at standard calibration isocenter}} \quad (25)$$

Sonography. The ultrasound beam is a sum of ultrasound waves, which arise from the mechanical oscillations of piezoelectric crystals in a transducer. The transducer converts electrical energy to mechanical (sound). These pulses of sound

are sent from the transducer through different density tissues and then return to the transducer as the reflected echoes. The returning sound is converted back to the electrical energy.

The ultrasound waves are reflected at the surfaces between the tissues of different density. Due to the significant difference of tissue densities, the sound is completely reflected (acoustic shadowing). Based on this principle, tissue density, acoustic resistance, and reflection coefficient can be estimated [107].

Considering that the physical density of irradiated dose gels depends on the irradiation dose, the applicability of the ultrasound imaging method for the evaluation of radiation-induced polymerization in gels was tested. For this reason, two cuvettes with nPAG^F gel: one non-irradiated and the other irradiated with 2 Gy dose in Gamma knife facility (gradient dose), were scanned using Esaote Biomedica AU5 Harmonic ultrasound imaging system (Fig. 30 A). 2.5 MHz micro-convex and 6.5 MHz endocavity ultrasound probes were used during the examination.

The irradiated samples were investigated in a water filled container (Fig. 30 B) in order to avoid the reflection of ultrasound waves and ensure the matching of acoustic resistivity.

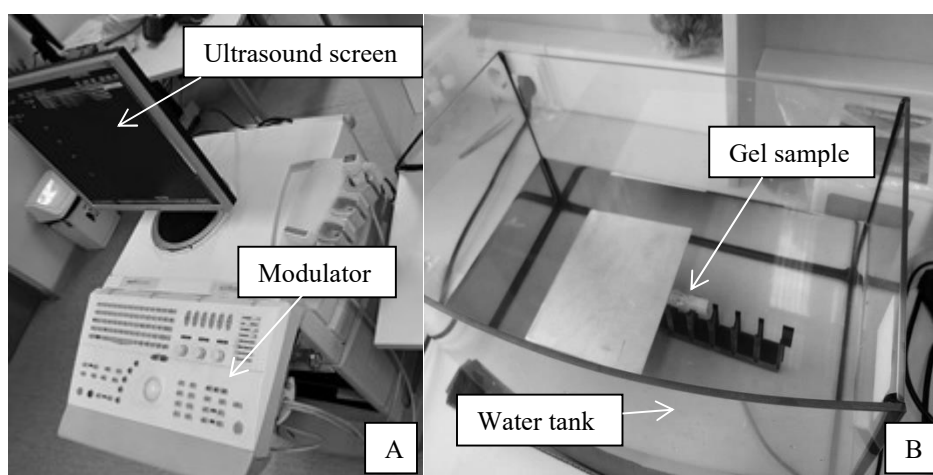


Fig. 30. Dosimetric sensitivity of electron beam irradiated nPAG dose gels at the selected wavelengths

The analysis of the results of measurements has shown that the pixel values within the whole ultrasound image area were from the narrow range. It was impossible to extract reliable dose distribution information by using both of the US probes.

Taking into account the low sensitivity of the method and complicated evaluation, the US method was not considered for further investigations.

A representative number of polymer gel samples were investigated when performing this research (Table 10). All measurements were repeated at least three times for one sample at different points of interest.

Table 10. nPAG^F and VIPARnd dose gel sample quantities used in the experiments

Method	nPAG ^F		VIPAR nd	
	Samples, units	Source	Samples, units	Source
UV-VIS	11	⁶⁰ Co	11	⁶⁰ Co
	11	e-beam		
Refractometry	17	⁶⁰ Co	20	⁶⁰ Co
Raman spectroscopy	4	X-rays	4	⁶⁰ Co
	4	e-beam		
X-CT attenuation	6	X-rays		
	6	⁶⁰ Co		
MRI calibration curve	6	⁶⁰ Co		
Dose mapping	5	⁶⁰ Co		
nPAG vs. VIPAR	2	⁶⁰ Co	2	⁶⁰ Co
Dose resolution	8	⁶⁰ Co	8	⁶⁰ Co
Gelatin, R2	30	⁶⁰ Co		
Free standings	6	¹⁹² Ir		
Adhesion force	6	¹⁹² Ir	6	¹⁹² Ir
Free standing, according TPS	2	¹⁹² Ir		
Microdosimetry	5	⁶⁰ Co		
Total	129		51	

It should be stated that several parameters, such as room temperature, room illumination, etc., have an impact on the performed measurements reliability. The uncertainties were determined by using an extended equation of uncertainties estimation during the measurements (Eq. 26) and calculated individually. In most cases, U(D) did not exceed $\pm 5\%$:

$$U(D) = (U_{cal}^2 + U_{eqp}^2 + U_E^2 + U_T^2 + U_{BS}^2)^{\frac{1}{2}}; \quad (26)$$

where U_{cal} is the calibration uncertainties related to ⁶⁰Co Gamma knife, ⁶⁰Co Rokus M, ¹⁹²Ir sources; U_{eqp} – uncertainties influenced by the read-out method; U_E – uncertainties related to the source radiation energy; U_T – uncertainties influenced by the temperature differences during the manufacturing and read-out procedures; U_{BS} – back scattering influence.

4. RESULTS AND DISCUSSION

4.1. Modified dose gels evaluation

This research was performed with the purpose to modify, analyze, and functionalize specific ionizing radiation sensitive dose gels for individual clinical dosimetry application. It was particularly addressed to:

1. Formation and analysis of polymer dose gels suitable for small scale high dose dosimetry applications;
2. Development and formation of ionizing radiation based 3D printing concept of free standing gels;
3. Implementation of a pilot study on the dose gel use for individual patient dosimetry in high dose small-scale radiotherapy and radiosurgery.

Taking into account the flexibility of gel modification, normoxic acrylamide-based (nPAG) and vinylpyrrolidone-based (VIPAR) were selected for the development of radiosensitive polymerizable gels that are suitable for clinical dosimetry applications in the dose range up to 45 Gy.

4.2. Characterization of the dose gel properties

In order to achieve the objectives of the research, different batches of nPAG and VIPAR gels were prepared, varying the concentrations of initial constituents (acrylamide, BIS-acrylamide, gelatin, water and oxygen scavenger for nPAG gel and *N*-vinylpyrrolidone, BIS-acrylamide, gelatin, water, copper sulfate and oxygen scavenger for VIPAR) in the gel composition and following the dose preparation method that was described in Methods and Materials section. The modifying of chemical content of the gel's different areas of application (micro dosimetry, ionizing radiation-based 3D printing) was considered as well.

After the irradiation of the prepared gels with gamma rays, electrons, and X-ray photons, using different medical irradiation facilities, the properties of irradiated gels were analyzed.

4.2.1. Evaluation of radiation sensitivity of experimental gels using UV-VIS spectrophotometry

Radiation sensitivity of irradiated dose gels is one of the most important parameters, characterizing the applicability of the gels for clinical dosimetry purposes. It might be expressed in terms of normalized response signal intensity changes per absorbed dose of 1.0 Gy or a slope of the curve, i.e., "gel's response versus absorbed dose curve" [108]. It should be noted that the dosimetric sensitivity of gel depends on the irradiation type and evaluation method.

Usually, the dosimetric sensitivity is relatively low and depends on the concentrations of gel constituents and the type of radiation. In the case of UV-VIS evaluation, it varies: for nPAG gels, in the range of 0.03–0.11 Gy⁻¹ and for VIPAR, in the range of 0.01–0.06 Gy⁻¹, when the irradiation doses are from the range of 0–8.0 Gy [109]. The sensitivity might be enhanced by varying the composition of gels or admixing additional constituents. It should be noted that the mentioned dose sensitivity is sufficient for dosimetry in external radiotherapy; however, the sensitivity

of gels at high doses (> 40 Gy), which are used for patient treatment in Gamma knife facility, is below the registration limits [110].

Different compositions of nPAG and VIPAR type gels were evaluated after their irradiation to various doses using UV-VIS spectroscopy. Most promising of them were the following: nPAG^F containing of acrylamide 3 wt%, *N,N*'methylene bisacrylamide 3 wt%, 5 wt% of gelatin, 10 mM THPC with additives, ~ 89 wt% pure water and VIPARnd containing of *N*-vinylpyrrolidone 8 wt%, gelatin 7.5 wt%, *N,N*'methylene bisacrylamide 8 wt%, 32 mM cooper sulfate pentahydrate $\text{CUSO}_4 \cdot 5\text{H}_2\text{O}$, 0.0007 wt% of ascorbic acid. These composites were selected for a more detailed investigation.

Two batches of samples, containing 22 cuvettes filled with nPAG^F, and 11 cuvettes filled with VIPARnd were prepared. After storage for at least 24 hours, nPAG^F samples were irradiated up to 40 Gy in a linear accelerator (6 MeV electron beam) and both VIPARnd and nPAG^F gels in gamma knife facility (1.25 MeV, Co-60 source). A 16 mm open field collimator was selected for the dose realization, and all samples were irradiated at cuvette isocenter.

It should be noted that in order to avoid overheating of the accelerator system, e-beam doses to samples were delivered in sequences, 10 Gy each.

The dosimetric sensitivity of irradiated polymer gels was analyzed by using UV-VIS spectral characteristics of the irradiated samples that are provided in Figures 31–33.

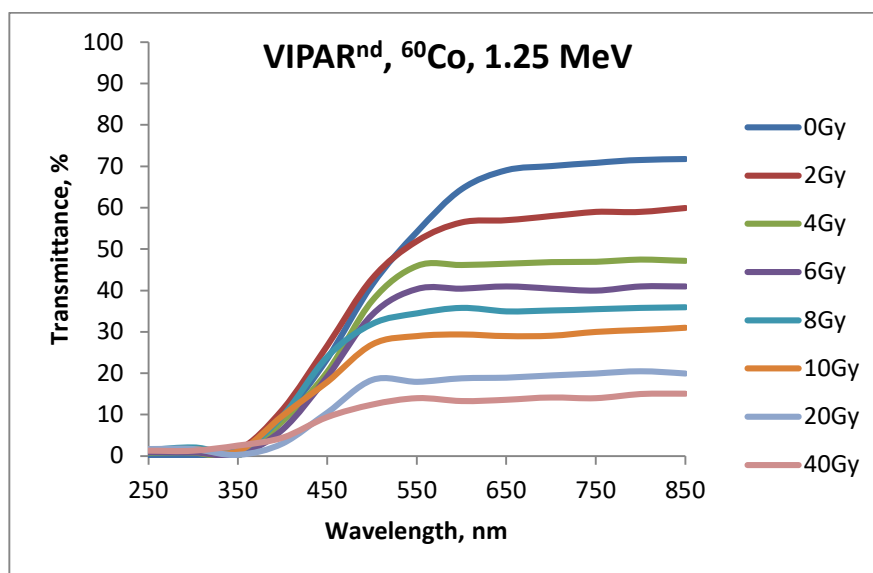


Fig. 31. Transmittance spectra of gamma irradiated VIPARnd gel

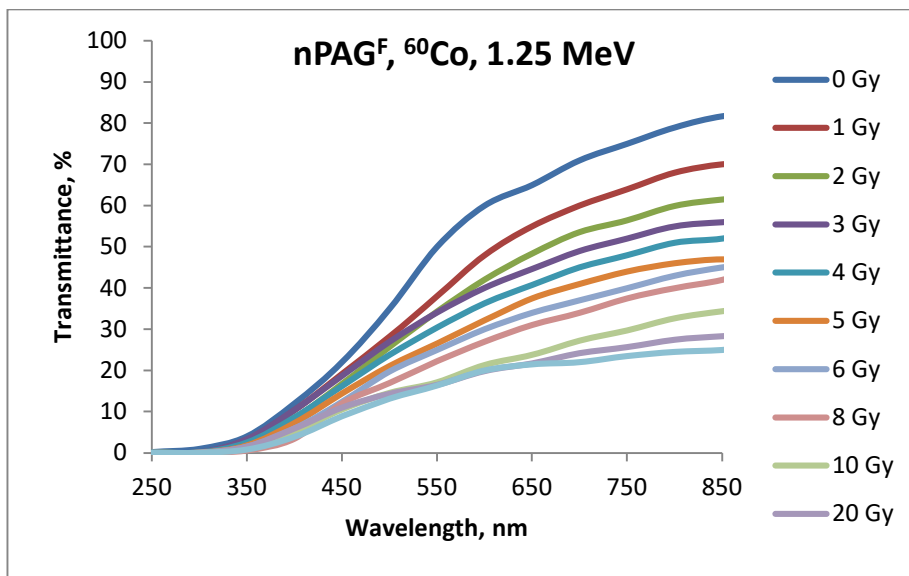


Fig. 32. Transmittance spectra of gamma irradiated nPAG^F gel

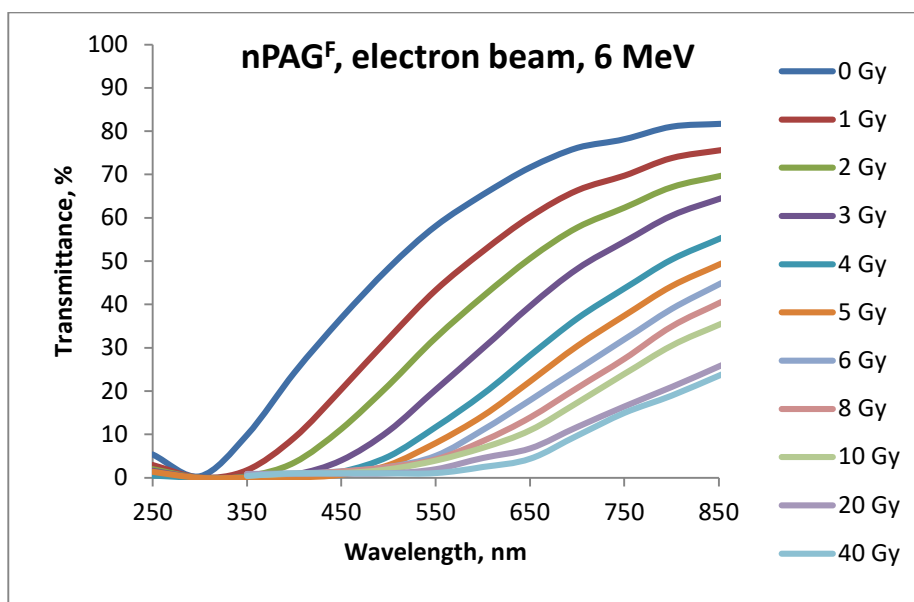


Fig. 33. Transmittance spectra of electron irradiated nPAG^F gel

It is known [101] that radiation induces polymerization in dose gels. Lower transmittance indicates higher yield of vibrational bonds in a sample, which may respond to the light from UV-VIS spectrophotometer [111, 112]. The yield of produced vibrational bonds depends on the dose absorbed by the gels and is directly linked with the polymerized amount of the irradiated sample. The polymerized part of the gel occupies the dose dependent volume and changes its color from almost

transparent to milky white at higher doses (ex. Fig. 22 d) and Fig. 24 b)). The irradiation of samples with higher doses leads to the formation of a denser polymer network.

Experimental UV-VIS spectroscopy results indicate that the polymerization proceeds differently in gels that are irradiated with gamma photons compared to the irradiation with electrons. Both types of gels irradiated in gamma knife facility show a similar decreasing tendency of transparency with the increasing irradiation dose. However, in the case of electron irradiation, the decreasing tendency of transmittance is followed by the “red shift” of gel’s maximum transparency at a certain irradiation dose. It may be explained by the different interaction processes of charged electrons and neutral gamma photons with a hydrogel. The electron beam is responsible for the direct interactions with monomer molecules (direct ionization), leading to the creation of different sized polymerized structures. Photons firstly interact with water in hydrogel creating active radicals, which are interacting with monomer molecules in the second step (indirect ionization). Due to this, the polymerization may start when a certain amount of radicals are created. The behavior of monomers upon irradiation will be discussed by analyzing the results of Raman spectroscopy.

Dosimetric sensitivity of polymer gels was assessed by analyzing the changes of their optical density (OD) at 750 nm wavelength after the irradiation with different beams (Fig. 34–36). The dosimetric sensitivity of gels was evaluated in two dose intervals: one ranging from 0 Gy to 10 Gy and the other one ranging from 10 Gy to > 40 Gy.

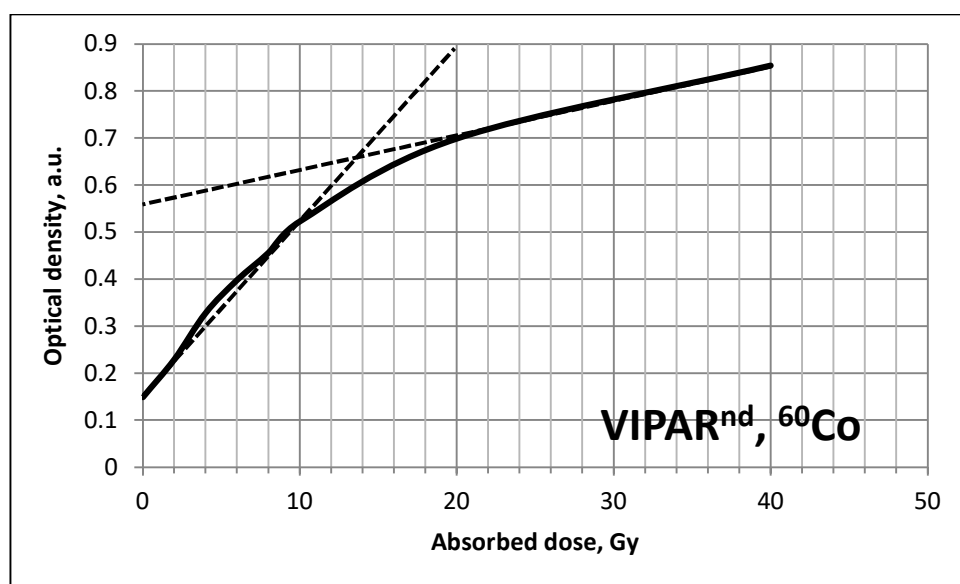


Fig. 34. OD changes of VIPARnd dose gel irradiated with gamma photons at 750 nm wavelength

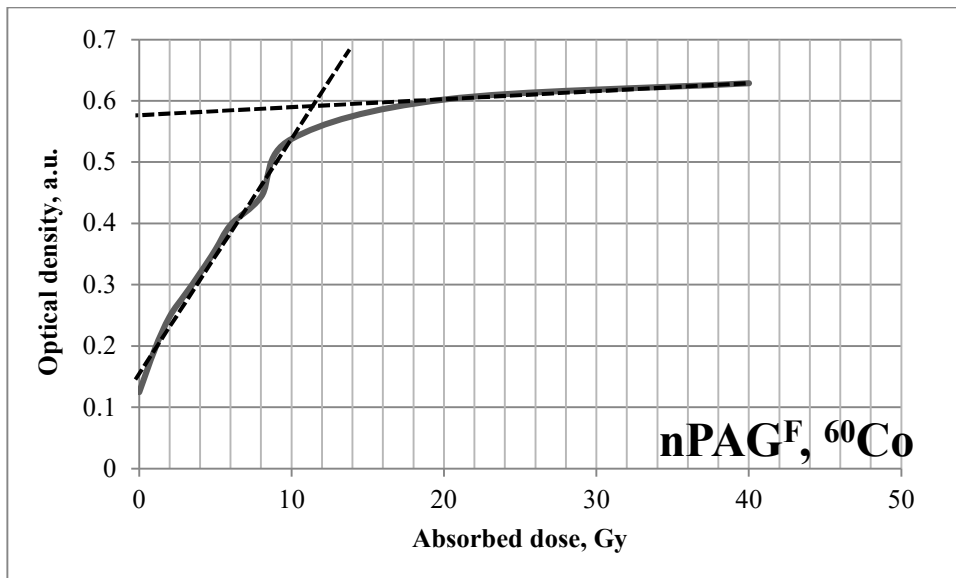


Fig. 35. OD changes of nPAG^F dose gel irradiated with gamma photons at 750 nm wavelength

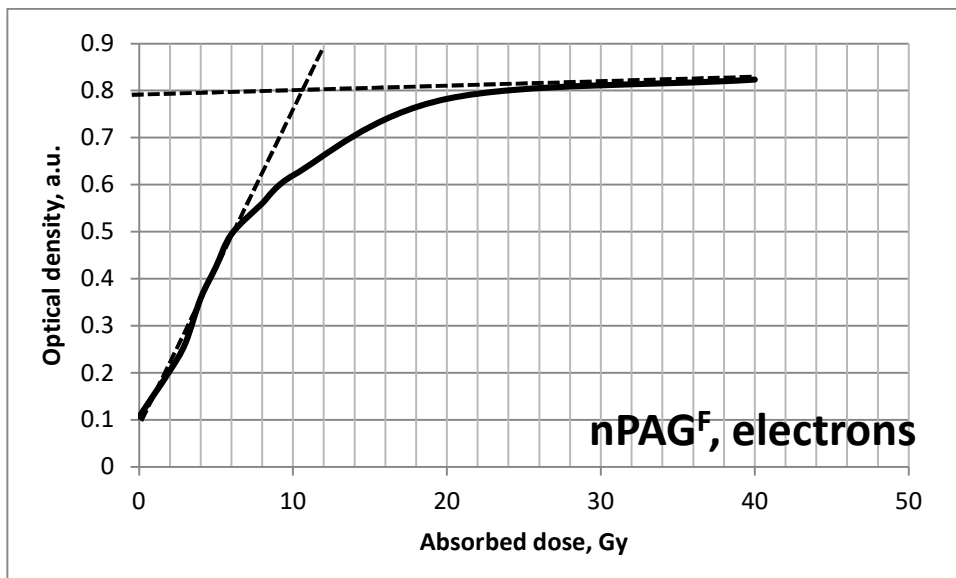


Fig. 36. OD changes of nPAG^F dose gel irradiated with electron beam at 750 nm wavelength

It has been found that all investigated gels were sensitive enough in the low dose region (0–10 Gy); however, the linearity in this range between the dose and OD was kept for ⁶⁰Co irradiation only. In the case of nPAG^F gel irradiation with electrons, a linear dependency was observed up to 6 Gy, indicating dose sensitivity of 0.0667 Gy⁻¹

¹. The estimated dose sensitivity of both gamma photons irradiated gels were 0.0516 Gy⁻¹ and 0.0357 Gy⁻¹ for nPAG^F and VIPARnd, respectively.

It was found that high dose (10 Gy to 40 Gy) irradiated VIPARnd dose gel demonstrated detectable sensitivity of 0.0075 Gy⁻¹, which is a very promising result for its application in the clinical radiosurgery treatment of patients when exploring the advantages of the gamma knife facility. The sensitivity of nPAG^F dose gels irradiated to high doses was below the acceptable detection limits.

4.2.2. Investigation of the optical density changes in the irradiated gels

It is known that the changes of mass density and optical density of irradiated gels are present due to the radiation-induced polymerization. The mass density of irradiated polymerized gels does not differ significantly from the freshly prepared gels; however, these changes are directly linked to the changes of the refraction index of irradiated material [112]. This correlation may be explained, according to the molecular optics, because refractive index results from the collective response of electric dipoles that are excited by the external applied field, and the number of dipoles in a given volume is closely related to the mass density. However, the optical density of material relates to the sluggish tendency of the atoms of a material to maintain the absorbed energy of the electromagnetic wave in the form of vibrating electrons before re-emitting it as a new electromagnetic disturbance. Taking into account that the radiation-induced polymerization process in dose gels depends on the absorbed dose and is based on the rearrangement of chemical bonds due to the redistribution of the supplied energy in the molecular structure, the optical density changes record the status of polymerization in the irradiated gel structures. Since the optical density is directly proportional to the refractive index of the investigated materials, the refraction index measurements may provide supplementary information regarding the radiation-induced polymerization of samples.

The variations of refractive index were investigated in nPAG^F and VIPARnd gels irradiated with gamma photons up to 10 Gy in the gamma knife facility. The samples were irradiated from the bottom side, delivering the maximum dose to the preselected isocenter at a certain depth in the vial. This irradiation geometry was selected with the purpose of achieving the step dose gradient at the boundary between the treated volume and the rest of the gel.

After the irradiation of samples, *Controlled heating method* that is described in Materials Characterization Methods chapter was applied in order to separate the polymerized part of the gel (solid structure) of each sample from the non-polymerized part of the gel, which was liquefied due to pre-heating of samples. The refraction index values measured for the not-polymerized gel parts of all samples have not indicated any significant changes that could be attributed to the application of different irradiation dose (Fig. 37).

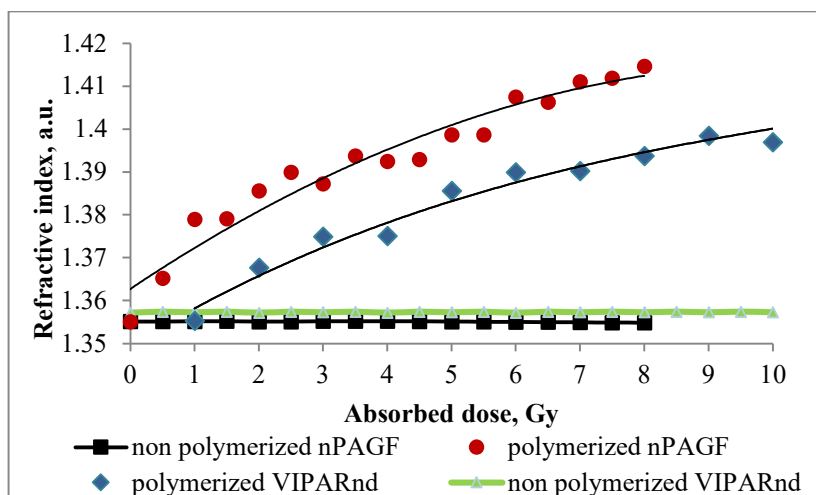


Fig. 37. Absorbed dose related refractive index of polymerized gels irradiated with gamma photons

The separated parts of polymerized gels were liquefied by the additional heating, and the refraction index measurements were performed. The obtained refractive index values indicated increasing but not linear tendency with the growing absorbed dose value for both investigated gels. nPAG^F gel showed slightly higher sensitivity as compared to VIPARnd gel, thus supporting dosimetric sensitivity assessment results that were obtained by analyzing the optical density changes related to UV-VIS spectroscopy results. The observed small deviations from direct dose dependency of the refractive index may be attributed to the fact of heating, which was applied for the liquefaction of gels, since additional, even small, amount of energy was supplied to the polymerizable structures. Similar tendencies of refraction index changes were observed by other authors as well [113, 114].

4.2.3. Analysis of polymerization processes in irradiated dose gels using Raman spectroscopy

In order to assess the radiation-induced polymerization of gels, Raman spectroscopy was applied. The polymerization processes in the irradiated dose gels are related to molecular level structural changes that are mainly related to the breakage of C=C or C=O bonds and formation of single-bonded structures, like C-C, C-H, and others. These processes may be assessed by investigating Raman scattering phenomena in irradiated gel samples; however, prior to start Raman spectra analysis of irradiated dose gels, Raman spectra of pure materials (Aam, BIS, gelatin, VIPE-*N*-vinylpyrrolidone), which are provided by manufacturers, were examined (Fig. 38).

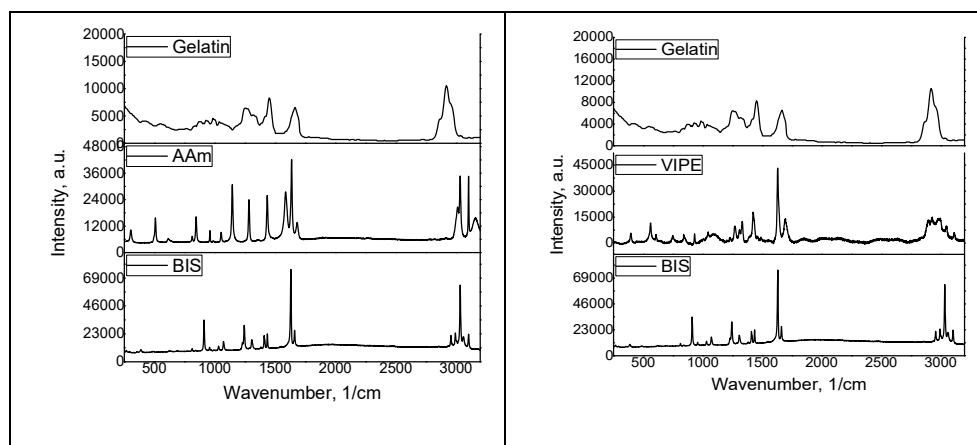


Fig. 38. Raman spectra of pure materials

The main Raman peaks of interest were identified as follows:

- **AAm:** 1142 cm^{-1} ($\nu\text{C-C}$, polyacrylamide), 1294 cm^{-1} (vinyl δCH), 1438 cm^{-1} ($\delta\text{CH}_2 + \nu\text{C-N}$), 1450 cm^{-1} (alkyl δCH_2 , gelatin/polyacrylamide), 1643 cm^{-1} ($\nu\text{C}=\text{C}$), 2936 cm^{-1} (alkyl νCH , gelatin/polyacrylamide), 3002 cm^{-1} (νSCH_2).
- **BIS:** 1249 cm^{-1} (vinyl δCH), 1429 cm^{-1} ($\delta\text{CH}_2 + \nu\text{C-N}$), 1634 cm^{-1} ($\nu\text{C}=\text{C}$), 3032 cm^{-1} (νSCH_2).

nPAG^F dose gels: two experiments have been performed. In the first experiment, the differences of polymerization processes in X-ray beam (Fig. 39) and electron beam (Fig. 40) irradiated (energy of both beams 6 MeV, low dose irradiation) nPAG^F gels were analyzed. The sample irradiation with X-ray photons was chosen for the simplification of the experiment, because X-photon and e-beam irradiation may be realized in the same linear accelerator.

It should be noted that the initial Raman peak position of gel components in gel solutions were different, compared to the pure materials; however, the appearance tendency of the peaks in Raman spectra remained.

The main Raman peaks, which are recording the status of polymerization in X-ray irradiated nPAG^F gels, were identified at 1114 cm^{-1} ($\nu\text{C-C}$, polyacrylamide), 1249 cm^{-1} (vinyl δCH , BIS), 1284 cm^{-1} (vinyl δCH , acrylamide), 1440 cm^{-1} ($\delta\text{CH}_2 + \nu\text{C-N}$, polyacrylamide/gelatin), 1630 cm^{-1} ($\nu\text{C}=\text{C}$, BIS), 1639 cm^{-1} ($\nu\text{C}=\text{C}$, acrylamide), and 2940 cm^{-1} (alkyl νCH , gelatin/polyacrylamide).

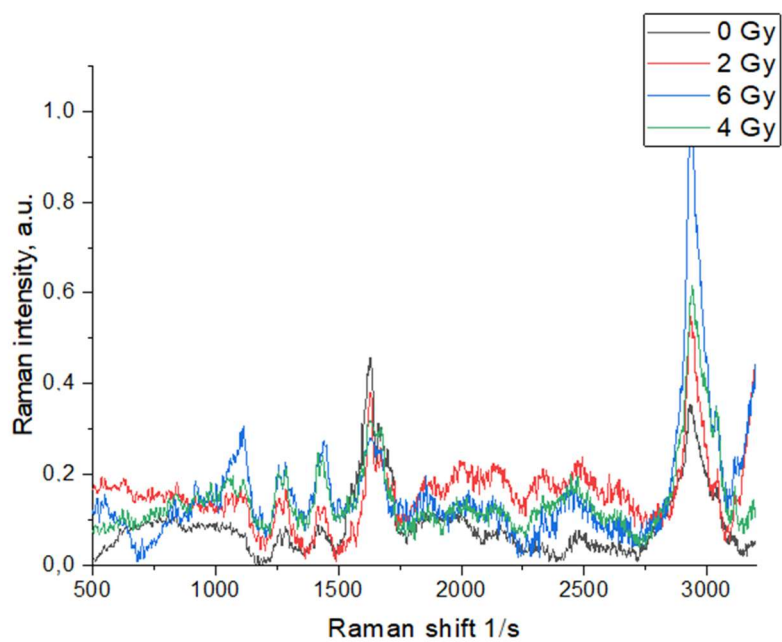


Fig. 39. Full Raman spectrum of nPAG^F dose gels irradiated with 6 MeV X-ray photons

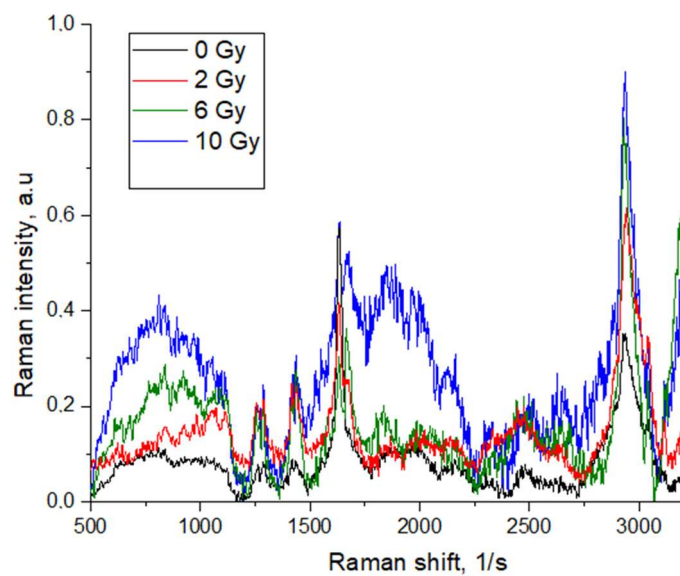


Fig. 40. Full Raman spectrum of nPAG^F dose gels irradiated with 6 MeV electrons

In the case of nPAG gel irradiation with electrons, the following peaks were identified: 1113 cm^{-1} ($\nu\text{C-C}$, polyacrylamide), 1263 cm^{-1} (vinyl δCH , BIS), 1288 cm^{-1}

¹ (vinyl δ CH, acrylamide), 1436 cm^{-1} (δ CH₂+ ν C-N, polyacrylamide/gelatin), 1631 cm^{-1} (ν C=C, BIS), 1639 cm^{-1} (ν C=C, acrylamide), and 2936 cm^{-1} (alkyl ν CH, gelatin/polyacrylamide). The increasing tendency of Raman spectrum at $> 3200 \text{ cm}^{-1}$ that is clearly seen in the Raman spectra of irradiated gels is related to hydrogen in water, and the peaks in the range of 600–1000 cm^{-1} may correspond to THPC, which can fulfil the function of oxygen scavenger or react with other constituents [115–117].

A detailed information, regarding the measured Raman peaks in X-ray and electron beam irradiated nPAG^F gels that has been provided by other authors is shown in Table 11.

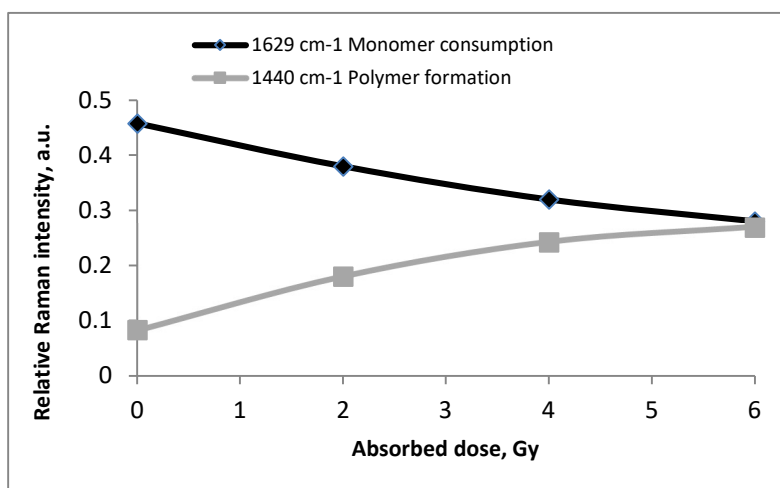
Table 11. The main vibrational band assignments for nPAG gels

nPAG gels					
Chemical component	Vibrational band assignments for nPAG gels	Band position, cm^{-1}			
		Pure materials /from https://spectra base.com/	In dose gels/ (e-beam)	In dose gels/ X-rays	Other authors
Polyacrylamide	ν C-C	1126			
	δ CH ₂ + ν C-N	1450	1436	1440	1439 [115]
Acrylamide		1114	1113	1114	
	vinyl δ CH	1294	1288	1285	1253 [114] 1256 [118] 1280 [115] 1285 [116]
	ν C=C	1634		1639	
BIS acrylamide	vinyl δ CH	1256	1263	1260	1629 [114] 1654 [119]
	ν C=C	1629	1631	1629	
Water		3256	3221	3221	3256 [116] 3360 [120]
THPC		838	839	838	785 [115] 1064 [118]
Gelatin/ polyacrylamide	alkyl ν CH	2936	2931	2929	

The tendencies of Raman peak intensity changes are signaling the polymerization processes, the most important of which is monomer to polymer transformation. The radiation-induced polymerization is a basic process of various materials (including dose gels) formation. The properties of these materials are dependent on the polymerization level, which is directly related to the absorbed dose. The irradiation dose defines the polymerization level, the properties of which are dependent on the level of polymerization.

The level of polymerization is strongly dependent on the radiation-induced chain reactions, which transform C=C bonds (monomer) into C-C bonds (polymer) [121]. In this research, several Raman peaks were addressed to C=C double bonded monomers, i.e., in acrylamide (1285 cm^{-1} and 1639 cm^{-1} in X-ray irradiated gels and 1288 cm^{-1} for electron beam irradiated gels) and BIS (1260 cm^{-1} and 1629 cm^{-1} in X-ray irradiated gels and 1631 cm^{-1} in e-beam irradiated gels). Due to the consumption of monomers, the intensities of these bands were decreasing with the increasing irradiation dose.

However, the intensities of Raman peaks at 1440 cm^{-1} and especially at 2940 cm^{-1} for X-ray irradiated gels and 1436 cm^{-1} and 2936 cm^{-1} for e-beam irradiated gels were steadily increasing, since they recorded vinyl group formation (C-C bonds in polymerized structure) in the gelatin matrix. The effectiveness of polymerization was assessed by comparing the consumption of monomers and the formation of polymers. According to the literature sources [123], this can be done by comparing Raman intensity changes of BIS at $\sim 1630\text{ cm}^{-1}$ that are corresponding to the vibrational mode of ($\nu\text{C}=\text{C}$) and polyacrylamide at $\sim 1436\text{ cm}^{-1}$ ($\delta\text{CH}_2 + \nu\text{C}-\text{N}$, polyacrylamide/gelatin). The changes in gelatin in the low dose region are mainly caused by THPC and completed before the irradiation. Therefore, the band at $\sim 1436\text{ cm}^{-1}$ is applicable for the evaluation of the radiation generated pure CH_2 (C-C bonds). Both monomers, acrylamide and BIS acrylamide, are participating in the polymerization process; however, BIS acrylamide was chosen for the evaluation. The selection of BIS as reference monomer was based on the fact that this monomer is responsible for crosslinking and formation of polymer network. The evaluation of polymerization processes in X-ray and e-beam irradiated gels is provided in Fig. 41. A and B.



A

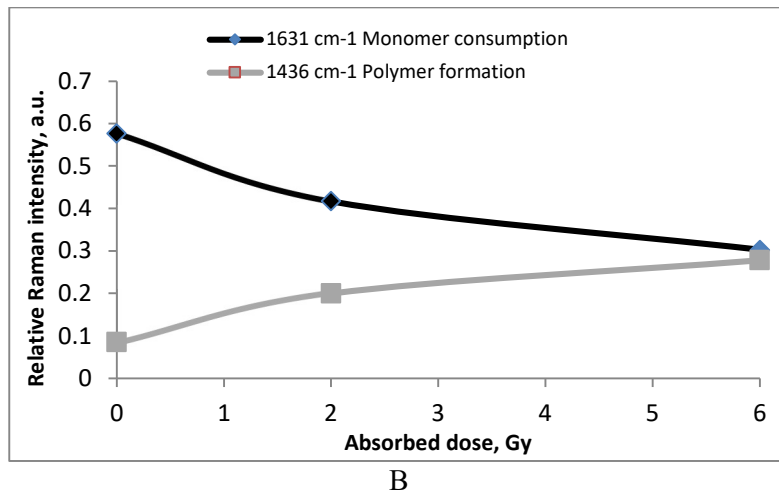


Fig. 41. Polymerization of nPAG^F dose gels: A) irradiated with 6 MeV X-ray photons, B) irradiated with 6 MeV electron beam

It has been found that with the increased dose monomer consumption generally followed a monoexponential decay curve, as it was shown in [75, 116]. Since e-beam interaction with matter is responsible for direct ionization, the polymerization processes were faster in e-beam irradiated nPAG^F gels. It has been found as well that a clear separation of corresponding Raman peaks for e-beam irradiated nPAG gels was possible only for relative low doses (up to 6 Gy), as it is shown in Fig. 41. Due to the direct ionizing radiation-induced relative fast generation of a high number of monomer radicals and possible their interaction with gelatin, the characteristic Raman peaks of monomers were starting to overlap with gelatin peaks at higher doses. This result fits well with the previous findings obtained when performing UV-VIS assessment of irradiated gel (see Fig. 34): the linearity of OD-Dose curve was observed in the range from 0 to 6 Gy as well.

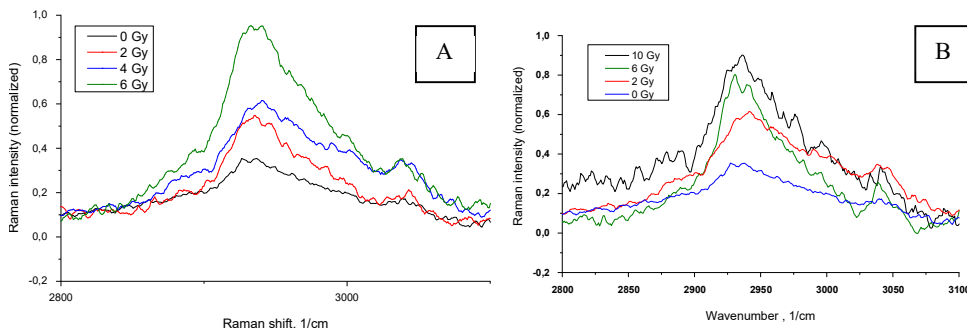


Fig. 42. Raman spectrum segments of nPAG gels: A) electron beam irradiated, B) X-ray irradiated

It should be noted that the polymer formation process may be assessed based on the changes of formation of a vinyl ν CH Raman peak at the position of $\sim 2936 \text{ cm}^{-1}$; however, there are some difficulties how to extract pure information about the polymer formation, since gelatin band and hydrogen water related spectral bands are overlapping. Nevertheless, the tendencies could be followed (Fig. 42).

VIPARnd dose gels: in order to access the polymerization properties in higher dose irradiation, Raman spectroscopy was applied, and the structural changes at molecular level were examined in VIPARnd dose gels irradiated in Gamma knife unit with ^{60}Co source up to 40 Gy (Fig. 43). Since the main constituents in this gel are *N*-vinylpyrrolidone (syn. 1-vinyl-2-pyrrolidone), crosslinker BIS acrylamide, gelatin and water, the positions of the main Raman peaks for each component was extracted from the standard spectra provided by SpectraBase TM [<https://spectrabase.com>]:

- PV/PVP (VIPE): 1225 cm^{-1} (CH_2 twisting vibration), 1312 cm^{-1} (CH_2 wagging), triplet 1425 cm^{-1} , 1447 cm^{-1} , 1465 cm^{-1} (C-N stretching), 1659 cm^{-1} (C=O, carbonyl stretching vibration), and 2935 cm^{-1} (νCH),
- BIS acrylamide: 1249 cm^{-1} (vinyl δCH), 1429 cm^{-1} ($\delta\text{CH}_2 + \nu\text{C-N}$), 1634 cm^{-1} ($\nu\text{C=C}$), 3032 cm^{-1} (νsCH_2).

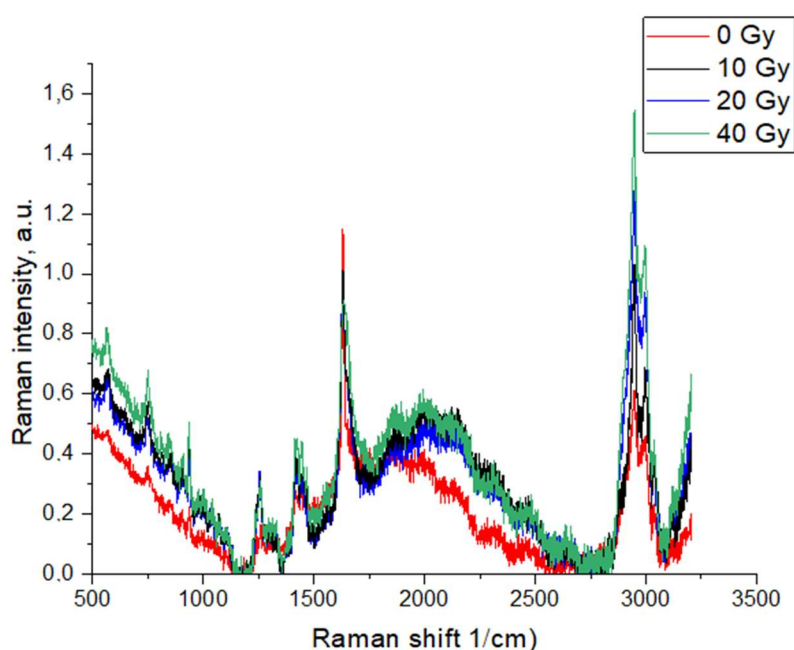


Fig. 43. Full Raman spectrum of VIPARnd dose gels irradiated with ^{60}Co gamma photons

The Raman peak positions identified for *N*-vinylpyrrolidone based VIPARnd gel are provided in the Table 12.

Table 12. The main Raman vibrational band assignments for VIPARnd gels

VIPAR nd				
Chemical component	Vibrational band assignments for	Band position, cm ⁻¹		
		Pure materials /from https://spectrabase.com/	In dose gels/ Gamma photons	Other authors
<i>N</i> -vinyl pyrrolidone	δCH ₂	1125	1108	
	CH ₂ wagging	1312		
	C-N stretching	1425	1425	
		1447	1446	1436 [120]
		1465	1465	
	C=O stretching	1659	1665	1685[117] 1690 [118] 1659 [119]
BIS acrylamide	vinyl δCH	1256	1255	1221 [119]
	vC=C	1629	1630	1630 [118]
Water		3256		
THPC	v(C-COOH)		969	
<i>Poly</i> -vinylpyrrolidone/gelatin	vC-H stretching	2935	2947	2933 [119]

The **behavior of** VIPARnd dose gels irradiated to high gamma **photon** doses (up to 40 Gy) were analyzed by using Raman scattering information at 1630 cm⁻¹, related to BIS acrylamide **monomer** consumption (breaking of C=C bonds). It should be noted that this peak is usually located relatively close to the peak, characterizing carbonyl stretching vibrations (C=O), which are usually characterized by the Raman peak at ~ 1658 cm⁻¹ [117]. Carbonyl stretching vibrations (C=O) are sensitive to the physical condition of the sample preparation and examination [124]. Due to the irradiation and water absorption, the stretching vibrations of carbonyl group are intending to decrease and might shift from higher frequency to lower values. In this case, the intensity of this peak at 1665 cm⁻¹ was very low/negligible, since freshly prepared gels were immediately tightly sealed in vials, trying to avoid any atmospheric influence on their properties.

Gamma photon-induced polymerization was assessed by analyzing the increasing with the dose intensities of Raman peaks that are characterized by symmetric C-H stretching modes at 2947 cm⁻¹ and 2997 cm⁻¹. Due to the specific structure of polymer network in irradiated VIPARnd gels, these vibrational modes almost do not overlap with other bands up to high doses [115] and provide more accurate information, regarding the polymer formation processes. Raman spectrum

segments that are corresponding to the discussed molecular bonds are provided in Fig. 44.

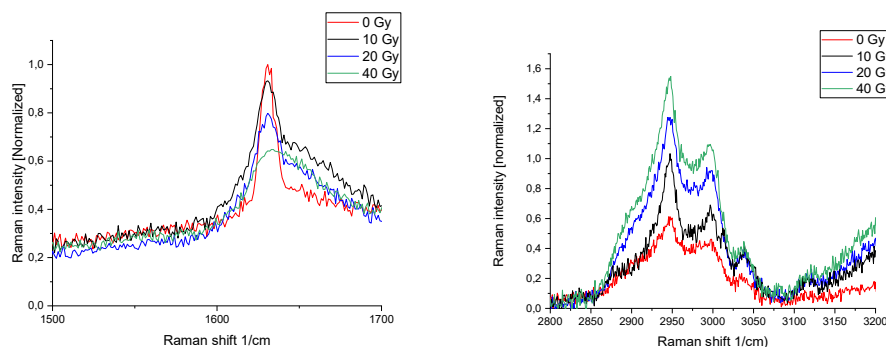


Fig. 44. Raman spectrum segments for gamma irradiated VIPARnd gels

Based on the performed analysis, the polymerization tendencies were estimated (Fig. 45).

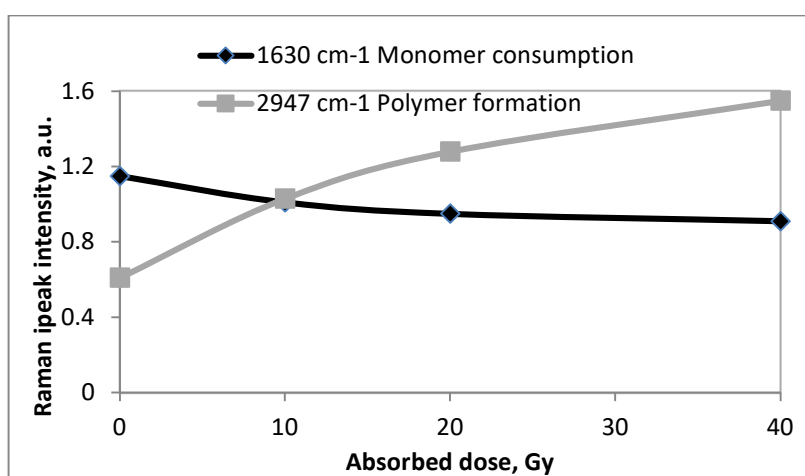


Fig. 45. Raman spectrum segments for gamma irradiated VIPARnd gels

It has been found that in both competing processes, i.e., monomer consumption and polymer formation, the rates were similar and slightly more intense for the polymerization part. The process was observed within a very broad dose region, indicating the potential of VIPARnd gels for high dose dosimetry applications.

It should be noted that overall, in each gel component, the amount of this component in gel solution is contributing to the shape of the Raman spectrum.

4.2.4. X-ray attenuation properties of dose gels

One of the main points in dosimetry is the tissue equivalency of detector material. This can be assessed by performing CT scans and obtaining Hounsfield units (or CT units), which are automatically calculated when performing CT scans.

For this reason, nPAG gel filled cuvettes (Fig. 47) were irradiated with 6 MeV electrons and underwent CT scanning.

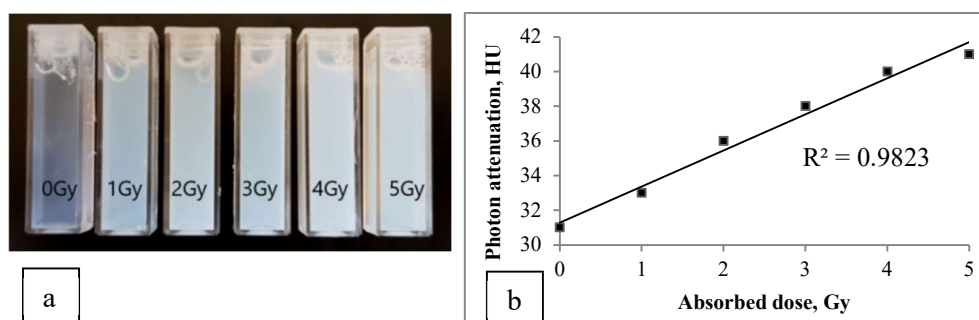


Fig. 46. a) nPAG cuvettes irradiated in linear accelerator with 6 MeV electrons b) dose dependency of e-beam attenuation in the irradiated gels

It has been found that the absorption of e-beam, as expressed in CT units, was slightly (linearly) increasing in the irradiated gels (Fig. 46. b) with the increased dose and was well in line with the CT values provided for the soft tissue [+ 30 - + 80] HU, thus indicating the applicability of the dose gels for medical dosimetry purposes.

Taking into account that the results provided in this thesis will be implemented in clinical routine and especially in radiosurgery, another batch of nPAG^F gels was irradiated in Gamma knife facility with gamma photons up to 24 Gy. As in the previous case, the irradiated gels were scanned in CT unit, and the attenuation properties in terms of CT units were analyzed.

The obtained results demonstrated a linear dose dependency of photon attenuation up to 12 Gy (Fig. 47).

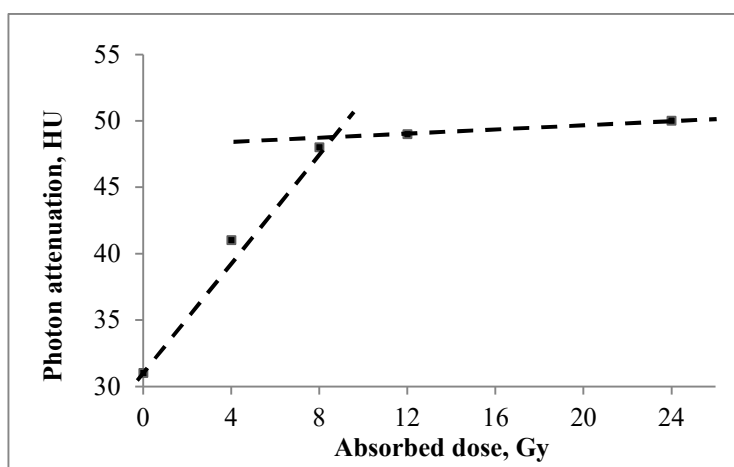


Fig. 47. Dose dependency of X-ray attenuation in nPAG^F gels irradiated with gamma photons

This fits well with the results of other authors [125, 126]. There were some attempts to assess the dose sensitivity in the relationship with CT units; however, it was found that the normalized dose sensitivity for doses up to 12 Gy was 0.0425 Gy^{-1} , compared to the very low dose sensitivity in the high dose region, where it was 0.005 Gy^{-1} only. The obtained results were similar to those provided by other researchers [127–129]. Having in mind that additional X-ray exposure (additional dose, which is not accounted) for the already irradiated samples is needed, this method was not considered for further developments.

4.2.5. Evaluation of polymerized gel properties using magnetic resonance imaging

Seeking to find out the most sensitive method for the evaluation of developed gels, MR imaging was explored for the assessment of radiation-induced changes in the irradiated gels.

The MR imaging is considered a golden standard for the visualization of dose distribution in the irradiated gels; however, due to the high examination costs and high load of facility in the clinic, its exploration is limited. The outlined situation explains why only very limited research information could be found regarding the MRI evaluation of high dose irradiated dose gels. Another almost unexplored issue is the possible application of MRI for the assessment of doses in small-scale (millimeter range) dosimetry, which might be easily realized by using dose gels.

4.2.5.1. Evaluation of dose sensitivity using MRI scanning method

Seeking to find out the most sensitive method for the evaluation of developed gels, MR imaging was explored for the assessment of radiation-induced changes in the irradiated gels.

A set of nPAG^F gels was irradiated with gamma photons in Leksell Gamma Knife© Icon™ unit. The experimental samples were irradiated with doses of 1, 2, 4, 6, and 8 Gy, respectively, keeping the same dose rate of 3.182 Gy/min. In order to minimize the uncertainties, the coordinates of the irradiation center (X, Y, Z: 100, 100, 100 mm) were the same for all gel samples. The irradiated gels were scanned by using MRI unit Siemens MAGNETOM Avanto 1.5T, choosing a 64 multiple spin-echo pulse sequence as a T2 weighted base sequence and a head coil (He 4,4). Two TE parameters were chosen: 89 ms and 145 ms, slice thickness was 2.5 mm, repetition time 4320 ms, and FoV 453*500 mm² and 348*512 mm², respectively.

The scanned images of irradiated gel samples were evaluated by analyzing the pixel values at the points of interest within the irradiated area, and the average pixel intensity that is corresponding to the irradiation dose was found for different echo times that were applied during the scanning, as it is shown in Fig. 48.

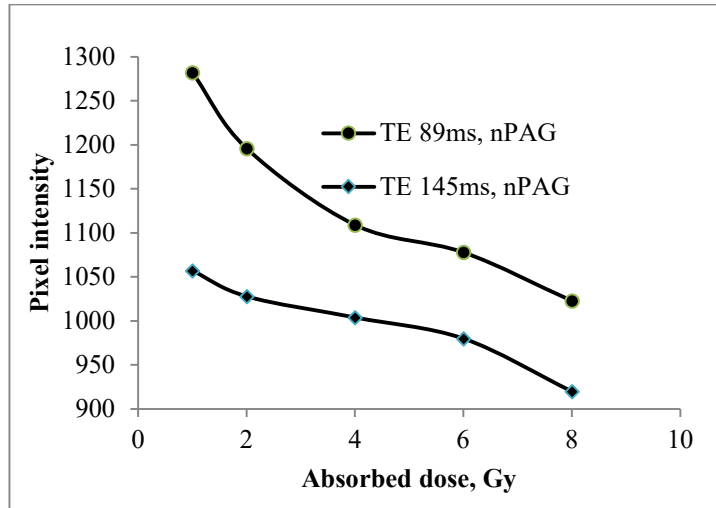


Fig. 48. Variations of pixel intensities with a dose of nPAG^F samples at the selected points in MRI scans obtained by applying different echo times

It is known that the optical density is a parameter, which responds to gel property changes due to the radiation-induced polymerization. However, the optical density of a material is a common parameter for the evaluation of gel dose sensitivity, using different analysis methods. Due to this pixel values that were registered, the MRI scans were converted to the corresponding optical density, and a dose sensitivity curve for Gamma knife irradiated nPAG^F samples was constructed (Fig. 49).

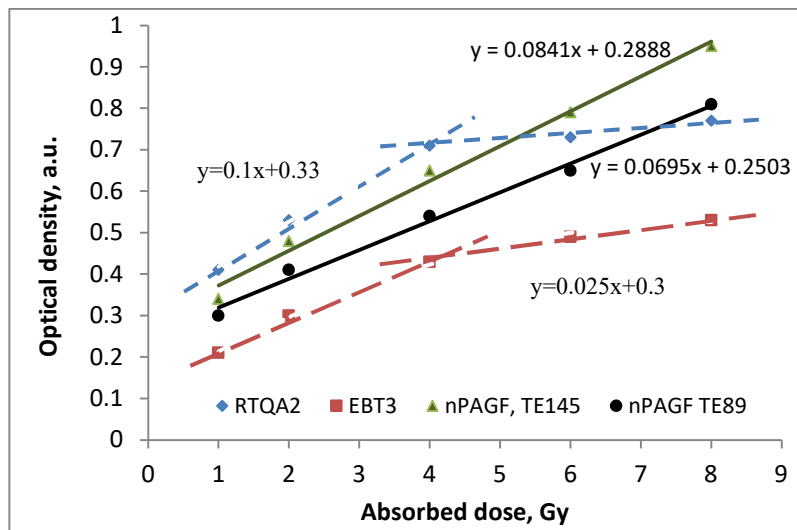


Fig. 49. Comparison of dose assessment sensitivity using MRI and Gafchromic films

The results of a standard film dosimetry are shown in Fig. 49. This method was used in order to verify the dose evaluation results that were obtained by using MRI, two types of Gafchromic films, RTQA2, EBT3, were prepared for the irradiation (see Methods sub-chapter 3.3.2.) and placed in the central position inside a specific film holder of Gamma knife facility for the irradiation. The film holder is calibrated for performing gamma knife quality control procedures using gafchromic films. The central position of the film holder is the already known stereotactic space coordinate: (100, 100, 100) mm. Therefore, all the films were irradiated with doses in the range of 1, 2, 4, 6, and 8 Gy, under the same conditions as dose gels. The irradiated films were scanned by using open code software NAPS2 (version 6.1.2.25834) and analyzed using open code image analyzer software ImageJ (1.52p version). The scanned films are shown in Fig. 50.

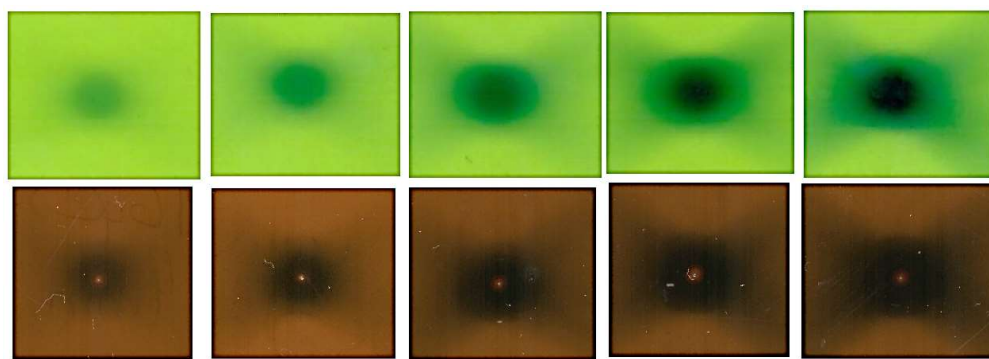


Fig. 50. Gafchromic EBT3 films (top row) and RTQA2 films (bottom row) irradiated in Gamma knife facility using 4 mm collimator to doses 1 Gy, 4 Gy, and 6 Gy, respectively

In order to compare the sensitivity of both methods, the registered pixel values that were obtained by analyzing gafchromic film images were converted to the optical density.

It has been found that the RTQA2 films were more sensitive compared to the scanned MR images; however, due to the specific features of the film composition, both films showed a saturation tendency at higher doses [130]. The MRI evaluated dose dependency of the irradiated gels was almost linear within the dose region up to 10 Gy. The method was a bit more sensitive when 145 s time echo sequence was used for the evaluation. The estimated highest sensitivity of nPAG^F gel was 0.0841 Gy⁻¹ and was higher compared to the one estimated from UV-VIS measurements.

Considering that in literature, the dosimetric sensitivity of irradiated dose gels is discussed sometimes in terms of spin-spin relaxation rate (R_2), which is one of the parameters of MRI evaluations [131], a normalized dependency between the absorbed dose and relaxation time was constructed from the MRI scans of dose gels (Fig. 51).

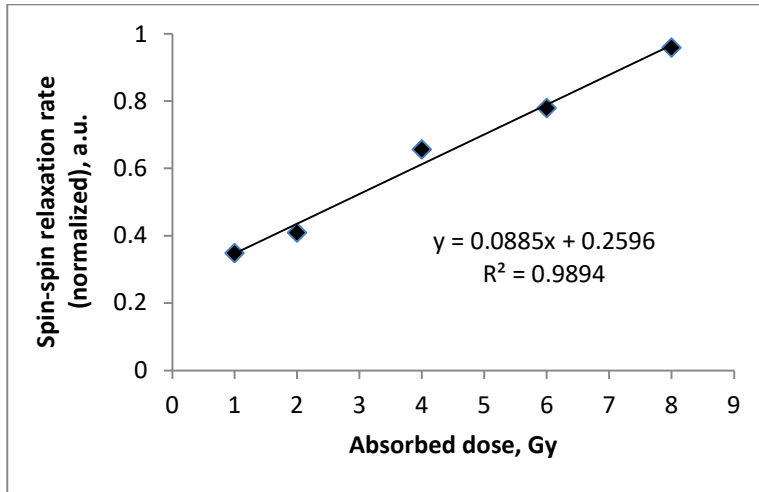


Fig. 51. Spin-spin relaxation rate R2 versus absorbed dose curve constructed for Gamma knife irradiated nPAG^F dose gels

The linear dose response was found for spin-spin relaxation rate in the dose range between 0–8 Gy, and the tendency was very similar to that reported by other authors for basic nPAG gel [132, 133]. The dosimetric sensitivity of nPAG^F gel that has derived from this measurement was 0.088 Gy⁻¹, which is very close to that evaluated for the same nPAG^F gel, keeping echo time of 145 ms as the main parameter.

4.2.5.2. Dose mapping using polymerizable nPAG^F gels

It is known [2] that gel dosimetry is the only method, which may record 3D dose distributions in the volume. The 3D images may be reconstructed from a set of 2D scans that are performed using MRI unit.

In order to assess the possibility of getting planar dose distributions (dose maps) from the MRI scans of high dose irradiated gels, five nPAG^F gel filled vials were irradiated with five different doses, ranging from 10 Gy to 43.3 Gy (10 Gy, 13 Gy, 18.6 Gy, 26 Gy, 43.3 Gy), respectively. The irradiation was performed in Gamma knife facility, according to the treatment plans that were simulated using Gammaplan treatment planning system, as it is indicated in Fig. 52. The irradiated dose gels were scanned with 1.5T MRI Siemens MAGNETOM unit, using the following parameters: FoV 208x230 mm², T2 sequence, sagittal axis, TE 89 ms and 145 ms, TR 4340s; Weasis v2.5.0 software was used for viewing images.

The MRI scans of the irradiated dose gels are provided in Fig. 53.

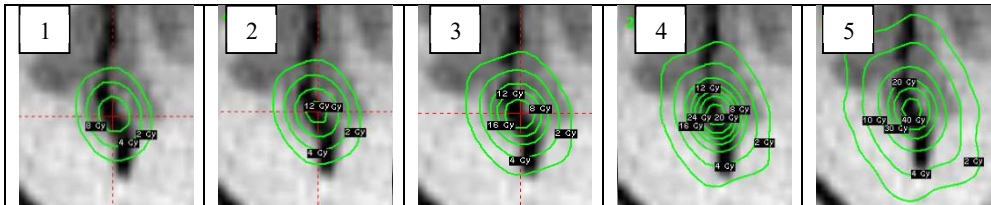


Fig. 52. Gammaplan TPS simulated dose distributions with D_{max} in the isocenter: 1–10 Gy, 2–13 Gy, 3–18.6 Gy, 4–26 Gy, 5–43.3 Gy

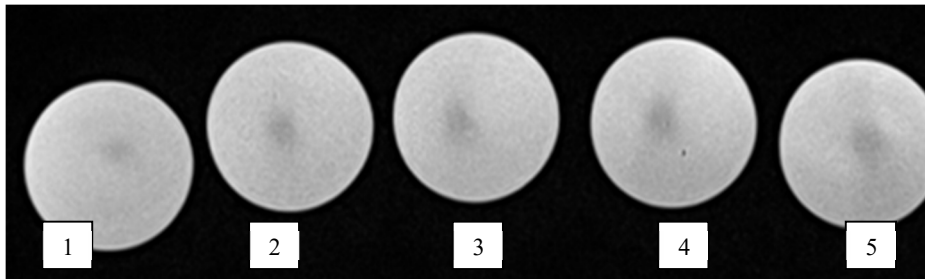


Fig. 53. MRI scanned nPAG^F dose gel image: 1–10 Gy, 2–13 Gy, 3–18.6 Gy, 4–26 Gy, 5–43.3 Gy

The pixel information that was obtained when analyzing MRI scans of the irradiated gels was used for the reconstruction of planar dose distributions in the form of dose maps that were created by applying a special homemade algorithm that was written by using the MatLab R2016b programming platform (see Annex 2). The dose mapping results (Fig. 54) allow demonstrating the polymerized part shape changes in the gels with the increasing dose and distinguishing between the differently irradiated points.

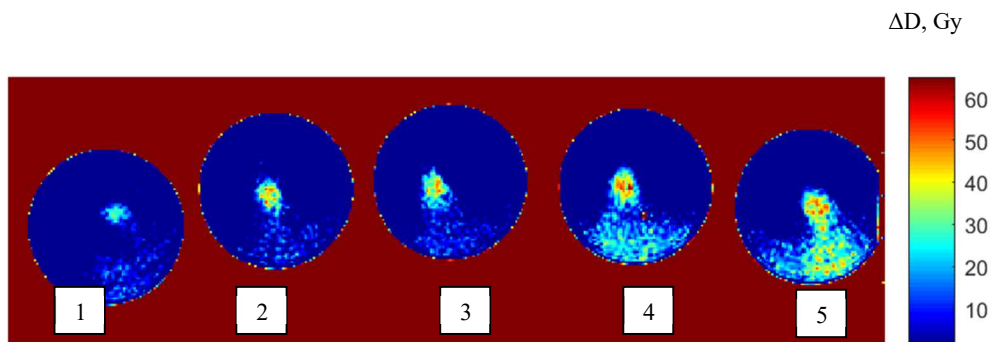


Fig. 54. Dose distribution maps of irradiated nPAG^F dose gels created using Matlab programming software: 1–10 Gy, 2–13 Gy, 3–18.6 Gy, 4–26 Gy, 5–43.3 Gy

The performed pilot investigation that is based on the reconstruction of MRI images and creating dose distribution maps of irradiated gels, using mathematical

approach, indicates a high potential of this method for clinical gel dosimetry applications, especially in radiosurgery, using gamma knife treatment where high doses are used to treat small-scale objects.

4.2.5.3. Comparison of dosimetric features of nPAG^F and VIPARnd gels

Radiation-induced polymerization processes are strongly dependent on the gel chemical constituents and their concentrations. This predicts that the polymerization processes will proceed differently in differently composed gels and will contribute significantly to the changes of properties of irradiated dose gels.

In order to assess the dose sensitivity of differently composed gels, two sets of nPAG^F and VIPARnd dose gel samples were prepared for the small-scale irradiation experiment by using Gamma knife IconTM unit. The irradiation was performed according to the simulated dose plan that was created using Gamaplan TPS. The collimators of 4 mm and 8 mm were used for the irradiation, which was performed in two shots for both nPAG^F and VIPARnd dose gels. The first shot was realized at (100, 130, 100) mm location, the second shot at (90, 120, 110) mm location. The treatment time for the first shot was 12.12 min, for the second 8.14 min; 12.0Gy@50% prescribed dose was used for the irradiation. The dose rate at the focus point was 1.91 Gy/min during the first shot and 2.85 Gy/min during the second shot. Both gels were scanned with MRI, using the same parameter settings: T2, TSE transversal sequence, head coil element, voxel size (0.4 x 0.4 x 5.0) mm³, FoV- 230 mm, TR 4080 ms, and a few variations of TE (11, 89, 145 ms) following the recommendations [134].

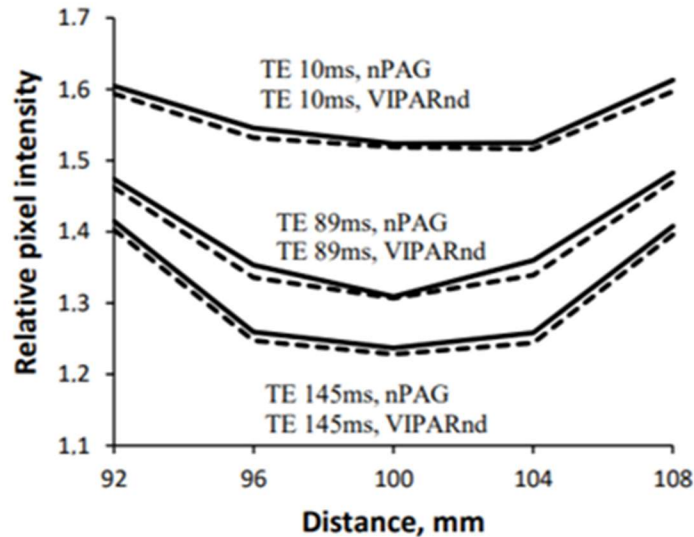


Fig. 55. Relative pixel intensity variations in MRI scanned irradiated dose images after the first shot at the first target

The results of the first shot for both gels are provided in Fig. 55 and the results of the second shot in Fig. 56.

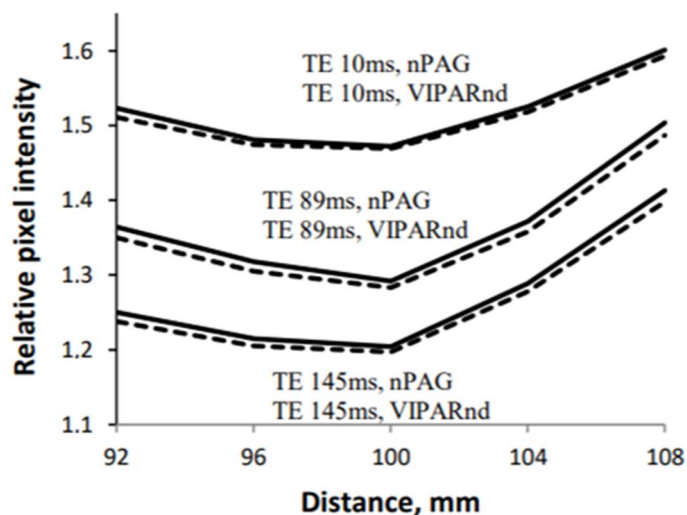


Fig. 56. Relative pixel intensity variations in MRI scanned irradiated dose images after the second shot at the second target

As it was already discussed in the previous chapters, the MR images are dependent on the echo time (TE) that is used for scanning. It was shown that the application of longer TE results in lower pixel intensities, which in turn contribute to the increased resolution of DICOM images [135] and allow for distinguishing more intensive (higher dose irradiated) parts of the scanned MR image. The obtained information was used for the calculation of T2 relaxation time, comparing the results that were obtained using different TE values in both gels and from both shots (Fig. 57 and Fig. 58).

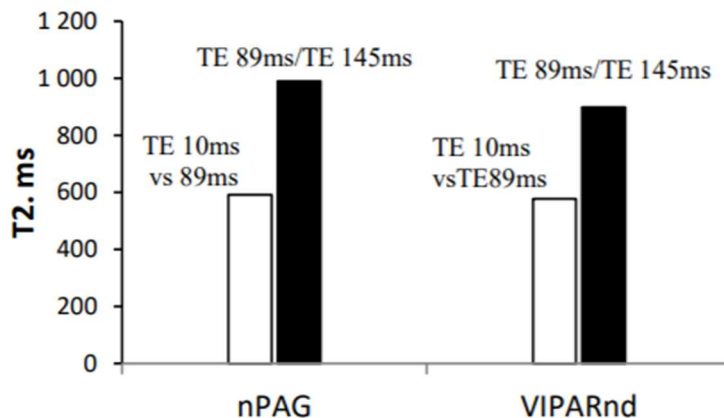


Fig. 57. Comparison of T2 time values that are needed for obtaining the irradiated dose gel images of the first target for both types of irradiated dose gels

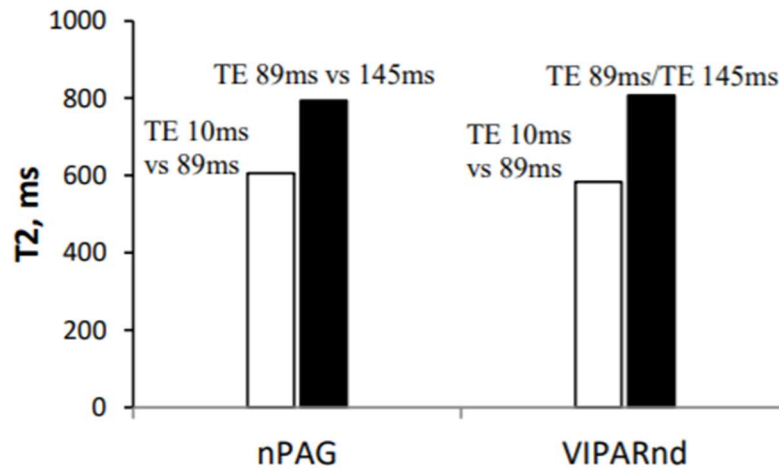


Fig. 58. Comparison of T2 time values needed for obtaining the irradiated dose images of the second target for both types of irradiated dose gels

The results of the performed experiment demonstrated the suitability of this technique for the estimation of irradiated gel response to the irradiation dose. A good agreement between the obtained results for the dose assessment in irradiated VIPARnd and nPAG^F dosimetric gels was found. The differences between the data values of the selected point at ROI and the data obtained at the isocenter of the first target did not exceed 0.5% for the evaluations that were performed by applying TE of 10 ms, 89 ms and 0.75%, applying TE of 145 ms for MRI scanning. The estimated differences in the second target were 0.5%, 0.7%, and 0.6% for TE 10 ms, TE 89 ms, and TE 145 ms [134]. It has been found as well that the relaxation time for VIPARnd dose evaluation was longer, and the corresponding pixel intensities were lower. This led to the suggestion that VIPARnd dose gels might be more sensitive to higher irradiation doses (up to 20 Gy) and have a broader dose response range, compared with nPAG gels.

4.3. Evaluation of dose resolution in irradiated gels

Dose resolution (see Equation 4) is an important parameter that is used for distinguishing the doses at two neighboring points that are separated by special resolution of the gel. The dose resolution is directly linked to the radiation-induced polymerization processes in the irradiated gels and gel property changes due to the polymerization level, as it was discussed in subchapter 2.4. Polymerization strongly depends on the amount of energy (dose) that was transferred and absorbed in the irradiated gel, which leads to the suggestion that the dose resolution is dependent on the absorbed dose.

In order to evaluate dose resolution at different absorbed energy levels, (different absorbed doses) batches (8 cuvettes in each) of nPAG^F and VIPARnd dose gels were produced and irradiated up to 40 Gy doses in Gamma knife unit. Two different echo times, i.e., 89 ms and 145 ms, were selected for obtaining MRI scans of irradiated gels.

In the first step, the dose sensitivity of both gels in low (0–10 Gy) and high up to 40 Gy regions was assessed by using spin-spin relaxation rate (R2) as the main parameter (Fig. 59).

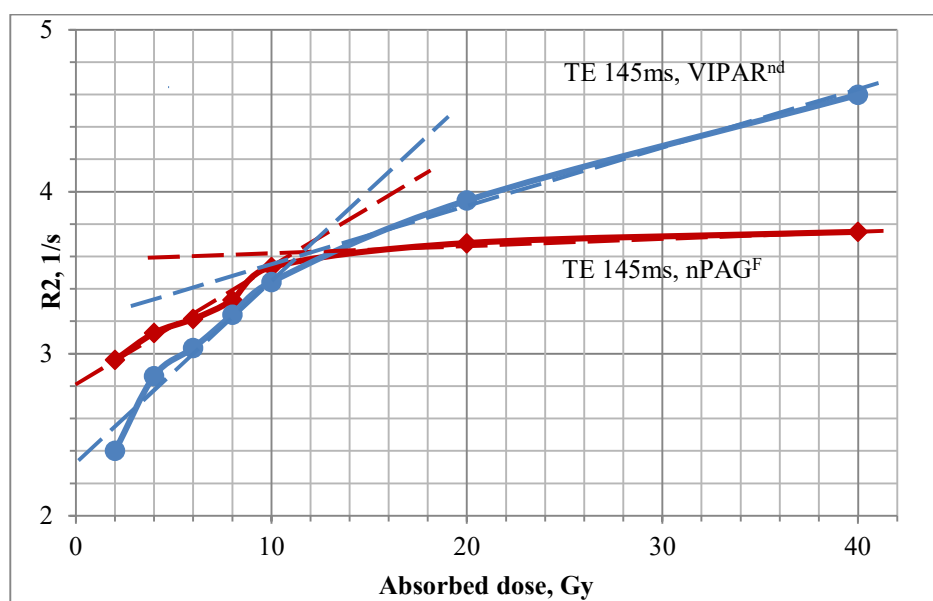


Fig. 59. R2 calculations for nPAG^F and VIPARnd dose gels with differently absorbed doses

It has been found that Gamma knife irradiated VIPARnd gels were more sensitive to the irradiation, compared to the nPAG^F gel. The estimated R2 related values in the low dose (up to 10 Gy) region were the following: 0.081 Gy⁻¹s⁻¹ and 0.121 Gy⁻¹s⁻¹ for nPAG^F and VIPARnd, respectively. VIPARnd gels were sensitive enough in the high dose region (10 Gy to 40 Gy), indicating 0.035 Gy⁻¹s⁻¹ sensitivity, which is a very promising result for dosimetry applications in high dose Gama knife radiosurgery. The R2 dose sensitivity of nPAG^F gel was negligible. These results are in line with the findings of [61], where it was shown that R2 dose response, which depends on the monomer concentration, temperature, and MRI scanning frequency, is typically linear up to 8–10 Gy for nPAG gels and keeps linearity in the high dose region for VIPAR (up to 30 Gy) and VIPARnd dose gels (up to 35 Gy).

Considering that in many cases, the irradiated dose gels are used for the verification of TPS produced 2D dose distributions, the analysis (dose mapping in the irradiated gels) has been performed by using MRI scanned images, evaluating the average pixel intensities with ImageJ2 code. The evaluated pixel intensity values were converted to the optical density, and the dose sensitivity curves were constructed (Fig. 60).

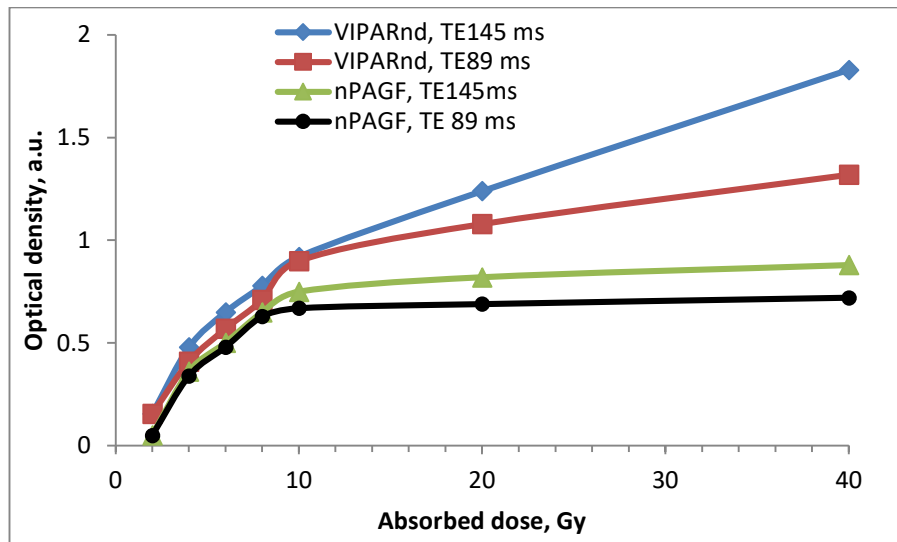


Fig. 60. Dose sensitivity of nPAG^F and VIPARnd dose gels evaluated at different echo times

It has been found that in the low dose region (up to 10 Gy), the dose sensitivity of both gels was similar, indicating slightly higher sensitivity when longer echo time was chosen for the MRI scanning. Particular dose sensitivity values for nPAG^F gel were the following: 0.0842 Gy⁻¹ for TE=145ms and 0.0765 Gy⁻¹ for TE=89 ms, and were well in line with the sensitivity values that had been obtained for this gel when performing other experiments. The estimated dose sensitivity of VIPARnd gel was 0.11 Gy⁻¹ for TE=145 ms and 0.0895 Gy⁻¹ for TE=89 ms. In high dose region (up to 40 Gy), the sensitivity of nPAG^F gel was negligible; however, for VIPARnd, it showed detectable dose sensitivity of 0.0302 Gy⁻¹ for TE=145 ms and 0.0137 Gy⁻¹ for TE=89 ms.

The estimated dose sensitivity values slightly differed, but were well in line with the previous findings (Fig. 59) that were obtained using R2 rate as a parameter.

Overall, the MRI evaluation-based dose sensitivity values were higher compared to those that were obtained using UV-VIS spectrophotometry. The main difference occurred in the low dose region where the estimated VIPARnd sensitivity was less than nPAG^F sensitivity, in contrary to the MRI evaluation results. This can be explained by the fact that UV-VIS method was applied for the gels that were irradiated in teletherapy unit with Co-60 source, which had a significantly lower dose rate compared to the gamma knife unit, which in turn influenced the polymerization processes in the irradiated gels.

The MRI scans that were obtained using TE=145 ms were used for the dose resolution D_{Δ} calculations (see subchapter 2.4) in both investigated gels. The calculations were performed within the selected 8.07 mm³ central region of the irradiated gel with a chosen voxel volume of (0.3 x 0.3 x 2) mm³. The calculation results for nPAG^F gel are provided in Fig. 61 and for VIPARnd, in Fig. 62.

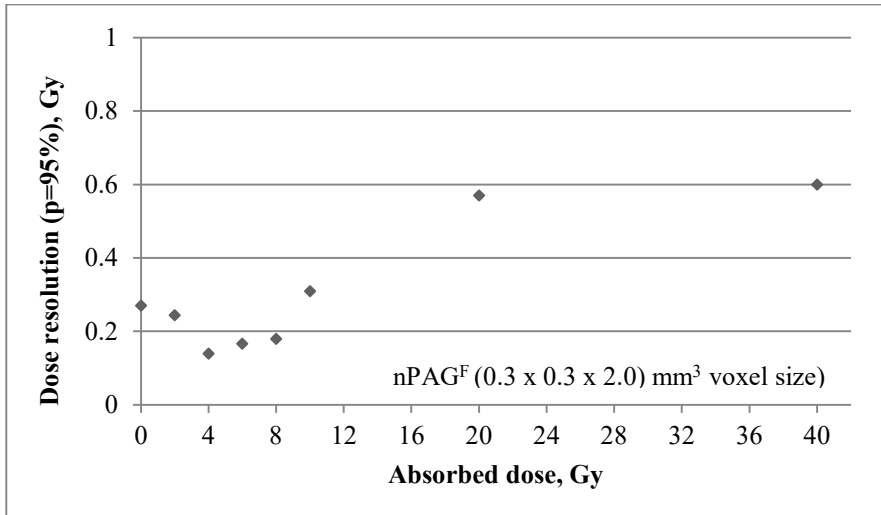


Fig. 61. Dose resolution (p=95%) calculations for nPAG^F dose gels

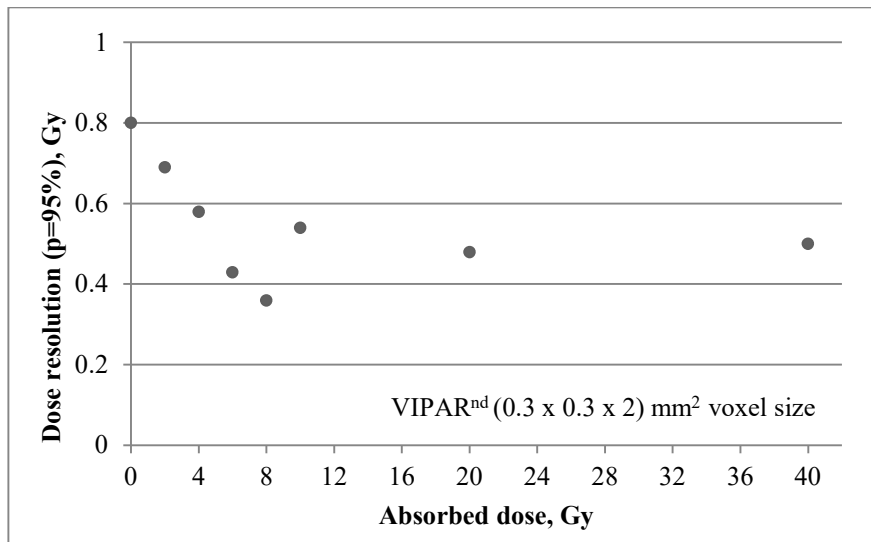


Fig. 62. Dose resolution (p=95%) calculations for VIPARnd dose gels

There was found a not well-expressed dependency between the dose resolution and absorbed dose value. However, some information was obtained from the performed calculations. It has been found that the dose resolution of nPAG^F dose gels was smaller in the low dose region (up to 8 Gy), compared with the high dose region.

Similar results for nPAG are provided in [135, 136], indicating that at the higher doses (20 Gy and more), the dose resolution was near to 1 Gy.

The opposite tendency was observed for VIPARnd gel: higher dose resolution values were observed for the doses from the low dose interval. In the high dose region, the dose resolution was moderate 0.45 Gy. These later findings fit well with the results obtained by the other authors [15].

It should be noted that the dose resolution depends on many factors, such as radiation type, quantity of investigated gel, dose gel preparation procedure, and chemical composition of the gel.

The performed experiments revealed that the changes in the irradiated dose gels that were caused by the MRI based dose evaluation, which is exploring the radiation-induced polymerization, can be applied for the assessment of 3D dose distribution in the small milli/micro scale targets (small tumors) that are commonly treated during the Gamma knife radiosurgery procedures. Both investigated gels, nPAG^F and VIPARnd, were verified for the potential application in gamma knife surgery; however, in the high dose region (up to 40 Gy), VIPARnd dose gel performed better, compared with nPAG^F: it was more dose sensitive and characterized with good spatial resolution (0.2 mm) and moderate dose resolution (0.45 Gy).

4.4. Ionizing radiation-induced 3D printing of free standing gels

It is known that the polymerization process is strongly dependent on the gel's chemical constituents and their concentrations. The influence of different gel components and concentrations on the dosimetric sensitivity of low dose irradiated basic dose gels (nMAG, nPAG, VIPET) was discussed in general in [109]. However, it was shown [29–31] that the gelatin concentration, especially in the higher dose region, may play an important role in gel's polymerization processes.

The influence of gelatin amount (2%, 3%, 5%) in the total gel solution was investigated for nPAG^F dose gels that were irradiated with different doses in Gamma knife facility. MRI scanner was used for the evaluation of irradiated gels, and the obtained results are provided in Fig. 63.

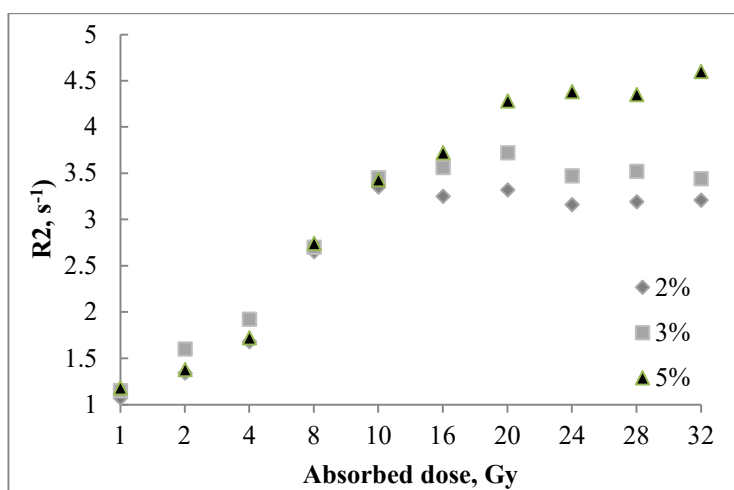


Fig. 63. Gelatin concentration related dose response in terms of relaxation rate R2 of gamma photons irradiated nPAG^F gels

It has been found that the amount of gel was not very significant in the low dose region (up to 10 Gy), and the dose responses of irradiated gels were almost linear; however, in the high dose region, some saturation tendencies were observed. The dose response was higher in gels with a higher amount of gelatin.

However, in [1, 16, 17], the increased amount of gelatin in polymer gels reduces the polymerization rate. The analysis of the gel samples has shown that 1.5–2.5 wt% of gelatin in the composition contributes to the faster liquification (Methods subchapter 3.3.1.) of dose gels after the irradiation, but do not assure the formation of a stable polymerized shape in the gel volume, which is definitely important when producing the free standing tumor-mimicking irradiated shapes. When the gelatin concentration increases up to 4.0–6.0 wt%, stable irradiated shapes might be produced, and they stay stable for a long period. A higher dose response to the irradiation, longer stability make gels with higher amount of gelatin attractive for the medical dosimetry applications [A2, 137].

It should be noted that the recipe of nPAG^F gel (3 wt% AAm and BIS, 5 wt% gelatin) together with the method of its fabrication are patented [138].

The amount of gelatin is extremely important in the formation of different polymerized gel shapes in the gel volume during the radiation-induced polymerization processes, since gelatin has a role of matrix, keeping the new formations stable. The shape of the formed structures depends on the maximum energy that is transferred/absorbed in the target (tumor), which is delivered according to the dose treatment plan of a real patient, simulated by a standard treatment planning system and surrounded by not polymerized part of the gel. The dose distribution in the shape volume is usually assessed by analyzing the gel-filled vial with polymerized part of the gel inside. This is not very convenient and leads to large uncertainties, since there is no possibility to physically investigate the changes of properties in the polymerized part of the gel. However, the precise evaluation and verification of dose distribution in small-scale objects are priorities for the radiosurgery treatment of patients.

Considering that the precise evaluation and verification of dose distribution in small-scale objects are the most important for radiosurgery treatment of patients, a concept for the development of free standing dose gels was proposed [103]. Free standing dose gels are radiation produced stable polymerized shapes of the gels that are mimicking tumors of real patients that might be removed from the rest volume of the gel.

The concept was explored to develop the ionizing radiation based 3D printing method of free standing dose gels [A2].

4.5. Formation of free standing gels

A batch of nPAG^F dose gels was manufactured, following the procedure that was described in subchapter 3.3.1. Materials characterization methods, and poured into glass bottles (D=2.5 cm, H=4.5 cm) with one centrally based catheter [137, 139]. The dose spread was 0.2 cm. The gel filled bottles that were irradiated to different doses are provided in Fig. 64.



Fig. 64. A – nPAG^F dose gel samples irradiated in Elekta Flexitron IconTM in brachytherapy unit with ¹⁹²Ir source with different doses, B – example with free standing dose gel shape inside the bottle, C – free standing polymerized gel removed from the whole gel volume

It was visually assessed that the dose distributions in irradiated gel samples were close to those that were theoretically planned in TPS. The tightly polymerized shape, which should correspond to the treatment target, was clearly seen in each irradiated bottle. After a few days, it was possible to remove the shapes from the residual gel and measure their size, shape, and optical and physical density. Raman spectroscopy was performed as well in order to assess the changes in molecular structure after the polymerization. In general, the spherical shapes changing to spheroid shapes were produced. The size, which was varying with dose, was measured several types using digital caliper (Fig. 65), and the evaluated mean values were compared with those indicated in the dose plans that were created using the treatment planning system Oncentra. The difference between the measured linear dimensions of the shapes and the values obtained from the planning system was < 5%.

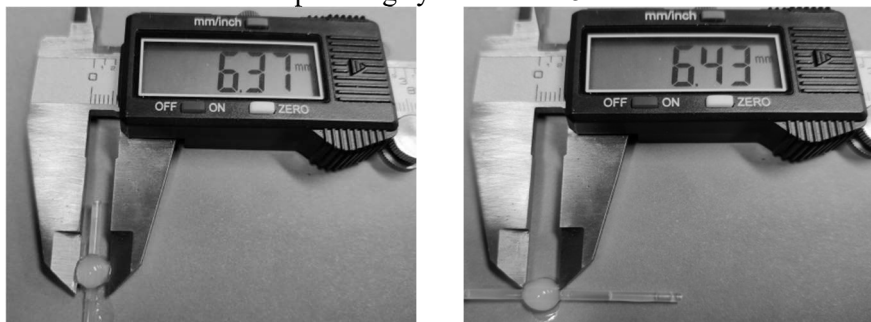


Fig. 65. Measurement of the polymerized shape with digital caliper

Similar results related to the irradiated shape and size of modified nPAG gels, irradiated with 1 Gy and 5 Gy, were obtained when performing the pilot study based on the development of the concept for the creation of free standing dose gels [103].

The conducted experiments were performed just for the approval of the free standing dose gel concept; thus, only simple shapes that were obtained after performing irradiation at one single point were investigated.

The next experiment was performed [A2] with nPAG^F dose gels when two centrally pre-arranged 4 Fr (D=2 mm) catheters for the insertion of brachytherapy source were inserted in gel filled borosilicate beakers (DIN 12 331. ISO 3819; D=4.8

cm, H=8.0 cm). Following the recommendations of PARIS system, the distance between catheters was 1 cm.

Radiation-induced local polymerization of dose gels was realized by irradiating samples in high dose rate (HDR) brachytherapy unit MicroSelectron v2 via insertion of ^{192}Ir source at certain positions in the catheters, according to the preplanned irradiation plan in Oncentra TPS. The randomly selected source locations in the catheter (2 catheters arrangement) and randomly chosen irradiation doses were used for the preparation of treatment dose plan (Fig. 66).

The performed rough calculations revealed relatively good agreement in size between the theoretically calculated and experimentally obtained shapes. The average standard deviation of 7% has been estimated.

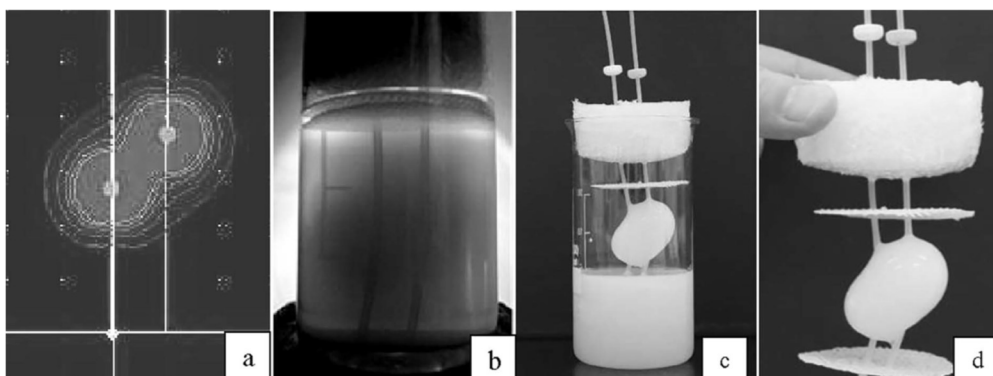


Fig. 66. Comparison of TPS proposed treatment volume (2D dose distribution map, transverse view from TPC) (a) with radiation produced polymerized free standing dose gel volume: (b) image of just irradiated gel filled beaker with a polymerized part in gelatin matrix, (c) separation of polymerized gel part from the gelatin, (d) image of radiation produced 3D free standing polymerized gel shape; notice that the scales are different

The horizontal line at the bottom of Fig. 66 a) corresponds to the bottom of the beaker; two vertical lines represent the inserted catheter locations, keeping 1 cm distance between them (normal practice during the surgical pre-implantation). Two bigger gray-colored points indicate the stopping positions of the ^{192}Ir source. Isocurves around these points demonstrate TPS planned dose distribution with irradiated volume. The first task of this experiment was to get 3D printed free standing dose gel shapes using high energy gamma photons. The second task was to find out whether the shape of the fabricated 3D object repeats the shape of the pre-calculated dose distribution map and evaluate the size deviations. It is evident that both shapes are similar. In order to be more certain, 3D gel shape surface was divided into specific segments, and the corresponding dimensions were measured.

The dose gels, demonstrating specific characteristics upon high energy photon irradiation, have been developed and used for the realization of radiation-induced formation of free standing 3D polymerized gel shapes (radiation based 3D printing). The first approach for the implementation of this 3D printing concept was done when

exploring the catheter based brachytherapy treatment procedures. Gel filled beakers with inside arranged catheters were used as the experimental samples for the investigation of radiation-induced dose gel changes. The comparison of fabricated free standing 3D polymerized gel shapes with the pre-planned irradiation volume, calculated using the algorithm of a standard brachytherapy treatment planning system, has shown the shape similarity and relatively good size agreement of both volumes. The average standard deviation of 7%, related to the local size measurements, was estimated.

The advantages and disadvantages of radiation based 3D printing of free standing dose gel shapes are summarized in the Table 13.

Table 13. Radiation based 3D printing of free standing dose gel shapes

Advantages	Disadvantages
Irradiated volume visualization	High precision when performing treatment is required
Possibility to compare the shape with the preplanned for the treatment volume (tumor)	Quite long preparation, read-out period
Possibility to physically perform the measurements and evaluate physical/chemical properties of polymerized gel material	Specific knowledge is necessary to use and read-out
Possibility to investigate the impact of radiation-induced polymerization processes on material (gel) properties	

Natural separation of irradiated and non-irradiated parts in dose gel is related to the gelatin chain helix decomposition, which may take some time under normal conditions. In order to overcome this problem, two methods were proposed to achieve faster gel liquefaction and removal of polymerized gel shape from the entire volume: controlled heating method and dry air method. The technical conditions for the application of these methods were described in the Methods section.

For this purpose, 6 nPAG^F samples and 6 VIPARnd samples with inserted catheter were prepared for the assessment of suitability of the proposed mechanical removal methods. The samples were irradiated to one single dose of 5 Gy in the brachytherapy unit Elekta Flexitron IconTM. The details of method applications are provided below.

The application of dry air method. The irradiated gels were dried at certain conditions in the air, and after each period of 4 hours, tensile force that is necessary for the separation of polymerized part from the whole gel was measured, assuming that the adhesion force between the polymerized gel and catheter material is sufficient enough to keep the shape on the catheter. The results of performed experiment for nPAG^F gel are provided in Fig. 67.

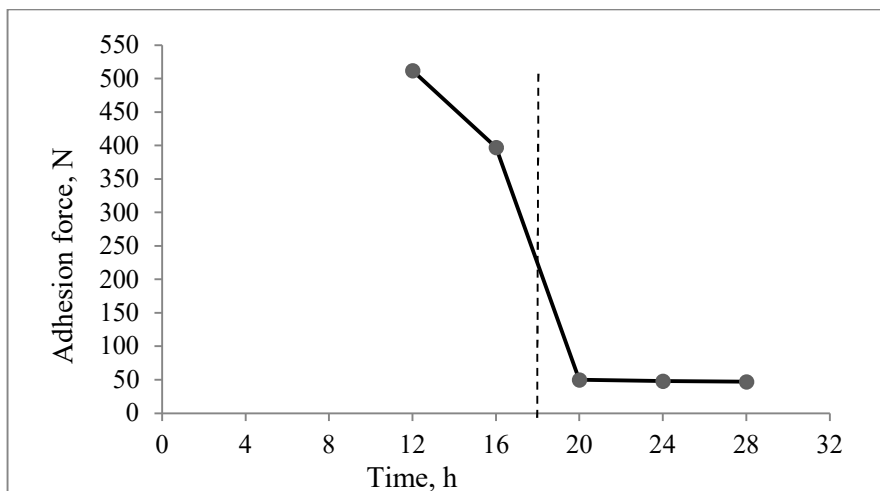


Fig. 67. Adhesion force versus time for nPAG^F gels, applying the dry air method

The experimental results demonstrated that the irradiated/polymerized volume could be separated after 20 hours relatively easily. However, the time is too long for the implementation in clinical applications.

The same experiment was repeated with irradiated VIPARnd dose gels; however, it turned out that the time needed to separate the polymerized part of the gel from the whole gel was significantly longer (> 24 h), compared with nPAG^F gels, making this method ineffective if used in clinical applications. Besides, a larger force should be applied, since the concentration of gelatin in VIPARnd is almost twice as high as in nPAG^F dose gel.

Controlled heating method. It was presumed that the application of high temperature gradients may lead to the fast separation of polymerized part from the rest of the gel volume. When applying this method, different temperature gradients were applied to heat the irradiated nPAG^F gel samples. In this case, the faster liquefaction of non-irradiated dose gel part and easier separation of polymerized part were achieved, compared with Dry air methods (Fig. 68). It should be noted that all high temperature experiments lasted no longer than 30 sec.

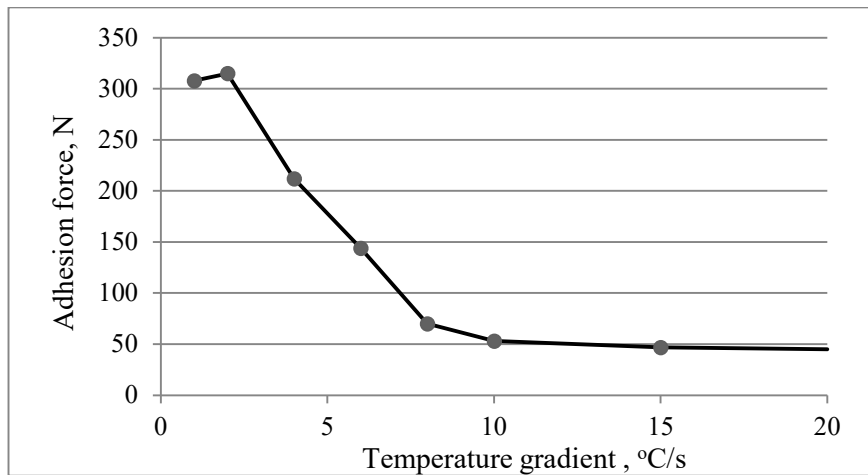


Fig. 68. Adhesion force versus temperature gradient time for nPAG^F gels, applying controlled heating method

There were not obtained any reliable results during the experiment performed with VIPARnd gels.

The performed experiments revealed that the controlled heating method could be easily applied to the separation of polymerized part of the gel from the whole volume in clinical dosimetry, where relative fast solutions are needed in order to provide the optimized treatment for the patient.

4.6. Clinical exploration of polymerizable gel properties

This chapter is particularly addressed to the following:

1. Clinical application of ionizing radiation based 3D printing of free standing gels;
2. Application of dose gels for individualized dosimetry;
3. A pilot study on the dose gel use for individual patient dosimetry in small-scale radiotherapy and radiosurgery.

4.6.1. Clinical application of free standing gel shapes

The advantages of creation of free standing polymerized dose gel shapes were explored by performing the dose verification for the real head and neck cancer patient with squamous cell lip carcinoma. For this purpose, nPAG^F filled borosilicate beaker (DIN 12 331. ISO 3819; D=4.8 cm, H=8.0 cm) with 4 prearranged catheters was prepared for the examination. The dose plan with indicated irradiation geometry for the treatment of this patient (Fig. 69) was simulated by using the standard treatment planning system Oncentra brachy planning.

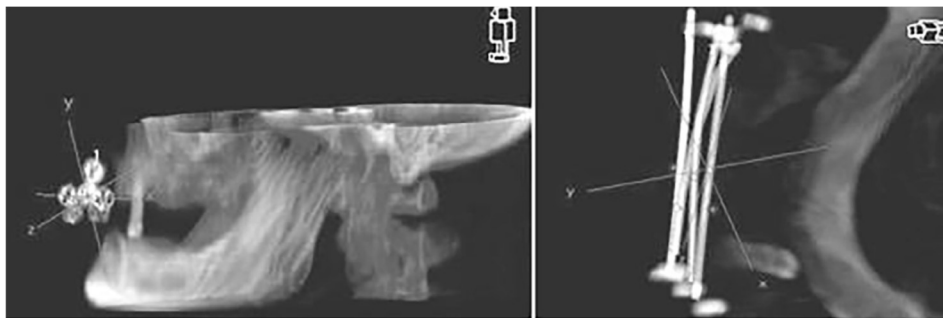


Fig. 69. Views of TPS plan prepared for head and neck cancer patient with squamous cell lip carcinoma

According to the plan, 5 Gy dose (dose rate: $1.871 \text{ cGy} \cdot \text{m}^2/\text{h}$) delivery position corresponded to the distance of 2 cm up from the beaker bottom in the first catheter; 7 Gy dose (dose rate: $1.871 \text{ cGy} \cdot \text{m}^2/\text{h}$) delivery location was 3 cm up from the bottom in the second catheter, and 6 Gy dose ($1.871 \text{ cGy} \cdot \text{m}^2/\text{h}$) delivery location was 4 cm up from the bottom in the third catheter (Fig. 70). Catheter No. 4 was not used during this treatment fraction, because after the reconstruction of catheter positions, it was found that maintaining the highest quality of treatment, the optimal plan can be created using only three catheters. The same method was used in other works [139, A2] for individual patient dosimetry evaluation.

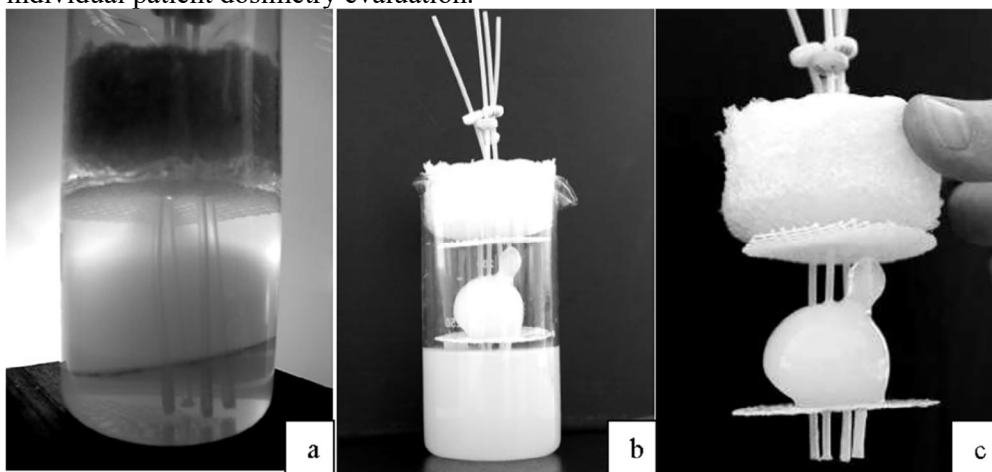


Fig. 70. The high energy photon based 3D printing of free standing gel shape: (a) image of just irradiated gel filled beaker with a polymerized part in gelatin matrix, (b) separation of polymerized gel part from the gelatin, (c) image of radiation produced 3D free standing polymerized gel shape; notice that the scales are different [A2]

The calculated deviations for the gel dosimetry related to the size of shape, compared with the size of the real treated area, was 7%, but the evaluated dose to the isocenter differed from the simulated dose by 3.5% only. Taking into account that the

spatial resolution of nPAG^F gel is 0.2 mm, this method is promising for the application in clinical dosimetry.

4.6.2. Application of dose gels for individualized dosimetry

An individual dosimetry method, which is exploring dose gels, has been proposed and realized by performing in vivo catheter based brachytherapy procedures for head and neck cancer patients. This suggestion was followed after the successful implementation of millimeter range TLD detectors for dose assessment in brachytherapy [A1].

TLD dosimetry. Prior to the treatment, 5 Fr catheters were surgically pre-implanted into target volume (tumor) following PARIS system geometry for the positioning of ¹⁹²Ir source during the patient's treatment [90]. One extra implanted catheter was left empty for dosimetry purposes. In order to perform in vivo dose measurements, the stiff stainless steel brachytherapy needle was filled with small 6 mm long and 1 mm thick TLD 100-H mini rods (Thermo ScientificTM), arranged in a certain sequences with 5.5 mm long "QuickLinkTM Cartridge Synthetic absorbable Seeding" plastic spacers, and inserted into the allocated catheter [93].

The pointed end of the needle was cut off before the insertion of dosimeters. In order to fix stable positions of dosimeters in the needle, the spacers from both ends of dosimeter chain were placed additionally. It should be noted that this method is applicable for straightly inserted catheter geometry (without loops) only.

All patients with pre-implanted empty catheters underwent a computed tomography (CT) scanning with a slice thickness of 2.5 mm [90]. These scans were sent to the treatment planning system (TPS) Nucletron Oncentra MasterPlanTM (version 3.2) and used for the reconstruction of catheter positions as well as dose calculations at the detector positions. During this study, the idea of theoretically modulated dose distribution in the target was formed by using polymer dose gel measurements that were performed [A1] for Head&Neck cancer (Fig. 71) patient.

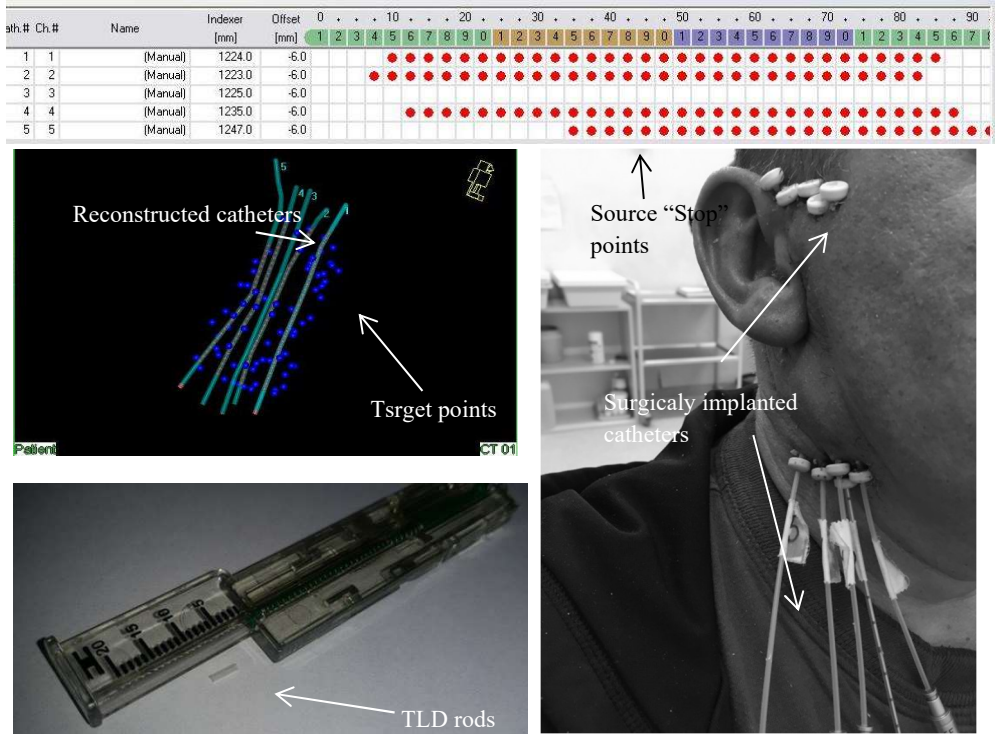


Fig. 71. Catheter implantation process in brachytherapy

The comparison of theoretical and experimental dose values was made for each measured fraction. Moreover, in vivo measured doses were verified with treatment planning system (TPS) planned doses Fig. 72 (dashed line).

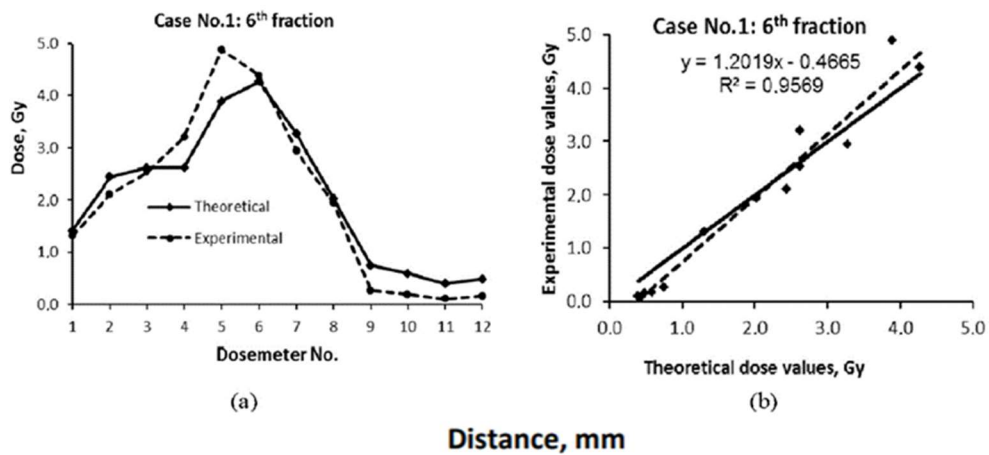


Fig. 72. Comparison of measured dose errors during two independent treatment sessions

Comparison of dose errors that were estimated during two separate fractions of the same patient is provided in (Fig. 73). It has been found that due to the specificity of the catheter based brachytherapy procedures, 7–11 dosimeters are needed for dose measurements to cover the whole range of interest.

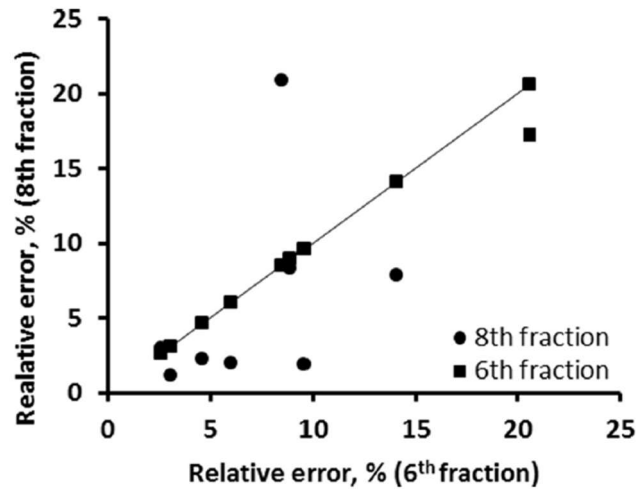


Fig. 73. Relative errors, % between two independent fractions

The comparison of treatment planning system (TPS) calculated doses with the experimentally measured dose values and their analysis has shown some promising tendencies for the implementation of catheter based IVD in brachytherapy: the margin of the average error for all performed IVD measurements was < 20% and was in line with the recommendations of the Report of AAPM task group No. 138. The average dose error that was obtained during independent IVD control measurements varied from 4.02% to 12.93% for Head&Neck patients.

Gel dosimetry. The performed study using TLD led to the application of polymer dose gels for in vivo dosimetry. During the clinical procedure, one catheter was filled with nPAG^F dose gel (Fig. 74 A, B) and used for in vivo dosimetry purposes for a patient irradiated with ¹⁹²Ir gamma source of brachytherapy unit, according to the created TPS plan (Fig. 74 C). The comparison of measured and calculated doses is provided in Fig. 74 D.

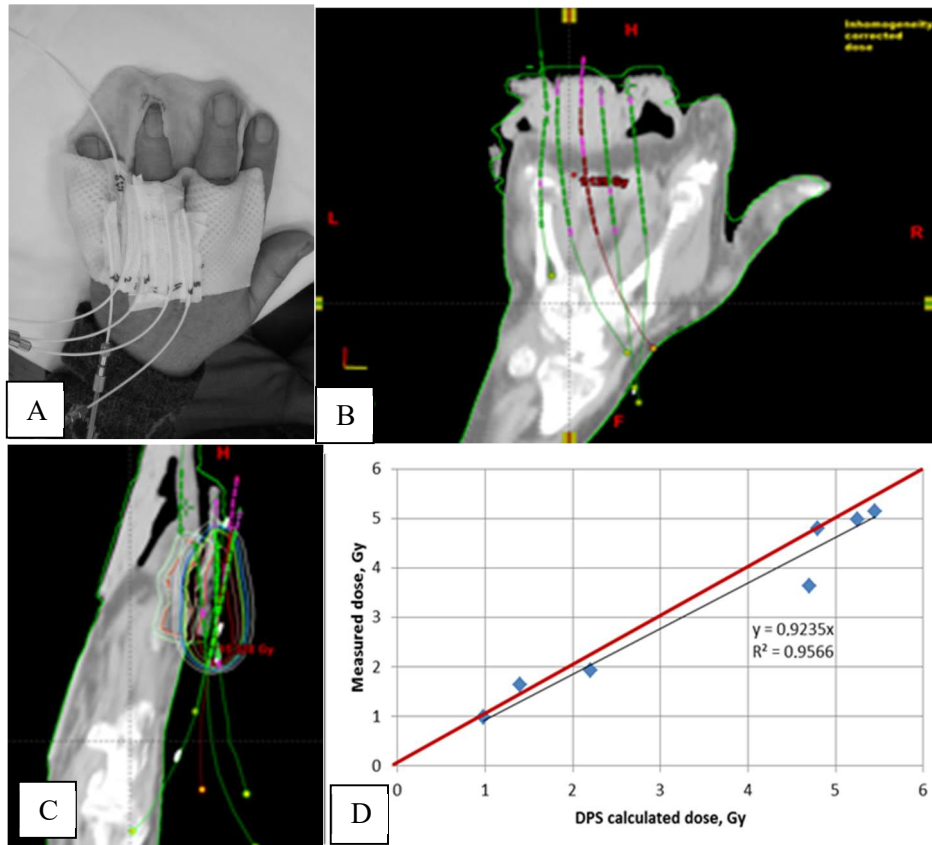


Fig. 74. Comparison of the in vivo dosimetry results using of nPAG^F gel filled catheter as a dosimeter in catheter based dosimetry

4.6.3. Clinical microdosimetry concept

Modified polymer dose gels were applied for milliscale target pre-treatment imitation using Lexell Gamma knife IconTM unit [A3]. The main aim of this study was to modify the gel dosimeters and analyze their capability to micro/milli scale target imitation and high dose assessment in small irradiated volumetric shape with the purpose to continue further dose gels applications in clinical dosimetry and implement routine verification of microscale target treatment procedures in radiosurgery.

Two sets of freshly prepared nPAG^F gels were irradiated in Lexell Gamma knife IconTM (⁶⁰Co) facility. The irradiation doses were delivered according to the real patient treatment plans, which were simulated by using treatment planning system “Gammaplan”; differently sized collimators were used. In both cases, the same 3.445 Gy/min mean absorbed dose rate, which is necessary for using the largest collimator, was applied.

Three samples from the first set (S1.1, S1.2, and S1.3) were irradiated under the same conditions in one single beam shot with 16.0 Gy@50% prescribed dose, using a collimator of 8 mm. The prescribed target coordinates (x, y, z) were 100 mm, 130 mm, 100 mm, respectively.

Three separate beam shots, using the smallest possible 4 mm diameter collimator, with all opened blocking sectors were applied to irradiate each of the three samples from the second set (S2.1, S2.2, and S2.3). The irradiation conditions were the same for all 3 samples from the second set. 2.0Gy@50% was delivered to the point (I) with coordinates (100 mm, 115 mm, 100 mm), 4.0Gy@50% to the point (II) with coordinates (100 mm, 130 mm, 100 mm), and 8.0Gy@50% to the point (III) with coordinates (100 mm, 145 mm, 100 mm), respectively. The irradiation parameters are summarized in Table 14.

Table 14. Irradiation parameters of nPAG^F gel samples in Gamma knife facility

<i>Sample</i>	<i>Shot no</i>	<i>x</i>	<i>y</i>	<i>z</i>	<i>Gamma Angle (Deg)</i>	<i>Prescribed dose (Gy) @50% isodose</i>	<i>Max (Gy)</i>	<i>Collimator (mm)</i>	<i>Grid size (mm)</i>
S1 (1-3)	I	100	130	100	90	16	32	8	60
	II	100	115	100	90	2	4	4	60
S2 (1-3)	II	100	130	100	90	4	8	4	60
	III	100	145	100	90	8	16	4	60

The irradiated gel samples were scanned using 1.5 T MRI unit Magnetom Avanto (Siemens) 24 hours after their irradiation. MR read-out was performed by using head scan coil. The vials were centrally positioned to ensure proper signal detection. The following parameters were used to read-out the samples: T2 weighted pulse sequence, voxel size 0.4 x 0.4 x 3.0 mm³, slice thickness 3 mm, Field of view (FoV) 210 mm, repetition time (TR) 4080 ms, and three echo times (TE): 10 ms, 89 ms, 145 ms. The relative pixel intensities or relaxation rate R2 from MRI images were calculated by using methods and formulas described in Methods subsection 3.3.2.

The MR images of irradiated samples that were obtained after the calculation of T2 values were subsequently analyzed using open-source software Weasis v2.5.0 and ImageJ2. The obtained results were compared with Gammaplan dose distribution maps that were created at the selected locations, using TMR 10 algorithm and Sigmaplot 14.0 visualization. It should be noticed that the pixel values in the MRI images of the second set (S2) samples were evaluated by selecting the same point at the isocenter in the same image slides of each sequence with the different echo time.

Single shot geometry. In order to realize the clinically realistic investigation, the irradiation of dose gels was performed, according to the treatment plan of a real patient, using Gammaplan simulation [A3]. The treatment plan with indicated isodoses that were selected from the range of 2–16 Gy is presented in Fig. 75 alongside with a horizontal dose cutting profile for a single shot irradiation of gel samples, which was created using open software Matlab 2016b. The profile indicates the size of the open irradiated area that was obtained using 8 mm collimator. The estimated polymerized gel volume is 2.42 cm³. The highest estimated dose difference between the calculated and measured absorbed doses was < 5%.

A photograph of irradiated gel sample S1.2 and MR-scanned image of the same sample in transverse plane are provided in Fig. 76 A and B, respectively.

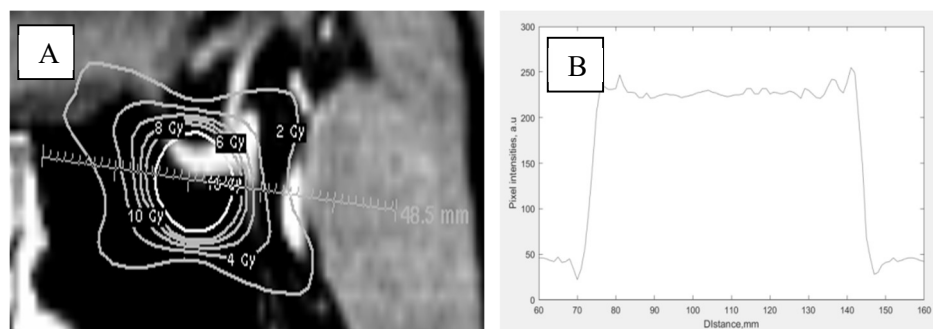


Fig. 75. A – distribution of isodoses in the target simulated by the Gammaplan treatment planning system for single shot geometry, where the yellow line indicates 8 mm collimator area, corresponding to the delivery area of 16 Gy, B – the horizontal dose profile within the area, irradiated with open field of 8 mm collimator

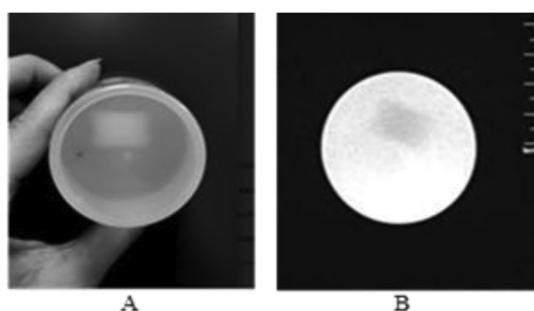


Fig. 76. Images of irradiated S1.2 gel samples: A – a photograph, B – MR-scanned image

In order to evaluate the possibility to assess the polymerization induced changes in a small irradiated gel volume using the MRI method, the pixel intensity values at the selected data points, along the dose profile line, in the same MRI scanned image slices were extracted and analyzed at different echo times (TE), as it is shown in Fig. 77. Each point in the graph represents the average absorbed dose of all S1 sequence samples at the point of interest.

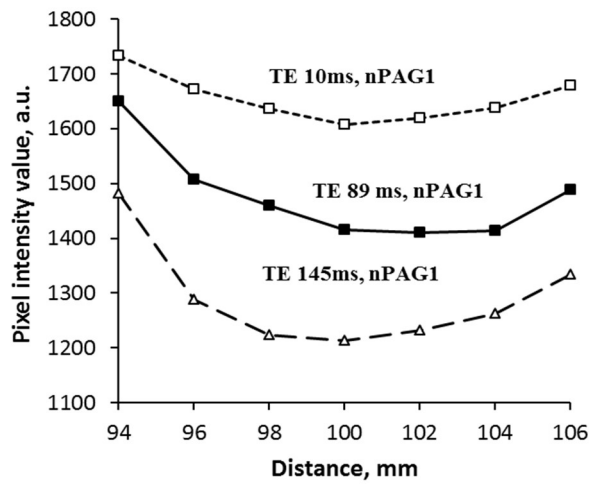


Fig. 77. Variations of pixel intensities of nPAG^F samples at the selected points in MR scans obtained at different TE

It has been found that the relative difference between the signal intensities in any two evaluated echo time sequences for each single shot varied in the range of 92.5–95%, as it is shown in Fig. 78.

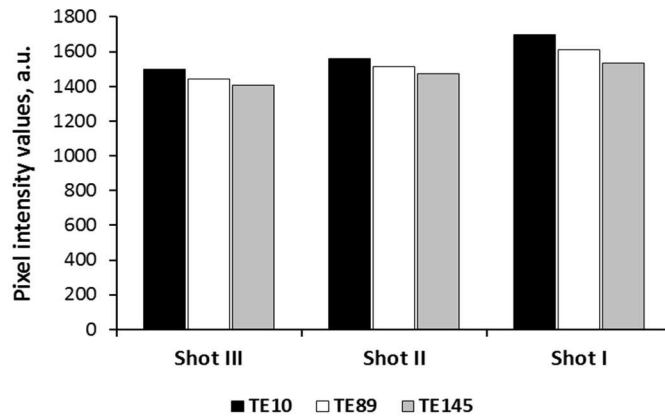


Fig. 78. Variations of pixel intensity values in MRI images of the irradiated nPAG^F gels for each of three single dose delivery shots at different echo times (TE)

The obtained results demonstrated the high importance of the TE selection when the irradiated volume is analyzed in the overall view of the MRI scan, thus indicating that the echo time selection might have a significant influence on the target detection and further data analysis of micro/milli scale targets. It has been found that the MR scans of dosimetric gels that were performed at the selected T2 sequence and different echo times provided higher image resolution at lower pixel intensities when longer TE was applied. Longer echo time allows for better image contrast.

Multiple shot geometry. The irradiation of nPAG^F gel samples in the multiple-shot geometry was realized by using the irradiation parameters of Gamma knife modality and experimental setup that is indicated in the Table 13, whereas each of S2 sequence samples was treated with three different doses that were delivered to the identical locations in all three samples. The irradiation and evaluation procedures were similar, like those described in the *single shot* experiment.

The prepared dose treatment plan indicates dose delivery in three separate shots (the doses at each shot were different) and provides corresponding 2, 4, 6, 8, 10 Gy isodose distribution at three isocenters (Fig. 80 A) together with the evaluated dose profile that is shown in Fig. 79 B. It could be seen that due to the lower prescribed primary doses, the dose profiles around the first isocenter with coordinates (100, 115, 100) mm and the second isocenter with coordinates (100, 130, 100) mm are flatter, compared with a relative sharp dose maximum at the third isocenter with coordinates (100, 145, 100) mm where the delivery of 8.0Gy@50% was planned.

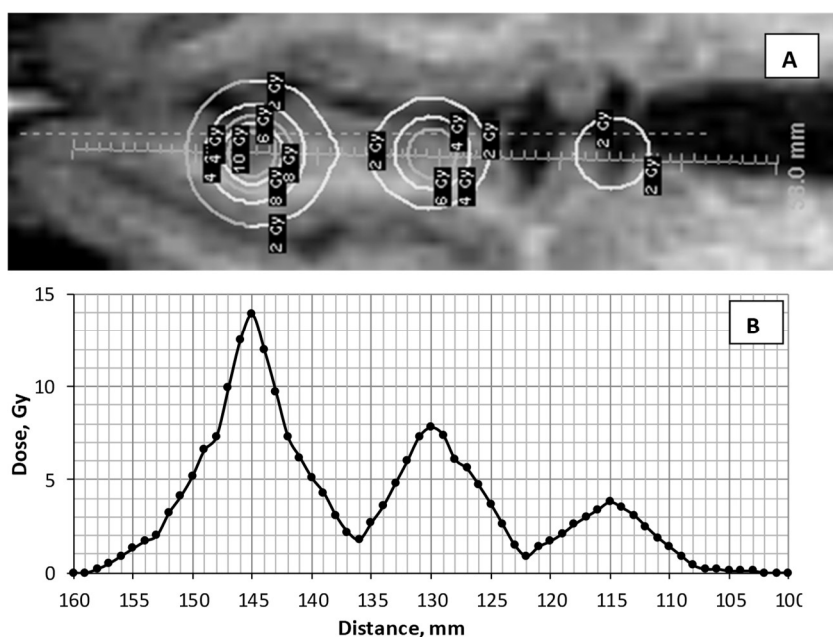


Fig. 79. A – Distribution of isodoses in three treatment isocenters simulated by the Gammaplan treatment planning system for multiple shot geometry, B – dose profile along the distance, covering all three dose isocenters

It should be noticed that the irradiation dose to the gel samples was delivered from the bottom side of the vial as it is shown in (Fig. 80 A).

The investigated polymerized gel volume (Fig. 80 B) in this case was 0.25 cm³. A slightly higher variation (7%) of the polymerized gel parameters between the samples of the second set (S2) were estimated, compared to the first set of the samples (S1). The highest estimated uncertainty was < 5%.

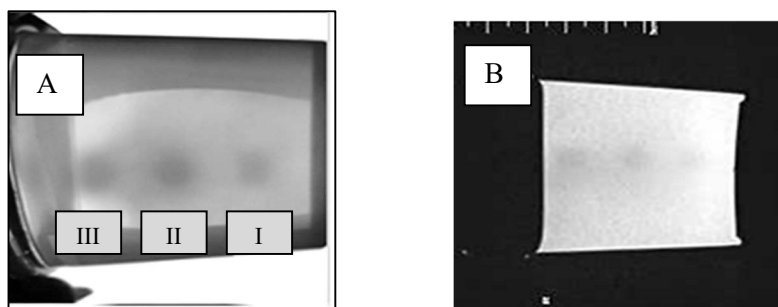


Fig. 80. Images of S2.3 sample: A– photograph of nPAG^F gel-filled vial after 3-shot irradiation with clearly seen three polymerized 3D shapes at the selected isocenters, indicated as I, II, and III, B – corresponding MRI DICOM view of the same sample

Since the MRI scanned images are provided in DICOM format, it was verified whether the spatial resolution provided by DICOM platform is sufficient to visualize very small, irradiated volumes. For this reason, the calculation of the output factor (OF) was proposed and realized for the adjustment of the dose to the target values when isocenter coordinates are not standard (100, 100, 100) mm.

The calculated output factor (see Eq. 25) was compared with the values, provided by the manufacturer for different collimator sizes in a standard (100 x 100 x 100) mm field. The results of the output factor calculations for the shifted isocentres are provided in the Table 15.

Table 15. Comparison of the output factors

Output factors	8 mm collimator, S1 samples	4 mm collimator, S2 samples		
		Shot No.	1	2
Shot No.	1	1	2	3
D _{max} /shot (planned)	32 Gy	4 Gy	8 Gy	16 Gy
Measured	1.037	1.045	1.078	1.092
Provided	1.043	1.016	1.043	-
Deviation %	0.01	2.78	3.20	-

Due to the size of the investigated gel samples (100 ml capacity plastic batch), y coordinates of the irradiation field varied in the range between 100–145 mm, thus exceeding the standard dosimetry field size and leading to the output factor value >1. Nevertheless, the calculated output factors demonstrated a good agreement with the values provided by the manufacturer, and the observed deviations were close to the recommended 3% limit. Better results and smaller output's factor deviation from the standard value was observed for the 8 mm collimator. The latter should be considered when adjusting Gamma knife dose plans for the patient's treatment.

It has been previously shown (Fig. 77) that the selection of the echo time (TE) when performing MRI scans may influence the detection sensitivity of micro-scale targets and further analysis of the data that was extracted from DICOM images. For

this reason, steep dose gradients were created in nPAG^F dose gel samples that were irradiated with Gamma knife facility by applying different size applicators. An example of dose profiles, obtained after the MRI scanning of three samples irradiated with the same 4 Gy dose and applying different collimators, is provided in Fig. 81 a. In Fig. 81 b), c), and d), the dose profiles from the Gammaplan treatment planning system for 16 mm, 8 mm, 4 mm size collimators are demonstrated.

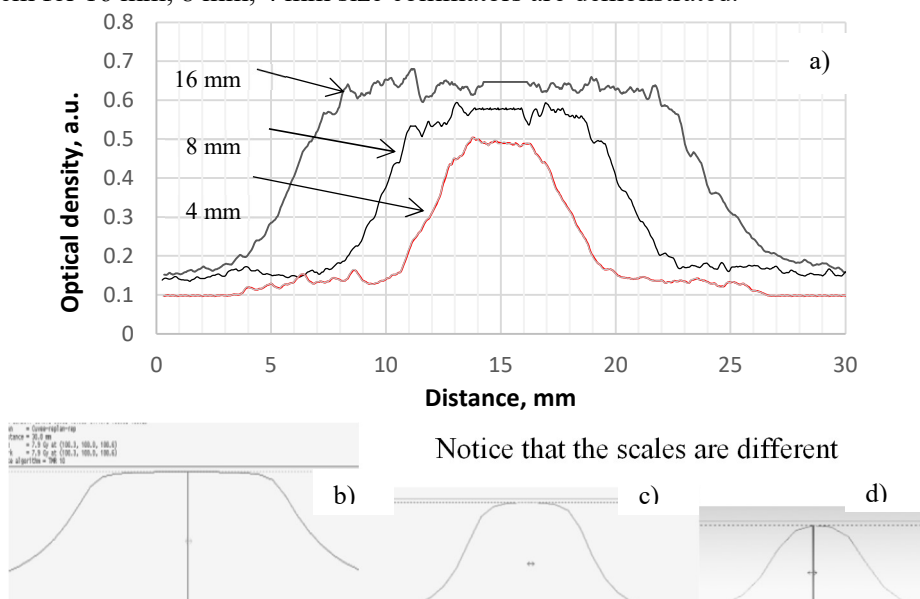


Fig. 81. Dose profiles obtained for the nPAG^F samples: a) irradiated with 4 Gy dose in Gamma knife facility by applying different collimators and from TPS Gammaplan irradiated using b) 16 mm, c) 8 mm, and d) 4 mm open sector collimators

The dose profiles along the z axis repeated those in the treatment planning system. Because of the small field when using 4 mm applicator, it may have a slightly larger margin of errors in measuring the optical values. It has been found that the dose profiles that were reconstructed from MRI scans were similar to those created by using the Gammaplan treatment planning system. The estimated average deviation between the results of measurements and simulation results did not exceed the recommended 5% limit, including the highest deviation of 4.7%, which was obtained by applying 4 mm collimator.

Overall, the presented results indicate a potential of nPAG^F dose gel for the applications in gamma knife radiosurgery where milli/micro scale tumors are treated, since these gels show good polymerization ability upon irradiation, are characterized by a good spatial resolution (at least 0.2 mm), and have relatively high dose sensitivity.

CONCLUSIONS

1. Dose gels with modified content have been fabricated, characterized, and functionalized for medical dosimetry applications in broad (0–40 Gy) absorbed dose regions.
2. The performed research has shown that both types of selected dose gels (nPAG^F and VIPARnd) were sensitive to the irradiation doses up to 10 Gy, indicating linear dose dependency. The dose sensitivity that was evaluated using UV-VIS spectrophotometry of nPAG^F gel irradiated with 6 MeV electrons was 0.0667 Gy⁻¹ and 0.0516 Gy⁻¹ for the gel irradiated with gamma photons (⁶⁰Co source). The sensitivity of VIPARnd gel irradiated with gamma photons was lower, i.e., 0.0357 Gy⁻¹; however, only this gel indicated detectable sensitivity of 0.0075 Gy⁻¹ to gamma photon doses up to 40 Gy.
3. The Raman spectroscopy results indicated a higher and more intensive polymerization of nPAG^F irradiated with electron beam due to the direct ionization induced processes in gels, compared to the photon irradiation. The initial molecular structure of VIPARnd was responsible for the higher polarizability of these gels in the broad dose region (up to 40 Gy).
4. In order to evaluate the sensitivity of dose evaluation method in irradiated gels, two evaluation methods, i.e., UV-VIS spectrophotometry and Magnetic Resonance Imaging, were compared. It has been found that MRI evaluated dose sensitivity was dependent on the scanning parameters, and the highest values were achieved by using the longest echo time (TE) of 145 s. The estimated R2 related sensitivity values of gels irradiated with gamma photons in Gamma knife facility in the low dose (up to 10 Gy) region were the following: 0.081 Gy⁻¹s⁻¹ and 0.121 Gy⁻¹s⁻¹ for nPAG^F and VIPARnd, respectively. VIPARnd gels were as well sensitive enough in the high dose region (10 Gy to 40 Gy), indicating 0.035 Gy⁻¹s⁻¹ sensitivity, which is a very promising result for dosimetry applications in high dose Gamma knife radiosurgery. The R2 dose sensitivity of nPAG^F gel was negligible.
5. The indirect MRI evaluation method, using optical information of the scanned images, which can be applied for 2D dose mapping, indicated similar dose sensitivity values: 0.0842 Gy⁻¹ for nPAG^F gel and 0.11 Gy⁻¹, for VIPARnd gel in the low dose region, compared to the direct MRI evaluation. The evaluated dose sensitivity of VIPARnd gel in the high dose region (up to 40 Gy) was 0.0302 Gy⁻¹. The higher dose evaluation sensitivity, using MRI compared to UV-VIS spectrophotometry, is based on the physical processes behind the MRI evaluation that are targeted in the excitation of hydrogen atoms in E/M field and following the relaxation processes.
6. The investigated polymer dose gels were used (in pilot project) for individual dosimetry in high dose small-scale radiotherapy treatment (brachytherapy, gamma knife radiosurgery). Both gels were applicable in the dose region (0–10 Gy); however, VIPARnd gel performed better in the high dose region (10–40 Gy), indicating 0.45 Gy dose resolution and at least 0.2 mm spatial resolution (MRI evaluation). The discrepancies between TPS calculated dose values were

lower than 3.0%, indicating the potential applicability of VIPARnd gel dosimetry in Gamma knife radiosurgery.

LIST OF REFERENCES

1. DE DEENE, Y. Essential characteristics of polymer gel dosimeters, *J of Phys: Conference Series* 3, 2004, p. 34-57; <https://doi:10.1088/1742-6596/3/1/006>;
2. WATANABE, Y., WARMINGTON, L., GOPISHANKAR, N. Three dimensional radiation dosimetry using polymer gel and solid radiochromic polymer: From basics to clinical application. *World J Radiol*, 2017, 9 (3), p. 112 – 125; <https://doi:10.4329/wjr.v9.i3.112>;
3. IZEWSKA, J., RAJAN, G. Chapter 3: Radiation Dosimeters. In: Podgorsak, E.B., Ed., *Radiation Oncology Physics: A Handbook for Teachers and Students*, International Atomic Energy Agency-IAEA, 2005, ISBN 92-0-107304-6;
4. PHILBERT, M. A., SAYES, C. M. *Comprehensive Toxicology (Second edition). Elsevier Science. Vol (2)*, 2010, p. 707 – 715. <https://doi.org/10.1016/B978-0-08-046884-6.00240-2>;
5. SPOREA, D., SPOREA, A. Radiation Effects in Optimal Materials and Photonic devices. 2016, *IntechOpen*. Doi: 10.5772/62547;
6. PRADHAN, A.S., LEE, J. I., KIM, J.L. Recent developments of optically stimulated luminescence materials and techniques for radiation dosimetry and clinical applications. *J Med Phys*. 33(3), 2008, p. 85 – 99. Doi: 10.4103/0971-6203.42748;
7. MCJURY, M., OLDHAM, M., COSGROVE, V.P. et al. Radiation dosimetry using polymer gels: Methods and applications. *British Journal of Radiology*. 73(873), 2000, p. 919 – 929. Doi: 10.1259/bjr.73.873.11064643;
8. GHOBASHY, M.M. Ionizing Radiation–Induced Polymerization. *Intechopen*. 2017, Doi: 10.5772/intechopen.73234;
9. DIAS, J.R., MANGUEIRA, T.F., LOPES, R.V.V., SALES, M.J.A., CESCHIN, A.M. Preliminary analysis of N-Vinylpirrolidone based polymer gel dosimeter. *Polimeros. Vol 28(5)*, 2018, <https://doi.org/10.1590/0104-1428.01718>;
10. MAITRA, J., SHUKLA, V.K. Cross_linking in Hydrogels – A Review. *American Journal of Polymer Science*. 4(2), 2014, p. 25 – 31. Doi: 10.5923/j.ajps.20140402.01;
11. SHERAZI, T.A. Graft Polymerization. In: Drioli E., Giorno L. (eds) *Encyclopedia of Membranes*. Springer, 2016, https://doi.org/10.1007/978-3-662-44324-8_274
12. DROBNY, J.G. Ionizing Radiation and Polymers. *Elsevier Inc*. 2013, p. 297. ISBN: 978-1-4557-7881-2;
13. From Basic to Modern Applications. Radiation Technology for Advanced Materials. Edited by Wu, G., Zhai, M., Wang, M. *Academic Press*, 2019, p. 337. ISBN: 978-0-12-814017-8;
14. PHILIPPOVA, O.E., KHOKHLOV, A.R. Basic Concept and Polymer properties. *Polymer Science: A Comprehensive Reference*. Elsevier, 2012, ISBN: 978-0-08-087862-1;
15. KARELLAS, A., THOMADSEN, B.R. Clinical 3D Dosimetry in Modern Radiation Therapy. Edited by Mijneer. *CRC Press. Taylor and Francis Group*, 2018, p. 674. ISBN: 9781482252217;

16. DE DEENE, Y. Dose-response stability and integrity of the dose distribution of various polymer gel dosimeters. *Phys. Med. Biol.* 47(14), 2002, p. 2459-2470. Doi: 10.1088/0031-9155/47/14/307;
17. BALDOCK, C., DE DEENE, Y., DORAN, S., IBBOTT, G. et al. Topical Review: Polymer Gel Dosimetry. *Phys Med Biol* 55(5), 2010, 1 – 63. Doi: 10.1088/0031-9155/55/5/R01;
18. FARHOOD, B., ABDAHI, S.M., GERALLY, G. Dosimetric characteristics of PASSAG as a new polymer gel dosimeter with negligible toxicity. *Rad. Phys. Chem. Vol (147)*, 2018, p. 91 – 100. <https://doi.org/10.1016/j.radphyschem.2018.02.010>;
19. ABTAHI, S.M., POURGHANBARI, M. A new less toxic polymer gel dosimeter: Radiological characteristics and dosimetry properties. *Physica Medica Vol (53)*, 2018, p. 137 – 144. Doi: <https://doi.org/10.1016/j.ejmp.2018.08.018>;
20. MESBAHI, A., JAFARZADEH, V., GHAREHAGHAJ, N. Optical and NMR dose response of N-isopropylacrylamide normoxic polymer gel for radiation therapy dosimetry. *Reports of Practical Oncology & Radiotherapy Vol 17 (3)*, 2012, p. 146–150. <https://doi.org/10.1016/j.rpor.2012.03.009>;
21. CHANG, Y.J., HSIEH, B.T. Effect of Composition Interactions on the Dose Response of an N-Isopropylacrylamide Gel Dosimeter. *J. Plos One Vol 7 (10)*, 2012, Doi: <https://doi.org/10.1371/journal.pone.0044905>;
22. KHODADADI, R., KHAJEALI, A., FARAJOLLAHI, A.R. et al. Dosimetric properties of N-isopropylacrylamide polymer gel using nonelectrophoresis grade BIS in preparation. *J. Of Cancer Research and Therapeutics Vol 11(3)*, 2015, p. 592–596. Doi: 10.4103/0973-1482.163732;
23. GORJIARA, T., HILL, R., KUNCIC, Z. et al. An evaluation of Genipin gel as a water equivalent dosimeter for megavoltage electron beams and kilovoltage x-ray beams. *J. Phys. Conf. Ser. Vol (250)*, 2010, 012036. <https://doi.org/10.1088/1742-6596/250/1/012036>;
24. KHAN, M., HEILEMANN, G., LECHNER, W., GEORG, D., BERG, A.G. Basic Properties of a New Polymer Gel for 3D-Dosimetry at High Dose-Rates Typical for FFF Irradiation Based on Dithiothreitol and Methacrylic Acid (MAGADIT): Sensitivity, Range, Reproducibility, Accuracy, Dose Rate Effect and Impact of Oxygen Scavenger. *Polymers 11(10)*, 2019, 1717. <https://doi.org/10.3390/polym11101717>;
25. JORDAN, K., AVVAKUMOR, N. Radiochromic leuco dye micelle hydrogels: I. Initial investigation. *Phys. Med. Biol.* 54(22), 2009, p. 6773 – 6789. Doi: 10.1088/0031-9155/54/22/00;
26. KIPOUROS, P., PAPPAS, E., BARAS, P. et al. Wide dynamic dose range of VIPAR polymer gel dosimetry. *Phys. Med. Biol.* 46(8), 2001, p. 2143 – 2159. Doi: 10.1088/0031-9155/46/8/308;
27. KOZICKI, M., MARAS, P., RYBKA, K. et al. On the Development of the VIPAR Polymer Gel Dosimeter for Three-Dimensional Dose Measurements. *Macromolecular Symposia 254(1)*, 2007, p. 345 – 352. <https://doi.org/10.1002/masy.200750850>;

28. PETROKOKKINOS, L., KOZICKI, M., PANTELIS, E. et al. Characterization of a new polymer gel for radiosurgery dosimetry using Magnetic Resonance Imaging. *Jinst Vol (4)*, 2009, P06018. Doi: Doi:10.1088/1748-0221/4/06/P06018;
29. PHILLIPS, G.O., WILLIAMS, P.A. Handbooks of hydrocolloids. *2nd Ed. CRC Press*, 2009, p. 1003. ISBN: 9781845694142;
30. FUXMAN, A.M., MCAULEY, K.B., SCHREINER, L.J. Modeling of Free-radical Crosslinking Copolymerization of Acrylamide and N,N'-Methylenebis(acrylamide) for Radiation Dosimetry. *Macromolecular Theory and Simulations Vol 12(9)*, 2003, p. 647 – 662. <https://doi.org/10.1002/mats.200350050>;
31. OSADA, Y., GONG, J.P. Soft and Wet Materials: Polymer gels. *Adv. Mater. 10(11)*, 1998, Doi: 0935-9648/98/1108-0827;
32. FUXMAN, A.M. Modeling of Free-radical Crosslinking Copolymerization of Acrylamide and N,N'-Methylenebis(acrylamide) for Radiation Dosimetry. *Macromolecular Theory and Simulations 12(9)*, 2003, p. 647 – 662. <https://doi.org/10.1002/mats.200350050>;
33. SPEVACEK, V., PILAROVA, K., KONCEKOVA, J., KONCEK, O. The influence of antioxidant THPC on the properties of polymer gel dosimeter. *Phys Med Biol Vol 59(17)*, 2014, 5141. <https://doi.org/10.1088/0031-9155/59/17/5141>;
34. MCAULEY, K.B., NASR, A.T. Fundamentals of gel dosimeters. *J.Phys.Conf.Ser. 444 012001*, 2013, Doi: 10.1088/1742-6596/444/1/012001;
35. JIRASEK, A., MCAULEY, K.B., LEPAGE, M. How Does the Chemistry of Polymer Gel Dosimeters Affect their Performance? *J. Phys.: Conf. Ser. 164 012003*, 2009, Doi:10.1088/1742-6596/164/1/012003;
36. RUDIN, A., CHOI, P. The Elements of Polymer Science and Engineering, 3rd Edition. *Academic Press*, 2012, . 584. ISBN: 9780123821782;
37. VENNING, A.J. Investigation of Radiation Sensitive Normoxic Polymer Gels for Radiotherapy Dosimetry. *Doctoral dissertation, Queensland University of Technology*, 2005, p. 237;
38. BALDOK, C., DE DEENE, Y., DORAN, S. et al. Polymer gel dosimetry. *Phys Med Biol 55(5)*, 2010, Doi: 10.1088/0031-9155/55/5/R01;
39. JIRASEK, A., DUZENLI, C. Effects of crosslinker fraction in polymer gel dosimeters using FT Raman spectroscopy. *Physics in Medicine and Biology 46(7)*, 2001, p. 1949 – 1961. Doi: 10.1088/0031-9155/46/7/315;
40. MARYANSKI, M.J., AUDET, C., GORE, J.C. Effects of crosslinking and temperature on the dose response of a BANG polymer gel dosimeter. *Phys. Med. Biol. 42(303)*, 1997, <https://doi.org/10.1088/0031-9155/42/2/004>;
41. PAPADAKIS, A.E., MARIS, T.G., ZACHAROPOULOU, F. An evaluation of the dosimetric performance characteristics of N-vinylpyrrolidone-based polymer gels. *Phys Med Biol. 52(16)*, 2007, p. 5069 – 5083. Doi: 10.1088/0031-9155/52/16/024;
42. ADLIENE, D., URBONAVICIUS, B.G., LAURIKAITIENE, J., PUIISO, J. New application of polymer gels in medical radiation dosimetry: Plasmonic sensors. *Radiation Physics and Chemistry. Vol (168)*, 2020, <https://doi.org/10.1016/j.radphyschem.2019.108609>;

43. NECASOVA, B., LISKA, P., KELAR, J., Slanhof, J. Comparison of Adhesive Properties of Polyurethane Adhesive System and Wood-plastic Composites with Different Polymers after Mechanical, Chemical and Physical Surface Treatment. *Polymers 11(3)*, 2019, 397. <https://doi.org/10.3390/polym11030397>;
44. YUAN, X., MAYANOVIC, R. A. An Empirical Study on Raman Peak Fitting and Its Application to Raman Quantitative Research. *Appl. Spectrosc. 71(10)*, 2017, p. 2325 – 2338. Doi: 10.1177/0003702817721527;
45. KHAN, M., HEILEMANN, G., LECHNER, W. et al. Basic Properties of a New Polymer Gel for 3D-Dosimetry at High Dose-Rates Typical for FFF Irradiation Based on Dithiothreitol and Methacrylic Acid (MAGADIT): Sensitivity, Range, Reproducibility, Accuracy, Dose Rate Effect and Impact of Oxygen Scavenger. *Polymers 11(10)*, 2019, 1717. Doi: 10.3390/polym11101717;
46. CRESCENTI, R.A., SCHEIB, S.G., SCHNEIDER, U., GIANOLINI, S. Introducing gel dosimetry in a clinical environment: customization of polymer gel composition and magnetic resonance imaging parameters used for 3D dose verifications in radiosurgery and intensity modulated radiotherapy. *Med. Phys. 34(4)*, 2007, p. 1286 – 1297. Doi: 10.1118/1.2712042;
47. SOUSA, R.V. Dose rate influence on deep dose deposition using a 6 MV x-ray beam from a linear accelerator. *Braz. J. Phys. 39(2)*, 2009, Doi: <http://dx.doi.org/10.1590/S0103-97332009000300009>;
48. SUNTHARALINGHAM, N., PODGORSK, E.B., HENDRY, J.H. Radiation Oncology Physics. Basic Radiobiology. Chapter 14. *IAEA in Austria*. 2005, p.696. ISBN: 92-0-107304-6;
49. MATSUYA, Y., MCMAHON, S.J., TSUTSUMI, K. et al. Investigation of dose-rate effects and cell-cycle distribution under protracted exposure to ionizing radiation for various dose-rates. *Scientific Reports 8* 8287, 2018, <https://doi.org/10.1038/s41598-018-26556-5>;
50. DE DEENE, Y., VERGOTE, K., CLAEYS, C., WAGTER, C. DE. The fundamental radiation properties of normoxic polymer gel dosimeters: a comparison between a methacrylic acid based gel and acrylamide based gels. *Phys. Med. Biol 51(3)*, 2006, 653. <https://doi.org/10.1088/0031-9155/51/3/012>;
51. ALEX, S., TIWARI, A. Functionalized Gold Nanoparticles: Synthesis, Properties and Applications--A Review. *J Nanosci Nanotechnol. 15(3)*, 2015, p. 1869 – 1894. Doi: 10.1166/jnn.2015.9718;
52. Edit. by SEEGENSCHMIEDT, M.H., SAUER, R. Interstitial and Intracavitary Thermoradiotherapy, *Springer – Verlag*. 1993, p. 401. ISBN: 13:978-3-642-84803-2;
53. SHEIB, S., VOGELSANGER, W. Normoxic polymer gel dosimetry. *Rad. Onc. 68(1) S110*, 2003, [https://doi.org/10.1016/S0167-8140\(03\)80329-8](https://doi.org/10.1016/S0167-8140(03)80329-8);
54. ROED, Y., WANG, J., PINKSY, L., IBBOTT, G. Polymer gels enable volumetric dosimetry of dose distribution from an MR-guided linac. *Rad. Onc. 125(3)*, 2016, p. 426 – 432. <https://doi.org/10.1016/j.radonc.2017.08.027>;

55. MANN, P., SAITO, N., LANG, C. et al. 4D dose calculations validated by combining 3D polymer gel dosimetry and the Calypso tracking system. *Rad. Onc. Vol(127)*, 2018, S958 – 959. Doi:[https://doi.org/10.1016/S0167-8140\(18\)32095-4](https://doi.org/10.1016/S0167-8140(18)32095-4);
56. SHIH, C.T., HSU, J.T., HAN, R.P., et al. A Novel Method of Estimating Dose Responses for Polymer Gels Using Texture Analysis of Scanning Electron Microscopy Images. *PLOS one 8(7)*, 2013, Doi:10.1371/journal.pone.0067281.g009;
57. LEPAGE M. Magnetic resonance in polymer gel dosimetry: techniques and optimization. *J. of Phys.* 56, 2006, p. 86-9;
58. AZADBAKHD,B., ZAHMATKESH,M.H., HADAD,K., BAGHERI,S. Verification of the PAGAT polymer gel dosimeter by photon beams using magnetic resonance imaging. *Iran. J. Radiat. Res Vol 6(2)*. 2008, p.83-87;
59. HENDRICK,R.E. Optimization of Breast MRI Imaging Protocols. *Conference Proceedings: Jointly sponsored CME by University of Kentucky HealthCare CECentra and Rperience*, 2009;
60. International Commission on Radiological Protection, Ed. By VALENTIN,J. Recommendations of the International Commission on Radiological Protection, 2007, Open access: [https://www.icrp.org/docs/ICRP_Publication_103-Annals_of_the_ICRP_37\(2-4\)-Free_extract.pdf](https://www.icrp.org/docs/ICRP_Publication_103-Annals_of_the_ICRP_37(2-4)-Free_extract.pdf);
61. KESHTKAR, M., TAKAVAR, A., ZAHMATKESH, M.H., MONTAZERABADI, A.R. Uncertainty Analysis in MRI–Based Polymer Gel Dosimetry. *J. Biomed. Phys. Eng.* 7(3), 2017, p. 299 – 304. Doi: 10.22086/JBPE.V0I0.436;
62. DUYN, J.H., GELDEREN, P., LI, T. et al. High-field MRI of brain cortical substructure based on signal phase. *PNAS 104(28)*, 2007, p. 11796 – 11801. Doi: <https://doi.org/10.1073/pnas.0610821104>;
63. DUYN, J., YANG, Y., FRANK, J.A., WEEN, J.W. Simple Correction Method for k-Space Trajectory Deviations in MRI. *Journal of Magnetic Resonance 132*, 1998, p. 150 -153. Doi: 10.1006/jmre.1998.1396;
64. HERNANDO, D., LIANG, Z.P., KELLMAN, P. Chemical Shift-Based Water/Fat Separation: A Comparison of Signal Models. *Magn. Reson. Med 64(3)*, 2011, p. 811 – 822. Doi: 10.1002/mrm.22455;
65. HARGREAVES, B. Quantitative/Mapping methods. *RAD 229 conference proceedings*, 2017, Open access: <https://web.stanford.edu/class/rad229/Notes/4d-Mapping.pdf>;
66. RAZAK, N., RAHMAN, A.A., KANDAIYA, S. et al. Role of anti-oxidants on normoxic methacrylic acid gelatin (mag) polymer gel dosimeter AT 6-MV photon beam using single spin echo MRI. *Malaysian Journal of Analytical Sciences 18(2)*, 2014, p. 423 – 433;
67. MARYANSKI, M.J., SCHULZ, R.J., IBBOTT, G.S. et al. Magnetic resonance imaging of radiation dose distributions using a polymer-gel dosimeter. *Phys. Med. Biol.* 39(9), 1994, p. 1437 – 1455. Doi: 10.1088/0031-9155/39/9/010;
68. DE DEENE, Y., BALDOCK, C. Optimization of multiple spin–echo sequences for 3D polymer gel dosimetry. *Phys. Med. Biol.* 47 3117, 2002, <https://doi.org/10.1088/0031-9155/47/17/306>;

69. HIROKI, A., YAMASHITA, S., SATO, Y. et al. New polymer gel dosimeters consisting of less toxic monomers with radiation-crosslinked gel matrix. *J. Phys. Conf. Ser.* 444 012028, 2013, Doi:10.1088/1742-6596/444/1/012028;
70. DIAS, J.R., MANGUIERA, T.F., LOPES, R.V. et al. Preliminary analysis of N-vinylpyrrolidone based polymer gel dosimeter. *Polimeros* 28(5), 2018, <http://dx.doi.org/10.1590/0104-1428.01718>;
71. CHACON, D., VEDELAGO, J., STRUMIA, M.C. et al. Raman spectroscopy as a tool to evaluate oxygen effects on the response of polymer gel dosimetry. *Applied Radiation and Isotopes Vol 150*, 2019, p. 43 – 52. <https://doi.org/10.1016/j.apradiso.2019.05.006>;
72. ABTAHI, S. M., AGHAMIRI, S. M. R., KHALAFI, H. Optical and MRI investigations of an optimized acrylamide-based polymer gel dosimeter. *Journal of Radioanalytical and Nuclear Chemistry* 300(1), 2014, p. 287-301. <https://doi.org/10.1007/s10967-014-2983-7>;
73. SHIH, C.T., CHANG, Y.J., HSU, J.T., et al. Image reconstruction of optical computed tomography by using the algebraic reconstruction technique for dose readouts of polymer gel dosimeters. *Physica Medica*, 31(8), 2015, p. 942-947.
74. XU, A.Y., WUU, C.S. Application of Optical CT Scanning in Three-Dimensional Radiation Dosimetry. In: CT Scanning-Techniques and Applications. *InTech*, 2011, Doi: 10.5772/20678;
75. ŠEPERIENĖ, N., ADLIENĖ, D. Comparison of low dose proton and photon irradiation induced polymerization processes in advanced nMAG gels using Raman spectroscopy. *J. Phys.: Conf. Ser.* 1305 012039, 2019, Doi:10.1088/1742-6596/1305/1/012039;
76. BUMBRAH, G.S., SHARMA, R.M. Raman spectroscopy – Basic principle, instrumentation and selected applications for the characterization of drugs of abuse. *Egyptian Journal of Forensic Sciences* 6(3), 2016, p. 209 – 215. <https://doi.org/10.1016/j.ejfs.2015.06.001>;
77. BAKER, M.J., HUGHES, C.S., HOLLYWOOD, K.A. Biophotonics: Vibrational Spectroscopic Diagnostics, chapter Raman spectroscopy. *Morgan and Claypool publishers*, 2016, p. 3 – 13. ISBN: 978-1-6817-4071-3;
78. RINTOUL, L., LEPAGE, M., BALDOCK, C. Radiation dose distribution in polymer gels by Raman spectroscopy. *Appl. Spectrosc.* 57(1), 2003, p. 51 – 57. Doi: 10.1366/000370203321165205;
79. MCAULEY, K. The chemistry and physics of polyacrylamide gel dosimeters: Why they do and don't work. *J. Phys. Conf. Ser.* 3(1), 2004, Doi: 10.1088/1742-6596/3/1/005
80. SHIH, C.T., CHANG, Y., HSIEH, B.T., WU, J. Microscopic SEM texture analysis of NIPAM gel dosimeters. *IEEE Transactions on Nuclear Science* 60(3), 2013, Doi: 10.1109/TNS.2013.2258038;
81. NOVOTNY, J. et al. Application of polymer-gel dosimetry in stereotactic radiosurgery. *J. Phys. Conf. Ser.* 3 (049), 2004, p. 288 – 292. Doi: 10.1088/1742-6596/3/1/049;
82. MOUTSATSOS, A., PETROKOKKINOS, L., KARAIKOS, P. Gamma Knife output factor measurements using VIP polymer gel dosimetry. *Med. Phys.* 36(9), 2009, p. 4277 – 4287. Doi: 10.1118/1.3183500;

83. VENNING, A., CHANDROTH, M., CHICK, B. Clinical experience of the normoxic PAG gel dosimeter using a flattening filter free beam for SABR treatments with MRI readout. *Physica Medica Vol (52)*, 2018, p. 168. <https://doi.org/10.1016/j.ejmp.2018.06.024>;
84. WUU, C.S., SCHIFF, P., MARYANSKI, M.J. et al. Dosimetry study of Re-188 liquid balloon for intravascular brachytherapy using polymer gel dosimeters and laser-beam optical CT scanner. *Med. Phys.* 30(2), 2003, p. 132 – 137. Doi: 10.1118/1.1533749;
85. MASILLON, G., MINNITI, R., MITCH, M.G. et al. The use of gel dosimetry to measure the 3D dose distribution of a ⁹⁰Sr/⁹⁰Y intravascular brachytherapy seed. *Phys. Med. Biol.* 54(6), 2012, p. 1661 – 1672. Doi: 10.1088/0031-9155/54/6/017;
86. FRAGOSO, M., LOVE, P.A., VERHAEGEN, F. et al. The dose distribution of low dose rate Cs-137 in intracavitary brachytherapy: comparison of Monte Carlo simulation, treatment planning calculation and polymer gel measurement. *Phys. Med. Biol.* 49(24), 2004, p. 5459 – 5474. Doi: 10.1088/0031-9155/49/24/005;
87. VIDOVIC, A.K., JUANG, T., MELTSNER, S. et al. An investigation of a PRESAGE® in vivo dosimeter for brachytherapy. *Phys. Med. Biol.* 59(14), 2014, p. 3893 – 3905. Doi: 10.1088/0031-9155/59/14/3893;
88. MAYNARD, E., HILTS, M., HEATH, E., JIRASEK, A. Evaluation of accuracy and precision in polymer gel dosimetry. *Med. Phys.* 44(2), 2016, p. 736 – 746. <https://doi.org/10.1002/mp.12080>;
89. MOUTSATSOS, A., KARAIKOS, P., PETROKOKKINUS, L. et al. Assessment and characterization of the total geometric uncertainty in Gamma Knife radiosurgery using polymer gels. *Med. Phys.* 40(3), 031704, 2013, Doi: 10.1118/1.4789922;
90. RUDZIANSKAS V, INCIURA A, JUOZAITYTE E, RUDZIANSKIENE M, KUBILIUS R, VAITKUS S, KASETA M, ADLIENE D. Reirradiation of recurrent head and neck cancer using highdose-rate brachytherapy. *PMS Vol 32(5)*, 2012, p.297–303;
91. ELTER, A., DORSCH, S., MANN, P. et al. Compatibility of 3D printing materials and printing techniques with PAGAT gel dosimetry. *Phys. Med. Biol.* 64(4) 04NT02, 2019, <https://doi.org/10.1088/1361-6560/aafef0>;
92. A Guide to Polyacrylamide Gel Electrophoresis and Detection. *Bio-Rad Laboratories Inc*, 2014, p. 92. Online: http://www.bio-rad.com/webroot/web/pdf/lsr/literature/Bulletin_6040.pdf;
93. ADLIENE, D., URBOVICIUS, B.G., LAURIKAITIENE, J., PUIISO, J. New application of polymer gels in medical radiation dosimetry: Plasmonic sensors. *Rad. Phys. Chem. Vol (168)*, 2020, <https://doi.org/10.1016/j.radphyschem.2019.108609>;
94. RAHMAN, W.N., WONG, C.J., YAGI, N., DAVIDSON, R., GESO, M. Dosimetry and its enhancement using gold nanoparticles in synchrotron based microbeam and stereotactic radiosurgery. *Conference on Medical Applications of Synchrotron Radiation Proceedings. Vol (1266)*, 2010, p.107-110. <https://doi.org/10.1063/1.3478186>;
95. CEBERG, S. 3D Verification of Dynamic and Breathing Adapted Radiotherapy using Polymer Gel Dosimetry. *Monography*, 2010, ISBN: 978-91-7473-041-8;

96. VANOSSI, E., GAMBARINI, G., CARRARA, M., MARIANI, M. Polymer gels for in phantom dose imaging in radiotherapy. *Applied radiation and Isotopes*. Vol (68), 2010, p. 772–775. <https://doi.org/10.1016/j.apradiso.2009.09.052>;
97. JIRASEK, A. Experimental investigation of polymer gel dosimeters. *J. Of Phys. Conf. Ser. Vol (56) 003*, 2006, <https://doi.org/10.1088/1742-6596/56/1/003>;
98. JASZCZAK, M., MARAS, P., KOZICKI, M. Characterization of a new N-vinylpyrrolidone-containing polymer gel dosimeter with pluronic F-127 gel matrix. *Rad. Phys. And Chem. Vol (177)*, 2020, <https://doi.org/10.1016/j.radphyschem.2020.109125>;
99. JAYARAMAN, S., LANZL, L.H. *Clinical Radiotherapy Physics: 20 chapter Radiation Safety in Brachytherapy*. Springer, 2004, p.523. ISBN: 978-3-642-18549-6;
100. BJORELAND, E., LINDVALL, P., KARLSSON, A., GUSTAVSSON, H. Liquid ionization chamber calibrated gel dosimetry in conformal stereotactic radiotherapy of brain lesions. *Acta Oncologica* 47(6), 2008, p.1099-1109. DOI:10.1080/02841860801888781;
101. DISPENZA, C., GRIMALDI, N., SABATINO, M. A. et al. Radiation-Engineered Functional Nanoparticles in Aqueous Systems. *Journal of Nanoscience and Nanotechnology* 15(5), 2015, p. 3445 – 3467. Doi: 10.1166/jnn.2015.9865;
102. GUSTAVSSON, H. *Radiotherapy Gel Dosimetry: Development and Application of Normoxic Polymer Gels*, 2004, Available: <https://portal.research.lu.se/>;
103. ADLIENE D., JAKSTAS K., VAICIUNAITE N., LAURIKAITIENE J., Cerapaitė-Trusinskienė R. Application of Dose Gels in HDR Brachytherapy. In: Jaffray D. (eds) *World Congress on Med. Phys. Biomed. Eng., IFMBE Proceedings, Vol 51*. Springer, 2015, https://doi.org/10.1007/978-3-319-19387-8_178;
104. KARLSSON, A., GUSTAVSSON, H., MANSSON, S. Dose integration characteristics in normoxic polymer gel dosimetry investigated using sequential beam irradiation. *Phys. Med. Biol.* 52(15), 2007, p.4697-4706. DOI:10.1088/0031-9155/52/15/021;
105. FARHOOD, B., GERRILL, G., ABTAHL, S.M. A systematic review of clinical applications of polymer gel dosimeters in radiotherapy. *Appl. Rad. Iso. Vol (143)*, 2019, p.47-59. <https://doi.org/10.1016/j.apradiso.2018.08.018>;
106. ŠČUPAKOVA, K., TERZOPOULOS, V., JAIN, S., SMEETS, D., HEEREN, R.M.A. A patch-based super resolution algorithm for improving image resolution in clinical mass spectrometry. *Scientific Reports Vol (9), 2915*, 2019, <https://doi.org/10.1038/s41598-019-38914-y>;
107. MASOUMI, H., DIZAJI, M.M., ARBABI, A. et al., Determine the Dose Distribution Using Ultrasound Parameters in MAGIC-f Polymer Gels. *Sage Journals Vol (14) 1*, 2016, <https://doi.org/10.1177/1559325815625647>;
108. TULEUSHEV, A.Z., HARISSON, F.E., KOZLOVSKIY, A.L., ZDOROVETS, M.A. Assessment of the Irradiation Exposure of PET Film with Swift Heavy Ions Using the Interference-Free Transmission UV-Vis Transmission Spectra. *Polymers Vol 13 (358)*, 2021, <https://doi.org/10.3390/polym13030358>;
109. ŠEPERIENĖ, N. The development of polymer gels and composites with the enhanced sensitivity to low-dose irradiation. *KTU, Technologija*, 2018, p.146. ISBN: 978-609-02-1487-9;

110. SANDILOS, P., TATSIS, E., VLACHOS, L., DARDOUFAS, C. et al. Mechanical and dose delivery accuracy evaluation in radiosurgery using polymer gels. *J Appl Clin Med Phys Vol 7(4)*, 2006, p.13-21. Doi:10.1120/jacmp.v7i4.2273;
111. HOSSAIN, M.K., RAHMAN, M.T., BASHER, M.K. Impact of ionizing radiation doses on nanocrystalline TiO₂ layer in DSSC's photoanode film. *Results in Physics Vol 11*. 2018, p.1172-1181. <https://doi.org/10.1016/j.rinp.2018.10.006>;
112. TRUMBO, T.A., SCHULTZ, E., BORLAND, M.G. Applied spectrophotometry: Analysis of a biochemical mixture. *Biochemistry and Molecular Biology Education 41(4)*, 2013, p. 242 – 250. <https://doi.org/10.1002/bmb.20694>;
113. OLDHAM, M. Optical-CT scanning of polymer gels. *J of Phys. Conf. Ser. Vol 3(011)*. 2004, p.122-135. Doi: 10.1088/1742-6596/3/1/011;
114. MANJAPPA, R., SHARATH, M.S., KUMAR, R., KANHIRODAN, R. Effects of refractive index mismatch in optical CT imaging of polymer gel dosimeters. *Med. Phys. Vol 42(2)*, 2015, Doi:10.1118/1.4905043;
115. JIRASEK, A., HILTS, M., SHAW, C., BAXTER, P. Investigation of tetrakis hydroxymethyl phosphonium chloride as an antioxidant for use in x-ray computed tomography polyacrylamide gel dosimetry. *Phys. Med. Biol. 51(7)*, 2008, 1891. Doi: <https://doi.org/10.1088/0031-9155/51/7/018>;
116. WU, F., WANG, H., ZHENG, X. Concentration-dependent frequency shifts of the C-S stretching modes in ethylene trithiocarbonate studied by Raman spectroscopy. *Journal of Raman Spectroscopy 46(6)*, 2015, p. 591 – 596. <https://doi.org/10.1002/jrs.4683>;
117. BONG, J., CHOI, K., YU, S.C. et al. Raman Spectroscopy of Irradiated Normoxic Polymethacrylic Acid Gel Dosimeter. *Bulletin Korean Chemical Society 32(2)*, 2011, Doi: 10.5012/bkcs.2011.32.2.625;
118. DASAN, B.G., SIR, N., KAVLAK, S., GUNER, A. A New Approach for the Electrochemical Detection of Phenolic Compounds. Part I: Modification of Graphite Surface by Plasma Polymerization Technique and Characterization by Raman Spectroscopy. *Food and Bioprocess Technology 3(3)*, 2009, p.473-479. Doi: 10.1007/s11947-009-0244-5;
119. ADENAN, M.Z., AHMAD, M., NOOR, N.M. A Study of N-Isopropyl Acrylamide (NIPAM)-Based Polymer Gel Dosimeter by Using Raman Spectroscopy. *Advanced Materials Research Vol (1107)*, 2015, p.103 – 107. <https://doi.org/10.4028/www.scientific.net/AMR.1107.103;67>.
120. TODICA, M., STEFAN, R., POP, C.V., OLAR, L. IR and Raman Investigation of Some Poly (acrylic) Acid Gels in Aqueous and Neutralized State. *Acta Physica Polonica A Vol (128)*, 2015, Doi: 10.12693/APhysPolA.128.128;
121. National Center for Biotechnology Information. PubChem Compound Summary for CID 6917, N-Vinyl-2-pyrrolidone. Retrieved June 28, 2021, <https://pubchem.ncbi.nlm.nih.gov/compound/N-Vinyl-2-pyrrolidone>;
122. BEHERA, M., RAM, S. Interaction between poly(vinyl pyrrolidone) PVP and fullerene C60 at the interface in PVP-C60 nanofluids—A spectroscopic study. *IOP Conf. Series: Materials Science and Engineering Vol 330*, 2018, Doi:10.1088/1757-899X/330/1/012016;

123. BALDOCK, C., RINTOUL, L., KEEVIL, S.F. et al. Fourier transform Raman spectroscopy of polyacrylamide gels (PAGs) for radiation dosimetry. *Phys. Med. Biol.* 43, 1998, 3617. <https://doi.org/10.1088/0031-9155/43/12/017>;
124. BASTARRACHEA, M.L., KAO, W.H., et al. A TG/FTIR study on the thermal degradation of poly(vinyl pyrrolidone). *Journal of Thermal Analysis and Calorimetry.* 2011, DOI:10.1007/S10973-010-1061-9
125. HILTS, M. X-ray computed tomography imaging of polymer gel dosimeters. *J. Phys. Conf. Ser.* 56 009, 2006, p. 95 – 107. Doi: 10.1088/1742-6596/56/1/009;
126. DENOTTER, T.D., SCHUBERT, J. Hounsfield Unit. *In StatPearls*, 2020, Online access: <https://www.ncbi.nlm.nih.gov/books/NBK547721/>;
127. VOLOBUEV, A.N., LUKACHEV, S.V., TOLSTONOGOV, A.P., KOLOMIN, I.V. Interaction of Photons with Electrons of a Metal during the Irradiation of Its Surface in Vector-Potential Space. *J. Synch. Investig. Vol (13).* 2019, p.658-666. <https://doi.org/10.1134/S102745101902040X>;
128. SPENCE, J.C. Outrunning damage: Electrons vs X-rays—timescales and mechanisms. *Structural Dynamics* 4, 2017, 044027. <https://doi.org/10.1063/1.4984606>;
129. CLELAND, M.R., GALLOWAY, R., BROWN, D.F. X-ray Scattering in the Shielding of Industrial Irradiation Facilities. *Physics Procedia* 90, 2017, p. 151 – 156. Doi: 10.1016/j.phpro.2017.09.049;
130. Ashland Inc, “Gafchromic TM RTQA2 film,” 2013
131. RUH, A., KISELEV, V.G. Calculation of Larmor precession frequency in magnetically heterogeneous media. *Concepts Magn. Reson. Part A Vol 47*, 2019, Doi: 10.1002/cmr.a.21472;
132. MACKIEWICH, B. Intracranial Boundary Detection and Radio Frequency Correction in Magnetic Resonance Images. *Monography*, 1995, p.166. Open access: <https://summit.sfu.ca>;
133. DAVIDOVITS, P. Chapter 17: Nuclear Physics. *Phys. Biol. Med 5th edition. Academic Press.*, 2019, p.291, ISBN 9780128137161. <https://doi.org/10.1016/B978-0-12-813716-1.00017-3>;
134. JASELSKĖ, E., KUDREVIČIUS, L., RUDŽIANSKAS, V., DIDVALIS, T., ADLIENĖ, D. First approach to 3D dosimetry verification using Leksell Gamma knife Icon™. *Med. Phys. Conf. Proceedings*, 2019, p. 48-51. ISSN 1822–5721;
135. MALKAJ, P. The dose profiles in the certain depth. *J. Chem. Biol. Phys. Sciences* 10(3), 2020, p. 101 – 107. Doi: 10.24214/jcbps.C.10.3.10107;
136. AUDET, C., HILTS, Jirasek, A., Duzenli, A. 3d dose verification of a stereotactic irradiation using an x-ray ct pag dosimetry technique. *Journal of Applied Clinical Medical Physics*, 3(2), 2002, p. 110–118.
137. JASELSKĖ, E., ADLIENĖ, D., RUDŽIANSKAS, V., JAKŠTAS, K. Free standing polymerized gels and in vivo TLD dosimetry in catheter-based HDR brachytherapy. *Med. Phys. Conf. Proceeding*, 2017, p.145-148. ISSN 1822-5721;
138. ADLIENĖ, D., URBONAVIČIUS, B. G., ŠEPERIENĖ, N., LAURIKAITIENĖ, J., JASELSKĖ, E. The radiation doses, obtaining to the patient during external radiotherapy procedures, visualization system and its manufacturing method, *Kaunas University of Technology*, 2021, Application nr. K158-35LT, patent nr. A61B 6/00;

139. ADLIENE, D., JAKSTAS, K., URBONAVICIUS, B.G. In vivo TLD dose measurements in catheter – based high – dose – rate brachytherapy. *Radiat. Prot. Dosimetry* 165(1-4), 2015, p. 477 – 481. Doi: <https://doi.org/10.1093/rpd/ncv054>;
140. SCHREINER, L.J. Review of Fricke gel dosimeters. *J. Phys: Conf. Ser.* 3 003, 2004, Doi: <https://doi.org/10.1088/1742-6596/3/1/003>;
141. JORDAN, K., AVVAKUMOV, N. Radiochromic leuco dye micelle hydrogels: I. Initial investigation. *Phys. Med. Biol.* 54(22), 2009, p. 6773-6789. Doi: 10.1088/0031-9155/54/22/002;
142. EBENEZEN S.B.S., RAFIC, M.K., RAVINDRAN, P.B. Basic investigations on LCV micelle gel. *J. Phys: Conf. Ser.* 444(1), 2013, p. 2027-. Doi: 10.1088/1742-6596/444/1/012027;
143. MOOK, K.J., HAN, L.D., RA, C.H., BUNG, H.S. et al. Analysis of Physical Properties for Various Compositions of Reusable LMG and LCV Micelle Gel. *Korea Science Vol* 27(4), 2016, p. 175-179. <https://doi.org/10.14316/pmp.2016.27.4.175>.

LIST OF PUBLICATIONS

Articles published in journals belonging to the scientific international databases Clarivate Analytics. Indexed in the Web of Science with Impact Factor

Related to the dissertation topic

A1. [S1; GB] **Jaselskė, Evelina**; Adlienė, Diana; Rudžianskas, Viktoras; Urbonavičius, Benas Gabrielis; Inčiūra, Artūras. In vivo dose verification method in catheter based high dose rate brachytherapy // *Physica Medica*. Oxford : Elsevier. ISSN 1120-1797. eISSN 1724-191X. 2017, Vol. 44, p. 1-10. DOI: 10.1016/j.ejmp.2017.11.003. [Science Citation Index Expanded (Web of Science); Scopus] [IF: 2,240; AIF: 3,002; IF/AIF: 0,746; Q2 (2017, InCites JCR SCIE)] [M.kr.: M 001, N 002] [Indėlis: 0,200];

A2. [S1; NL] Adlienė, Diana; **Jaselskė, Evelina**; Rudžianskas, Viktoras; Šeperienė, Neringa. First approach to ionizing radiation based 3D printing: fabrication of free standing dose gels using high energy gamma photons // *Nuclear instruments and methods in physics research, Section B: Beam interactions with materials and atoms*. Amsterdam : Elsevier. ISSN 0168-583X. eISSN 1872-9584. 2018, Vol. 435, p. 246-250. DOI: 10.1016/j.nimb.2018.01.033. [Science Citation Index Expanded (Web of Science); Scopus] [IF: 1,210; AIF: 2,497; IF/AIF: 0,484; Q3 (2018, InCites JCR SCIE)] [M.kr.: T 008, M 001] [Indėlis: 0,250];

A3. [S1; NL] **Jaselskė, Evelina**; Adlienė, Diana; Rudžianskas, Viktoras; Korobeinikova, Erika; Radžiūnas, Andrius. Application of polymer dose gels for millimeter scale target/tumor pretreatment imitation using gamma knife facility // *Nuclear instruments and methods in physics research. Section B: Beam interactions with materials and atoms*. Amsterdam : Elsevier. ISSN 0168-583X. eISSN 1872-9584. 2020, vol. 470, p. 56-60. DOI: 10.1016/j.nimb.2020.03.009. [Science Citation Index Expanded (Web of Science); Scopus] [IF: 1,270; AIF: 2,574; IF/AIF: 0,493; Q2 (2019, InCites JCR SCIE)] [M.kr.: T 008, M 001] [Indėlis: 0,200]

Others:

4. [S1; GR] Korobeinikova, Erika; Ugenskiene, Rasa; Insodaite, Rūta; Rudžianskas, Viktoras; **Jaselskė, Evelina**; Poškienė, Lina; Juozaityte, Elona. Association of angiogenesis and inflammation-related gene functional polymorphisms with early-stage breast cancer prognosis // *Oncology letters*. Athens : Spandidos publ LTD. ISSN 1792-1074. eISSN 1792-1082. 2020, vol. 19, no. 6, p. 3687-3700. DOI: 10.3892/ol.2020.11521. [Science Citation Index Expanded (Web of Science); MEDLINE] [IF: 2,311; AIF: 4,840; IF/AIF: 0,477; Q3 (2019, InCites JCR SCIE)] [M.kr.: M 001] [Indėlis: 0,142];

5. [S1; CH] Rudžianskas, Viktoras; Korobeinikova, Erika; Rudžianskienė, Milda; **Jaselskė, Evelina**; Adlienė, Diana; Šedienė, Severina; Kulakienė, Ilona; Padervinskis, Evaldas; Jurkienė, Nemira; Juozaitytė, Elona. Use of 18F-FDG PET/CT imaging for radiotherapy target volume delineation after induction chemotherapy and

for prognosis of locally advanced squamous cell carcinoma of the head and neck // *Medicina*. Basel : MDPI AG. ISSN 1010-660X. eISSN 1010-660X. 2018, vol. 54, iss. 6, art. no. 107, p. 1-18. DOI: 10.3390/medicina54060107. [Science Citation Index Expanded (Web of Science); Scopus; DOAJ] [IF: 1,467; AIF: 4,542; IF/AIF: 0,322; Q3 (2018, InCites JCR SCIE)] [M.kr.: M 001] [Indėlis: 0,100]

Publications indexed in the Web of Science database without citation index (JCR SCIE)

International publishers

1. [P1a; SG] Adlienė, Diana; Jaselskė, Evelina; Urbonavičius, Benas Gabrielis; Laurikaitienė, Jurgita; Rudžianskas, Viktoras; Didvalis, Tadas. Development of 3D printed phantom for dose verification in radiotherapy for the patient with metal artifacts inside // IFMBE proceedings: World congress on medical physics and biomedical engineering 2018, June 3–8, 2018, Prague, Czech Republic / L. Lhotska, L. Sukupova, I. Lacković, G.S. Ibbott (eds.). Singapore : Springer, 2019. ISBN 9789811090226. eISBN 9789811090233. ISSN 1680-0737. eISSN 1433-9277. 2019, vol. 68, iss. 3, p. 643-647. DOI: 10.1007/978-981-10-9023-3_119. [Conference Proceedings Citation Index - Science (Web of Science); Scopus] [M.kr.: N 002, M 001] [Indėlis: 0,166]

National publishers

1. [P1a; LT] Jaselskė, Evelina; Kudrevičius, Linas; Rudžianskas, Viktoras; Didvalis, Tadas; Adlienė, Diana. First approach to 3D dosimetry verification using Leksell gamma knife® ICON™ // *Medical physics in the Baltic States: proceedings of the 14th international conference on medical physics*, Kaunas, Lithuania, 7-9 November, 2019 / executive editor Diana Adlienė. Kaunas : Kaunas University of Technology. ISSN 1822-5721. 2019, p. 48-51. [Conference Proceedings Citation Index - Science (Web of Science)] [M.kr.: N 002] [Indėlis: 0,200]
2. [P1a; LT] Jaselskė, Evelina; Adlienė, Diana; Rudžianskas, Viktoras; Korobeinikova, Erika. Dosimetric characteristics of 3d printed materials // *Medical physics in the Baltic States: proceedings of the 13th international conference on medical physics*, Kaunas, Lithuania, 9-11 November, 2017 / edited by D. Adliene. Kaunas : Kaunas University of Technology. ISSN 1822-5721. 2017, p. 52-55. [Conference Proceedings Citation Index - Science (Web of Science)] [M.kr.: M 001, T 008] [Indėlis: 0,250]
3. [P1a; LT] Opulskis, Donatas; Jaselskė, Evelina; Didvalis, Tadas. Evaluation of overlapping doses for gynecologic cancer patients using semiconductor diodes // *Medical physics in the Baltic States: proceedings of the 13th international conference on medical physics*, Kaunas, Lithuania, 9-11 November, 2017 / edited by D. Adliene. Kaunas : Kaunas University of Technology. ISSN 1822-5721. 2017, p. 85-88. [Conference Proceedings Citation Index - Science (Web of Science)] [M.kr.: T 008, N 011] [Indėlis: 0,333]
4. [P1a; LT] Didvalis, Tadas; Vaitkus, Antanas; Jaselskė, Evelina. Evaluation methods for speed and positioning of multileaf collimator leaves // *Medical Physics*

in the Baltic States : Proceedings of the 12th International conference on Medical Physics : Kaunas, Lithuania, 5-7 November, 2015 / Kaunas University of Technology ; [Executive Editor Diana Adlienė]. Kaunas : Technologija. ISSN 1822-5721. 2015, p. 31-33. [Conference Proceedings Citation Index - Science (Web of Science)] [M.kr.: M 001] [Indėlis: 0,333]

5. [P1a; LT] Jaselskė, Evelina; Adlienė, Diana; Rudžianskas, Viktoras; Jakštas, Karolis. Free standing polymerized gels and in vivo TLD dosimetry in catheter-based HDR brachytherapy // Medical Physics in the Baltic States : Proceedings of the 12th International conference on Medical Physics : Kaunas, Lithuania, 5-7 November, 2015 / Kaunas University of Technology ; [Executive Editor Diana Adlienė]. Kaunas : Technologija. ISSN 1822-5721. 2015, p. 145-148. [Conference Proceedings Citation Index - Science (Web of Science)] [M.kr.: N 011] [Indėlis: 0,250]

In peer-reviewed conference proceedings

International publishers

1. [P1c; CH] Laurikaitienė, Jurgita; Puiso, Judita; Jaselske, Evelina. Investigation of X-ray attenuation properties in 3D printing materials used for development of Head and Neck Phantom // Recent advances in technology research and education: proceedings of the 17th international conference on global research and education InterAcademia – 2018 / editor: Giedrius Laukaitis. Cham : Springer Nature, 2019. ISBN 9783319998336. eISBN 9783319998343. p. 137-143. (Lecture notes in networks and systems, ISSN 2367-3370, eISSN 2367-3389; vol. 53). DOI: 10.1007/978-3-319-99834-3_18. [Scopus] [M.kr.: N 003] [Indėlis: 0,333]

Other conference abstracts and articles in unreviewed conference proceedings

1. [T2; KZ] Jaselske, E.; Adliene, D.; Radžiūnas, A. Polymer dose gels for microscale target/tumor pretreatment imitation // REY-20: 20th international conference on radiation effects in insulators, 19-23 August 2019, L.N. Gumilyov Eurasian National University, Nur-Sultan (Astana), Kazakhstan: book of abstracts. Nur-Sultan : L.N. Gumilyov ENU printing house. 2019, P2-7, p. [1]. [M.kr.: N 002]

2. [T1e; LT] Laurikaitienė, J.; Puišo, J.; Jaselskė, E. Investigation of X-ray attenuation properties in 3D printing materials used for development of head and neck phantom // Inter-Academia 2018: 17th international conference on global research and education, September 24-27, 2018 Kaunas, Lithuania: programme and abstracts. Kaunas : Kaunas University of Technology. ISSN 2538-8835. 2018, p. 74. [M.kr.: N 002]

3. [T1e; NL] Rudžianskas, Viktoras; Korobeinikova, Erika; Inčiūra, Arturas; Rudžianskienė, Milda; Jaselskė, Evelina; Adlienė, Diana. Reduction of target volume post induction chemotherapy using PET/CT in locally advanced HNSCC // Radiotherapy and oncology : ESTRO 37, 20-24 April 2018, Barcelona, Spain. Amsterdam : Elsevier. ISSN 0167-8140. 2018, vol. 127, suppl. 1, EP-1111, p. 628. [M.kr.: M 001]

4. [T1e; LT] Jaselskė, Evelina; Didvalis, Tadas; Urbonavičius, Benas Gabrielis; Rudžianskas, Viktoras; Korobeinikova, Erika. 3D printed phantom development and

first approach for verification of individual dose in radiotherapy // Science for health: 1st international doctoral students' conference, April 13, 2018, Kaunas, Lithuania: book of abstracts. Kaunas : LSMU, 2018. ISBN 9789955155300. p. 40-41. [M.kr.: M 001, T 008]

5. [T1e; LT] Korobeinikova, Erika; Rudžianskas, Viktoras; Jaselskė, Evelina; Laurikaitienė, Jurgita; Adlienė, Diana. Risk factors for mandible osteoradionecrosis in oral cavity and oropharyngeal cancer patients // 1st International doctoral students' conference "Science for Health" : book of abstracts : April 13, 2018, Kaunas, Lithuania / Lithuanian university of health sciences. LSMU Department of Research Affairs. Council of LSMU Doctoral Students ; [Edited by Indrė Šveikauskaitė]. Kaunas : Lietuvos sveikatos mokslų universiteto Leidybos namai, 2018. ISBN 9789955155300. p. 55-56. [M.kr.: M 001]

6. [T1e; FR] Jaselskė, Evelina; Adlienė, Diana. Free standing dose gels: first approach to ionizing radiation based 3D printing // REI-19: the 19th international conference on radiation effects in insulators, 2nd – 7th July 2017, Versailles, France : book of abstracts. [S. l.] : [s.n.]. 2017, p. 57-58. [M.kr.: N 002]

7. [T1e; FR] Šeperienė, Neringa; Adlienė, Diana; Jaselskė, Evelina. Proton irradiation induced radiation effects in dose gels // REI – 19: the 19th international conference on radiation effects in insulators, 2nd – 7th July 2017, Versailles, France : book of abstracts. [S. l.] : [s.n.]. 2017, p. 55-56. [M.kr.: N 002]

8. [T2; LT] Jaselskė, Evelina. Apšvitos dozių registravimas bei vertinimas kateterinėje didelės dozės galios brachiterapijoje // Fizinių ir technologijos mokslų tarpdalykiniai tyrimai 2017: 7-oji jaunųjų mokslininkų konferencija, 2017 m. vasario 9 d. : pranešimų santraukos / Lietuvos mokslų akademija. [Vilnius] : [LMA Matematikos, fizikos ir chemijos mokslų skyrius]. 2017, p. 14. [M.kr.: N 002]

Patent:

1. KAUNAS UNIVERSITY OF TECHNOLOGY (LT): The radiation doses, obtaining to the patient during external radiotherapy procedures, visualization system and its manufacturing method. Inventors: Diana ADLIENĖ, Benas Gabrielis URBONAVIČIUS, Neringa ŠEPERIENĖ, Jurgita LAURIKAITIENĖ, **Evelina JASELSKĖ**. Application nr. K158-35LT, patent nr. A61B 6/00 (2021).

ANNEXES

ANNEX 1

Dose gel	Gelatin %	mM H2SO4	mM Xylenol Orange	mM Ferrous Ammonium Sulphate	Water	Source
Fricke 3	5	50	0.5	0.3	3x gr gelatin weight	[140]
	w/w methacrylic acid (MMA) %	gelatin %	tetrakis THPC	water %		
nMAG 1	2	8	??(20)	80		[97]

Dose gel	<i>N,N'</i> -methyl en bisacrylamide (Bis) %	Acrylamide (AA) %	Gelatin %	Mm tetrakis (THPC)	Mm hydroquinone (HQ)	HPLC (water)%	Glucose %	Sucrose	Source
PAGAT 1	4.5	4.5	5	7	0.01	86			[55]
PAGAT 3	3	3	6	10		??			[97]
PAGAT 3	3	3	6	10		??	10		[58]
PAGAT 3	3	3	6	10		??	20		[91]
PAGAT 3	3	3	6	10		??		10	[97]
PAGAT 3	3	3	6	10		??		20	[97]
PAGAT 4	3	3	6	5					[58]
PAGAT 13	3.5	3.5	5	10	8	89			[91]
PAGAT 14	3	3	6	10			20	20	[97]
PAGAT 15	3	3	5	5		89			[97]
nPAG 1	3	3	5	10		80			[1]
nPAG 2	3	3	5	10		89			[17]

Dose gel	Water %	Gelatin %	Methacrylic acid	Boric acid	Tetrakis (THPC)	Source
MAGAT 1	87	8	5	0 and 25 mM	5 mM	[24]

Dose gel	Water %	Gelatin %	Trichloroacetic acid	Triton X100 surfactant	LCV	Ferrous ammonium sulphate	H2O2	NaHCO4	mM Cetyl Trimethyl Ammonium Bromide (CTAB) /source
leuco-crystal violet (LCV) micelle		5	25 mM	4 mM	1 mM	1 mM			[141]
leuco-crystal violet (LCV) micelle		5	25 mM	4 mM	1 mM		100 mM		[142]
leuco-crystal violet (LCV) micelle gelatin hydrogel 3sample		5	25 mM	4 mM	1 mM		300 mM	50 mM	[142]
LCV	96%	4	25 mM	4 mM	1 mM				[141]

micelle										
LCV micelle	96%	4	25 mM	120 Mm 2,2,2- trichloroet hanol (TCE)	0.7 mM					17/[143]

Dose gel	% Deionized water	% Gelatin	N-isopropyl- acrylamide (NIPAM) %	% <i>N,N'</i> methylene bisacrylamide (BIS, Sigma-Aldrich)	mM tetrakis hydroxymethyl phosphonium chloride (THPC)	Source
NIPAM	75	5	15	4.5	5	[97]
NIPAM	80	5	3	3	5	[97]

ANNEX 2

Matlab codes

```
%%MRI/document scanner data processing program%%
%%%%%%%%%%%%%%%%%%%%%%%%%%%%%%%%%%%%%%%%%%%%%%%%%%%%%%%%%%%%%%%%%%%%%%%%
%% calibration curve acquisition part
clc;
close all;
clear all;
I =
rgb2gray(imread('C:\Users\Evelina\Desktop\geliai.jpg'));
%read picture as an intensity image
%I = imread('geliai.jpg'); %read picture as an intensity
image
figure
imshow(I); %show picture
a05=mean(mean(imcrop())); %cut regions
a1=mean(mean(imcrop())); %cut regions
a2=mean(mean(imcrop())); %cut regions
a3=mean(mean(imcrop())); %cut regions
a4=mean(mean(imcrop())); %cut regions
%rearrange values to single vector
a=[a05 a1 a2 a3 a4];
% a=a/max(a); %normalization
P = polyfit(a,[10 13 18.6 26 43.3],1); %fit first order
polynomial
figure %draw calibration curve
hold on;
plot([10 13 18.6 26 43.3],a, 'o'); %plot data points
(relative pixel intensity)
plot(polyval(P, a), a); % plot approximation
hold off;
xlabel('Absorbed dose, Gy');
ylabel('Pixel intensity');

%R-squared calculation according to formula
B=[10 13 18.6 26 43.3]; % y values
f=polyval(P, a); %predicted y values
Bbar = mean(B);% mean
SStot = sum((B - Bbar).^2);
SSres = sum((B - f).^2);
R2 = 1 - SSres/SStot

filename='C:\Users\Evelina\Desktop\spectrums.txt';
%saving spectrums at each dose, manual folder selection
```

```

save(filename, 'P');
%% dose mapping part
clear all;
I =
rgb2gray(imread('C:\Users\Evelina\Desktop\geliai.jpg'));
%read picture as an intensity image
%I = imread('geliai.jpg'); %read picture as an intensity
image
filename='C:\Users\Evelina\Desktop\spectrums.txt';
load(filename);
%convert data to double type
I=double(I);
%apply model to data
I2=polyval(P,I);

%show dose map
figure
imshow(I2); % show dose map
colormap jet
colorbar
caxis('auto');
c=colorbar;
c.Label.String = 'Dose, Gy';
%set(gca,'XTickLabel',0:2:12)

Dose profile code

%%MRI/document scanner data processing program%%
%%%%%%%%%%%%%%%%%%%%%%%%%%%%%%%%%%%%%%%%%%%%%%%%%%%%%%%%%%%%%%%%%%%%%%%%
clc;
close all;
clear all;
%% dose mapping part
clear all;
I =
rgb2gray(imread('C:\Users\Evelina\Desktop\1shot.jpeg'));
%read picture as an intensity image
%I = imread('geliai.jpg'); %read picture as an intensity
image

%show dose map
figure
imshow(I); % show dose map
colormap jet
colorbar
caxis('auto');

```

```

c=colorbar;
c.Label.String = 'Dose, Gy';
%set(gca,'XTickLabel',0:2:12)

%dose profile part
V=rgb2gray(imread('C:\Users\Evelina\Desktop\lshot.jpeg')
);
[n,m]=size(V); %raw of interest
c=270;
K=zeros(m);
for i=1:1:m
K(i)= V(c,i); %profile line
end
figure
plot(K)%show plot

>>>
clear all;
Files=dir('C:\Users\Evelina\Desktop\Matlabai\measurement
s 05-04\nulis\*.txt');
j=1;t=1;
Csum=0; %sum of absorbance values at specific wavelength
for k=1:length(Files)
filenames='C:\Users\Evelina\Desktop\Matlabai\measurement
s 05-04\nulis\*.txt'; %acquire each name
Data=fileread(filenames); %read data
Data=strrep(Data,',',' '); %string replace , to .
fID=fopen(filenames,'w');
fwrite(fID,Data,'char'); %save modified data
fclose(fID);
fID=fopen(filenames);
C=textscan(fID,'%f %f','headerlines',13); %scan text
fclose(fID);
C1 =str2double(C{1,1});%column1 extract and convert
from string to double
C2 =str2double(C{1,2});%column2 extract and convert
from string to double
Csum=Csum+C2; % sum all absorbance values for mean
calculation
end
C05=Csum/36; %average of absorbance values at each
wavelength
filename='C:\Users\Evelina\Desktop\Matlabai\kalibariciai
.mat';
save(filename,'C05','C1','C2','C3','C4','C5','C6','C7');
load(filename);

```



```

for i=1:length(C1)
Caldata(i,:)=[C05(i) C1(i) C2(i) C3(i) C4(i) C5(i) C6(i)
C7(i)]; %gather calibration curve data at
Diffcaldata(i)=mean(diff(Caldata(i,:)));
end
[value, position]=max(Diffcaldata);
wavelength=C1(position);
P = polyfit(Caldata(position,:), [0.5 1:1:4],1); %fit
first order polynomial
figure
hold on
plot([0.5 1:1:4],Caldata(position,:), 'o'); %plot data
points
plot(polyval(P, Caldata(position,)),
Caldata(position,:)); % plot approximation
hold offm

```

SL344. 2021-*-* , * leidyb. apsk. I. Tiražas 12 egz. Užsakymas 255.
Išleido Kauno technologijos universitetas, K. Donelaičio g. 73, 44249
Kaunas
Spausdino leidyklos „Technologija“ spaustuvė, Studentų g. 54, 51424
Kaunas